DYNAMIC INTERLAMINAR TOUGHNESS OF GLASS FABRIC/EPOXY LAMINATES

By

HIMANSHU CHAUDHARY

DEPARTMENT OF MECHANICAL ENGINEERING

Indian Institute of Technology Kanpur

January, 2000

DYNAMIC INTERLAMINAR TOUGHNESS OF GLASS FABRIC/EPOXY LAMINATES

A Thesis Submitted
in Partial Fulfillment of the Requirements
for the Degree of

MASTER OF TECHNOLOGY

By

HIMANSHU CHAUDHARY

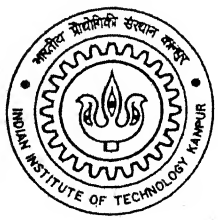

to the

Department of Mechanical Engineering
Indian Institute of Technology, Kanpur

January, 2000

CERTIFICATE

It is certified that the work contained in the thesis entitled **"Dynamic Interlaminar Toughness of Glass Fabric/Epoxy Laminates"**, *by* **Himanshu Chaudhary**, *has been carried out under my supervision and this work has not been submitted elsewhere for a degree.*

P Kumar

January,2000

(Dr. Prashant Kumar)
(Professor and Head)
Dept. of Mechanical Engineering
Indian Institute of Technology
Kanpur

ABSTRACT

Name of student: Himanshu Chaudhary Roll No: 9810512
Degree for which submitted: M.Tech. Dept. :Mechanical Engg.
Name of thesis supervisor: Prof. Prashant Kumar

Month and year of thesis submission: January, 2000

A combined experimental and finite element method is exploited to determine dynamic interlaminar fracture toughness of glass fabric/epoxy laminates. A 7-8 mm thick specimen made of 64 laminae and having a precrack of length 40 to 50 mm at the midplane of one of its edges is used in the present study. The front face of the specimen is bonded to a rigid block and the rear cantilever is screwed to a load bar. In the load bar, a compressive elastic stress pulse is generated by impacting it with a striker bar. When the incident compressive pulse reaches the specimen, a part of energy is reflected into the load bar and the rest passes to the specimen. The incident and reflected stress pulses are monitored by two strain gauges on the bar, which determine the deflection history of the cantilever end. The energy transferred to the specimen initiates growth of the precrack at high speed under the impact conditions. The propagation of crack tip is monitored by two strain gauges of width 0.9 mm and 2 mm length bonded ahead of the crack tip on the side face of the cantilever end. The first strain gauge is bonded very close to the crack tip. The crack velocity determines initiation time of crack propagation.

The experimental results, the deflection history of the cantilever end, the crack velocity, the initiation time of crack propagation, as well as material properties are used as input data in a finite element (FE) code to evaluate dynamic interlaminar fracture toughness of the laminates in terms of J-integral($\hat{J}$). A model of gradual release of nodal forces simulates the propagation of the interlaminar crack. The FE code gives the variation of J-integral with time. Two sets of specimens of having different crack lengths are investigated to study the effect of crack length. First set of the specimens employs a short crack of 40 mm while the other employs a long one of 50 mm. For both sets of experiments the velocity is kept between 660 and 2200 m/s. The initiation fracture toughness for the short crack length is found to be between 55 and 536 J/m^2 and that of for the long crack length between 38 and 400 J/m^2. On the other hand, the values of propagation fracture toughness lies between 6 and 18 J/m^2 for short crack length and between 3 and 20 J/m^2 for long crack length. The effect of the crack length was found insignificant.

Acknowledgement

I take this opportunity to thank and express my gratitude to Prof. Prashant Kumar for providing me invaluable guidance through out the thesis work. His wisdom, unflagging enthusiasm and constant encouragement are a source of constant inspiration for me.

I am also grateful to Prof. N.N. Kishore and Prof. Om Prakash for their expert guidance in Finite Element Methods and Composites respectively.

I feel obliged to the active and expert team working on projects of Aeronautical Research and Development Board in the ESA Lab. The members of the team Mr. Pankaj Singh Chandel, Mr. Divakar, Mr. Anurag Goel, Mr. B.D. Pandey and Mr. Ramchandra Tewari helping me in various ways during experiments.

My friends Manish Pandey, Vimal Jaiswal, Dhiraj Tamarkar, Sharad Dwivedi, Arjun Singh, Dinesh Swami, Kamlesh Bhatt and Ms. Padmaja deserve a special mention for their unlimited love that made my stay in IIT, Kanpur so wonderful. I shall always cherish this pleasant memory.

I am also grateful to M.L.V. Textile Institute, Bhilwara (An autonomous institute of Government of Rajasthan) and Government of Rajasthan for granting me study leave and giving me this opportunity to pursue my M.Tech. degree.

Contents

List of figures

List of Tables

Chapter 1

Introduction

1.1 Introduction

Glass, carbon, or kevlar-fiber-reinforced polymers (GFRP, CFRP, and KFRP) have emerged out as an important class of engineering materials. Since they offer outstanding mechanical properties (strength, stiffness and lightness), unique flexibility in design capabilities, and ease of fabrication, they are increasingly used as structural members. Additional attractive properties, they offer, are corrosion resistance, impact resistance, excellent fatigue strength and environmental stability. Therefore, though expensive, are finding increasing use in aerospace, transport and sporting goods. In addition, there are many opportunities for their wider application in other fields like hiking equipment, medical goods and even apparently insignificant things like speculator frames.

Most FRP composites used in structural applications are in laminate form. The laminate is commonly made by stacking prepags over each other and curing them at high temperature and pressure. High strength man made fibers (carbon & graphite, Kevlar, glass, boron) impart stiffness and strength in the plane of the ply but plies are bonded to each other with comparatively low strength matrix material; fiber do not reinforce the laminate through thickness. However, interlaminar strength is usually adequate for an FRP structure loaded under quasistatic conditions. Glass fibers are the most common of all reinforcing fibers for polymer matrix materials because of low cost and high strength although they have comparatively low modulus and poor abrasive resistance, which decreases its strength and adhesion to polymer matrix resin in presence of moisture.

The strength of an FRP laminate comes into question when a foreign body is impacted on it at subsonic velocity. An intense damage is observed at the center of the impact with fiber breakage, matrix cracking and fiber pull out. Further, the damage

spreads laterally to the considerably large area mainly through interlaminar separation even if the impacting body is of Low Mass (10-30 g) (Kumar and badri, 1993). On the other hand, when a foreign body impacts a metallic sheet, material at the impact center yields, resulting in formation of a small dent. Therefore, in such cases the FRP laminates are less tough than conventional materials. The speed of expanding fronts of delamination cracks is as high as 200-500 m/s (Takeda et al .,1982). When glass fiber reinforced epoxy laminates are impacted it was found that if the total delamination area between various plies is multiplied by the quasistatic energy release rate, the net energy exceeds the energy of the impacting mass (Kumar and Naraganan,1993). The gives an idea that the interlaminar cracks at high speeds propagate at lower toughness resulting in a fairly large damage area. Therefore, the characterization of the interlaminar fracture toughness under dynamic creak propagation is of prime concern of FRP laminates.

Experiments to determine dynamic fracture toughness have been mostly done on large plates having a through the thickness crack. This work is generally carried out through the method of caustics. Although a considerable amount of work has been done to study the fracture phenomena through numerical methods but only large rectangular double cantilever beam were given attention. Owen and Shantaram (1997) introduced the use of finite element method to study dynamic crack growth. Nishioka and Atluri (1982a, 1982b) investigated the crack propagation and arrest in a high strength steel DCB specimen using moving singular dynamic finite element procedure.

The study of fast moving delamination cracks in a laminate, whose thickness is usually less than 5 -8 mm, is complex from an experimental and numerical point of view. Modeling of dynamic propagation requires having measurement within a very short period during crack propagation. In case of static case the crack propagates when the fracture toughness exceeds a certain critical value. Crack propagation criterion for dynamic case is not well defined. Further, studies of dynamic crack propagation require accurate loading and measuring techniques. These techniques are readily not available with commercially available facilities. Keeping these views in mind, a combined technique is developed, which makes use of a numerical simulation using experimental data from a less sophisticated instrument.

1.2 Literature Survey

A large number of investigations have been carried out on dynamic crack propagation employing a through-the-thickness crack in a large plate. Stress waves are the continuously generated at the crack tip of fast moving crack. As these stress waves reach the boundary of the specimen, they are reflected. Some of these reflected stresses waves come back to the region infront of crack tip. Experiments with large size plate are controlled such that the monitoring of important parameters is complete before the reflected waves arrive. In other words, the experiments are controlled to isolate the effect of specimen edges. In case of an interlaminar crack in a fiber glass/epoxy laminate, which is usually not thicker than 6 to 8 mm, the free surfaces are always close to the crack tip and there is no way one can isolate the region of interest from the reflected waves. Therefore, a new approach is required to find dynamic toughness of interlaminar cracks.

An important aspect of dynamic crack propagation study is the measurement of crack velocity. Takeda et.al. (1982) used high speed photography to measure the interlaminar crack propagating speed in composite laminates. They observed that the interlaminar crack in composite laminates moves at 200-500 m/s, when impacted by foreign bodies.

Several groups did initial and extensive investigations on crack propagation of through the thickness crack in a large plate. Ravi Chandar and Knauss (1982, 1984a, 1984b, 1984c, 1984d) have done an exhaustive study of dynamic crack propagation phenomena using the method of caustics for Homalite-100. This included study of crack initiation and arrest, microstructure aspects, crack branching and interaction of stress waves with the crack tip. Rosakis, Duffy and Fruend (1984) performed dynamic crack propagation experiments on double cantilever beam specimen using wedge loading. Zehnder and Rosakis (1990) used optical method of reflected caustics combined with high-speed photography to investigate the dynamic fracture initiation and propagation in 4340 steel specimen.

These investigations, based on caustic have been very effectively used to study the fracture phenomena in a large plate with through the thickness crack. The method is not likely to be effective for the interlaminar crack in a slender sheet because the strength of the interlaminar bond is very weak and it will introduce very little strain in the bonded sheet making the size of the caustic negligibly small.

Ravichandran and Clifton (1989) developed a special technique to study the initiation and propagation of crack in the steel under dynamic impact loading. They presented a plate impact experiment and an associated finite difference model to study the fracture process that occurs in sub-micron loading. A disc containing a prefatigued edge crack on the midplane upto half way across the diameter is impacted by a thin flyer plate of same material. A compressive pulse propagates through the specimen and reflects from the rear surface as a tensile pulse of 1μs duration. Using the laser interferometer system monitors the motion of the rear surface.

Berger and Dally (1990a) used a series of strain gauges ahead of the crack tip at a certain predetermined location to monitor the strain and crack propagation. Berger, Dally and Sanford (1990b) also used strain gauges ahead of the crack tip to determine dynamic stress intensity factor associated with a propagating crack.

Nishioka and Atluri (1983) studied the use of path independent J -integral for dynamic crack propagation by the finite element method. Other path integrals were also investigated along with J -integral. Numerical results showed that combined use of J -integral and the finite element method is a useful tool to obtain the fracture parameters such as stress intensity factors and energy release rates.

Kolednik (1991) presented his theoretical study for physical interpretation of the J-a curves for elastic-plastic fracture. He derived the difference between the exact initiation toughness and crack growth toughness using energy balance under quasi-static conditions. He considered three point bend specimens each of that consists of two parts glued together along the ligament. The analysis was made on large specimens.

Verma (1995) developed a combined experimental and numerical technique to determine interlaminar dynamic fracture toughness under impact loading. An interlaminar crack is propagated at very high speed in DCB specimen made of two steel plates which are bonded together by epoxy with a precrack. Strain gauges of gauge length 0.2 mm are bonded ahead of crack tip for monitoring crack propagation speed. Using the experimentally obtained data (deflection of steel plate, initiation time and crack propagation history with time) to FE code J-integral is determined. Initiation toughness and propagation toughness are evaluated.

Sun and Grandy (1988) investigated dynamic delamination fracture toughness in a $[90/0]_{5s}$ T900/934 graphite/epoxy laminate using impact loading. Delamination cracks of different sizes were embedded at the midplane of the composite specimen. The threshold impact velocity that causes propagation of delamination crack was used in the dynamic analysis with the finite element method. From the finite element solution, the time-history of the strain energy release rate was calculated. The critical strain energy release rate was taken equal to that of maximum value of the response history.

Raman P. Singh et al. (1996) described various experimental observations for dynamic intersonic decohesion of bimaterial interfaces. Two separate but complementary optical methods are used in conjunction with high-speed photography to explore the nature of the large-scale contact and shock wave formation at the vicinity of running cracks in two different bimaterial systems.

R.W.Truss et al. (1997) had attempted to find interlaminar and intralaminar fracture toughness of uniaxial continuous and discontinuous carbon fiber/epoxy composites, using compact tension and double cantilever beam test geometry. The discontinuous carbon fiber/epoxy composites have been found to have a slightly misalignment of the fibers from the average fiber direction and this misalignment was found to increase both initiation fracture toughness and to greater extent the propagation fracture toughness. The increase in fracture toughness in discontinuous carbon fibers/epoxy samples was due to fibers bridging the crack and this has been modeled as if the the bridging fibers provide an increase in compressive stress across

the crack analogues to a craze at the crack tip.

John Lambros and Rosakis A.J (1997a) investigated dynamic delamination of thick fiber reinforced polymeric matrix composite laminates using optical techniques and high-speed photography. They had used 65% fiber volume fraction of Graphite/epoxy laminates consisting of 48 plies. Square plates of152 mm X 152 mm dimensions were impacted in an out-of-plane configuration using high speed (1m/s – 3 m/s) gas gun. Real time imaging of the laminate out-of-plane displacement was performed using lateral shearing of interferometer of Coherent Gradient Sensing in conjunction with high speed photography. Delamination speeds up to 1800 m/s were observed.

John Lambros and Rosakis A.J (1997b) investigated dynamic crack initiation and growth in unidirectional graphite/epoxy plates with high-speed photography. Edge notch plates are impact loaded in one point bend configuration using drop weight tower. Initiation fracture toughness data were reported and significant dynamic effects are observed through emission of stress waves from the propagating crack tip.

Ramakrishna (1996), Babu (1998) and Mallikharjuna (1998) attempted to investigate initiation and propagation toughness of unidirectional GFRP laminates under impact loading. In these studies, Verma's(1995) experimental technique was exploited with some changes. Ramakrishna (1996) found that the initiation toughness lies between 50 and 250 J/m^2 and propagation toughness between 20 and 50 J/m^2. Babu and Mallikhajuna (1998) used superior specimen and conducted experiments at crack velocity varying in the range of 517 to 1000 m/s. They used velocity strain gauges of smaller length (0.2 mm). They reported J-initiation between 245 and 620 J/m^2 and J-propagation between 45 and 83 J/m^2. Ramakrishna, Babu and Mallikharjuna used GFRP laminates to investigate interlaminar dynamic fracture toughness.

1.3 Present Work

To determine interlaminar dynamic toughness of glass fabric/epoxy laminates under impact loading, a technique developed by Verma (1995) are exploited. The technique is initially developed on a double cantilever beam specimen made from hardened steel strips bonded together with epoxy. One of the cantilevers is impacted. A FE code is developed to simulate the wave propagation in the DCB specimen and to determine the initiation and propagation toughness of the interlaminar crack. This hybrid technique is extended in the present work to determine initiation and propagation toughness of specimen made of glass fabric /epoxy laminate. The technique employs a combined experimental and numerical analysis.

The technique used for glass fabric/epoxy laminates consists of applying an impact load on a specimen with a precrack (Fig. 1.1). The portion that is on front side of the precrack remains straight during experimentation because it is bonded to a solid block. The rear portion of the specimen acts as a cantilever plate. Strain gauges are mounted ahead of the crack tip to monitor the crack velocity. The experimental work determines the end deflection of the cantilever, crack velocity and crack initiation time. These are used as inputs to the FE code to simulate the crack propagation.

Chapter 2 discusses the specimen preparation and experimental setup. The brief details of finite element code are covered in Chapter 3. Results of the present work and comparison of the same with that of other researchers are presented in Chapter 4. Chapter 5 concludes the present work and scope for further work.

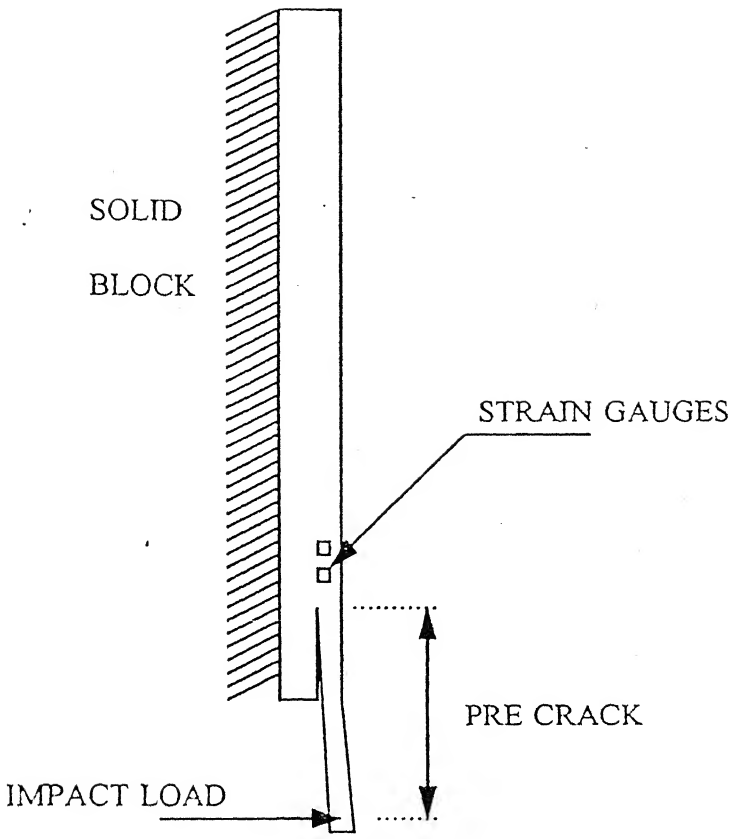

Fig.1.1 Specimen under impact loading

Chapter 2

Specimen and Experimental Set up

In the present study, a combination of experimental and a finite element package is employed to find interlaminar dynamic fracture toughness of polymer composites. Schematic diagram of the experimental setup is shown in Fig. 2.1 and the photograph of the setup in Fig. 2.2. Front face of the specimen is bonded to a rigid support and the rear cantilever is screwed to the load bar. The load bar is impacted with a striker bar. An air gun using compressed nitrogen gas is used for acceleration of the striker. Strain gauges mounted on load bar at an appropriate location measure the stress pulses propagating in the load bar. To monitor crack propagation two velocity strain gauges are bonded on side face of the DCB specimen.

In this section specimen preparation, experimental setup, experimental measurements and data processing are discussed.

2.1 Specimen

The specimen used in the present work is glassfibre fabric reinforced epoxy composite. This section describes the specimen geometry, raw materials, and preparation of laminates and preparation of specimen from laminate.

2.1.1 Specimen Geometry

The geometry of the specimen is shown in Fig. 2.3. Figure 2.4 shows the orthographic views of the same. It is 25 mm wide and 180 – 200 mm long with an edge precrack on mid plane of the specimen. The precrack is introduced during the fabrication of the specimen. The portion of the specimen, which is on front side of the precrack is cut and removed so that the load bar can impact the cantilever . A small hole of diameter 6.2 mm is drilled on the cantilever so that it can be screwed to the load bar with an M 6 cap screw and a specially designed washer.

2.1.2 Raw Materials

Fiberglass fabric and epoxy resin mixtures are used as raw materials of the specimen. Composition of epoxy resin mixture is as follows :

Araldite	LY556	100 parts by weight
Hardener	HT976	35 parts by weight
Accelerator	XY73	1 part by weight
Coupling Agent		0.5 part by weight
(γ-Amino prophyl triethoxy silane)		

Fiberglass fabric, purchased from M/s HARSH-DEEP INDUSTRIES, Ahemdabad, is used in the present work. The properties of fiberglass fabric are dependent on fabric construction, i.e., the number of yarn per cm in each direction, weave pattern, and yarn type. Specifications of the fiberglass fabric used as reinforcement material in the present work are as follows:

Number of yarn per 25 mm in warp = 40

Number of yarn per 25 mm in weft = 36

Area density = 146 gm/m^2.

2.1.3 Laminate Preparation

Prepregs of fabric and epoxy resin is made through a 150 mm wide prepreg-making machine available in the laboratory. It is prepared at 95°C and stored at – 18°C. For making a laminate, this prepregs is cut for required approximate length of 240 mm. Each cut lamina is stacked together to get required thickness; 60-64 lamina are generally required for a specimen of 7 to 8 mm thickness. Precrack length, 35 to 65 mm, is introduced by inserting a thin teflon film of 20 μm thickness at the midplane of the laminate at one of its edge. The stacked laminate is cured in hydraulic press at 120° C temperature. Initially laminate is pressed between two plates at gradually increasing pressure, 23.7 kPa per minute for half an hour. Then pressure of 710 kPa and temperature 120° C are maintained for 1 hour. Finally, maintaining the same pressure and increasing temperature to 150oC for two hours does post curing. The pressed laminate is then allowed to cool to room temperature. A diamond cutter cuts this cured laminate in required width of 25 mm.

2.1.4 Specimen from Laminate

Now the specimen is marked for drilling a hole to have the desired crack length. After drilling the hole of 6.2 mm diameter, the front portion of the specimen near the hole is removed through a saw. Furthermore, the front face of the specimen is serrated with a hacksaw for better bonding to the solid block. Final shape of the specimen is shown in Figs.2.3 and 2.4.

In the present study the specimen used is 7-8 mm thick, 25 mm wide and 220 mm long whereas crack length for one set of experiments is closed to 40 mm and for other set of experiments approximately close to 50 mm. The portion on the front side of the precrack remains straight during experimentation because it is bonded to the solid block. The rear portion of the specimen works as a cantilever.

2.2 Experimental Setup

Main integral components of experimental setup include air gun, striker, load bar, bridge circuits, digital storage oscilloscope and solid block (Figs. 2.1and 2.2). The slotted face of the specimen is bonded with araldite to the rigid block with the help of C clamps and the block is fastened to base of set up with two M12 bolts and washers. The load bar is screwed to the rear end of the specimen with a M6 screw 1Ua washer. When the load bar is impacted by a striker bar, from air gun, elastic compressive and reflected tensile stress pulses are generated in it. These elastic stress pulses are monitored by two strain gauges bonded on the bar in the longitudinal direction. They are connected to an oscilloscope through a bridge circuit. The two velocity strain gauges bonded ahead of crack tip are also connected to the oscilloscope each through another bridge circuit. The complete bridge circuit is discussed subsequently.

2.2.1 Striker and load bar

A compressive stress pulse is applied to the specimen through load bar, striker and air gun of nitrogen. The load bar is properly aligned with the centerline of barrel of the air gun. The striker bar is accelerated in the air gun and its impacting face is

spherical so that impact would be at center of end face of the load bar. Striker and load bar are made of cold rolled mild steel of 19 mm diameter. When the striker, from air gun, hits the load bar a longitudinal compressive stress pulse is generated in the load bar. As this compressive stress pulses reaches the specimen end of the load bar, part of it transmitted to the specimen and remaining is reflected back as tensile pulse.

Two strain gauges bonded at diametrically opposite locations on the load bar pick up these stress pulses. The reponses of the gauges are recorded in a storage oscilloscope through a bridge circuit.

2.2.2 Stress Pulses

When the striker bar impacts the load bar, the compressive incident pulse (σ_1) propagates towards the specimen and is recorded at location 1 as shown in Fig.2.1. The reflected tensile pulse (σ_3) is recorded at the same location but at different time and is denoted by point 3 in the t – x diagram (Fig. 2.5). A typical record of the incident and reflected pulses in load bar is shown in Fig.2.6.

To determine displacement of cantilever end one-dimensional wave propagation theory for elastic wave propagation in the load bar and the striker bar is used. Wave propagation in load bar is analyzed through relation along characteristic. Line 1 – 2 is the characteristic along positive direction and relation between the stress and particle velocity is given by

$d\sigma - \rho c dv = 0$ (along the positive characteristic, 1 – 2)

$d\rho + \rho c dv = 0$ (along the negative characteristic, 2 – 3)

where σ is stress, v is particle velocity and ρ is density of the load bar material. c is the longitudinal wave velocity in material of the load bar. By using above equations the relation along characteristic 1 – 2 simplifies to

$$\sigma_2 - \rho c v_2 = \sigma_1 - \rho c v_1. \qquad (2.1)$$

Along the characteristic 1 – 5

$$\sigma_1 + \rho c v_1 = \sigma_5 - \rho c v_5. \tag{2.2}$$

However, $\sigma_5 = 0$ and $v_5 = 0$ because the load bar is initially at rest and stress wave never reaches at point 5. The above equation gives

$$\sigma_1 = - \rho c v_1. \tag{2.3}$$

Substituting Eq. 2.3 in Eq. 2.1, one obtains

$$\sigma_2 - \rho c v_2 = 2\sigma_1. \tag{2.4}$$

Relation along characteristic 2 – 3 and 3 – 4 are

$$\sigma_3 + \rho c v_3 = \sigma_2 + \rho c v_2 \tag{2.5}$$

$$\sigma_3 - \rho c v_3 = \sigma_4 - \rho c v_4. \tag{2.6}$$

However, $\sigma_4 = 0$ and $v_4 = 0$ at point 4 because the striker and load bar are of same material and diameter and the striker comes at rest. The above two Eqs. Yield

$$\sigma_2 + \rho c v_2 = 2\sigma_3. \tag{2.7}$$

$$v_2 = \frac{\sigma_3 - \sigma_1}{\rho c}. \tag{2.8}$$

It is to be noted that nature of σ_1 is compressive and σ_3 is tensile and therefore the particle velocity of the cantilever end can be found by taking sum of the absolute value of incident and reflected pulse. Displacement u_2 at point 2 with time t is found by integrating Eq. 2.8

$$u_2(t) = \int_o^t v_2(t) = \int_o^t \left(\frac{\sigma_3 - \sigma_1}{\rho c}\right) dt. \tag{2.9}$$

The time, t, at cantilever end is measured only after the head of the incident pulse reaches the strain gauge of the load bar. Similarly time t, is measured for reflected pulse when head of the reflected tensile pulse reaches at the strain gauge of the load bar.

2.2.3 Details of Bridge Circuit

The bridge circuit converts the change in resistance of the strain gauges bonded to the load bar into potential difference. This potential difference is recorded by oscilloscope. Figure 2.7 shows the configuration of the bridge circuit used in the present study. R_1, R_2, R_3 and R_4 are four strain gauges each having a resistance of 120 ± 0.3 Ω. $R_1$and R_2 are mounted on the load bar whereas R_2 and R_4 represent dummy gauges. The dummy gauges are also mounted on a 19 mm diameter steel bar. The circuit is balance by connecting a 1.0 Ω resistance in series and two variable resistors 100 kΩ and 1.0 KΩ parallel to one of the dummy gauges R_2 and R_4. Balancing of bridge is necessitated to give zero voltage output for no change in resistance of the active strain gauges. A calibration resistance R_c is connected parallel to one of active gauge (R_1 in diagram) through a switch K. The value of calibration resistance is 47 kΩ. For a balance bridge circuit the output voltage (Δe) is given by

$$\Delta e = \frac{R_1 R_2 E}{(R_1 + R_2)^2}\left[\frac{\Delta R_1}{R_1} - \frac{\Delta R_2}{R_2} + \frac{\Delta R_3}{R_3} - \frac{\Delta R_4}{R_4}\right] \qquad (2.10)$$

where E is the voltage applied (9 V in this study) to the bridge circuit.

This equation shows that similar (both positive or both negative) changes in resistance of opposite arms of the bridge circuit are added up and dissimilar (one negative and other positive) changes are cancelled out. Thus, active strain gauges at opposite arms only records compressive pulse and bending effect is neglected.

The relation between the strain in strain gauge and corresponding change in its resistance is governing by the following equation

$$GF = \frac{\Delta R}{\varepsilon}$$

$$\varepsilon = \frac{\Delta R / R}{(GF)} \tag{2.11}$$

where GF is the gauge factor and ε is the strain recorded by the strain gauge. The change in resistance of arm CD after connecting R_c is given by

$$\Delta R_3 = R_3 - \left(\frac{R_3 R_c}{R_3 + R_c} \right) \tag{2.12}$$

which gives

$$\frac{\Delta R_3}{R_3} = \frac{R_3}{R_3 + R_c}. \tag{2.13}$$

Corresponding to this change in resistance a voltage difference (V_c) will occur between terminals A and C. Similar resistance change also occurs in R_3 when the load bar experiences the load pulses. Thus the simulated strain (ε_c) due to shunting the calibration resistance is given by

$$\epsilon_c = \frac{R_3}{2(R_3 + R_c)GF} \tag{2.14}$$

The strain corresponding to calibration voltage (V_c). It is worth noting that a factor ½ in Eq.2.14 is applied to average out the strain recorded by the two strain gauges R_1 and R_3, which are at opposite arms of the bridge circuit. The strain in the load bar corresponding to a voltage V recorded on oscilloscope is given as

$$\varepsilon = \frac{\varepsilon_c}{V_c} V \tag{2.15}$$

2.2.4 Digital Storage Oscilloscope

A 4-channel digital storage oscilloscope of DSO1624, Gould Inc., UK is used to monitor strain gauges response. It stores data in 50-memory block and can be recalled. It has 12 bit resolution is 4096 point on the screen in horizontal and 8 bit resolution i.e. 256 points in vertical direction. Therefore per channel storage points

available in horizontal direction are 1024 and that in vertical direction 64. The maximum sensitivity in the vertical direction is 0.025 V and that in horizontal direction is 0.25 μs. For 4 channel horizontal sensitivity become 1 μs. The stored data are transferred to a personal computer by the GPIB software.

2.2.5 Rigid Block

A rigid block of mild steel of dimensions 75mm X 75 mm X 150 mm is used to bond serrated face of the specimen. The Serrated face of block is kept towards the serrated face of specimen. Two holes in the block are oversize (18 mm diameter) so as to adjust the specimen normal to the load bar. The rigid block is bolted to the rigid base plate after aligning the specimen to the load bar. Care is to be taken to ensure that the crack plane is normal to the load bar; otherwise specimen will be preloaded and the numerical simulation would be inaccurate. To use same block repeatedly the block is cleaned by burning araldite and then cleaning with acetone.

2.2.6 Velocity Strain Gauges

The two type of gauges used are supplied by Tokyo Sokki Kenkyijo Co., Ltd. Japan of following specification :

(I) BFLA-2-8	Resistance :	120 ± 0.3 Ω
	Gauge factor :	2.11 ±1
	Length:	2 mm
	Width	1 mm
(II) BFLA-5-8	Resistance :	120 ± 0.3 Ω
	Gauge factor :	2.10 ± 1%
	Length:	5 mm
	Width	1.3 mm

Verma et.al (1995), Babu and Mallikharjuna (1998) used the strain gauge of type FLG-02-11, gauge factor 2.05 and gauge length 0.2 mm. Since Verma (1995) used specimen of isotropic steel plate as bonding face, they worked properly. In the

present study, the material used is heterogeneous therefore 0.2 mm length is unable to sense the singular strain peak properly. Furthermore, BELA strain gauges are more suitable for this study because they are specially designed for composites.

The backing film of the gauges is large in area and therefore a portion of the gauge is chopped (Figs. 2.8 and 2.9). The gauge is bonded on the side face of the specimen such that the top portion of the active portion is 0.5 to 0.8 mm away from the crack plane.

Before bonding the strain gauges, the faces of the specimen to be bonded are polished with the help of emery paper. Then it is cleaned by acetone. The first strain gauge is placed very close to the crack tip approximately 1-2 mm and the second strain gauge 3-5 mm from first the gauge. These strain gauges are perpendicular to crack plane. Fewi-quick supplied by Pedilite Industries is used to bond the gauges. Position of the gauges with crack tip and plane are shown in Fig. 2.10.

2.2.7 Crack Velocity

Crack velocity is obtained by monitoring the responses of the strain gauges bonded ahead of the crack tip (Verma 1995). Verma used to bond three strain gauges at a certain angle. In present work, a modification of the above technique is used. Only two strain gauges are used and both the strain gauges are kept at an angle 90° to the crack plane. It is noteworthy that strain gauges are kept at a short distance (0.5 to 0.8 mm) from the midplane or crack plane of the specimen. Since the strain gauge are very close the crack plane, the singular strain field of the crack tip gives a strain peak when the crack tip passes close to the strain gauge. There are two such velocity strain gauges; the distance between the two strain gauges is measured accurately through travelling microscope; the velocity can be found using formula (Fig.2.11)

$$\text{Velocity} = \frac{a_2 - a_1}{t_2 - t_1}.$$

2.2.8 Initiation Time

The initiation time could be found out by extrapolating the data procured by the crack velocity strain gauges as shown in Fig. 2.11. Extrapolation procedure to find initiation time is justified on the following observation.

- The first velocity strain gauge is very close to the tip of the precrack (in the range of 1 to 2 mm). The initiation time of propagation of these kinds of experiment is very small. This can be justified from the experimental work of John Lambros and Ares J. Rosakis (1997a) who conducted on impact loading test on a one-point bend edge-notched unidirectional graphite/epoxy composite plates. For obtaining crack initiation and monitoring crack growth, on experimental technique with high speed photography was used. The measured crack velocity Fig.2.12 is in microsecond domain; the crack, after initiation, acquires high velocity immediately with rise time much less that one μs. The experimental results show that the extrapolation invoked in this study in finding initiation time work reasonably good. It is observed clear from Fig.2.12 that crack velocity does not change drastically after initiation time.
- The crack velocity of interlaminar crack is very high (600 to 2000m/s) and it takes a short time for the crack to move to the first velocity strain gauge.

2.3 Experiment Procedure

The specimen bonded with velocity strain gauges is screwed to the load bar through M6 cap screw and the front plate is bonded to rigid block by araldite. To cure bonding materials, block and specimen together is kept for 12 hours under bulb heating. Leads of velocity strain gauge are soldered to bridge circuit arm as discussed in section of bridge circuit; bridge circuits are then balanced. Experiments are carried out as follows:

Approximately 3.5 bar pressurized gas is filled in air gun from cylinder. Before releasing pressure it is made sure that oscilloscope is checked for normal and storage mode. The pressurized air is released to accelerate the striker, which impact the load bar. A compressive stress induced in the load bar propagates through strain

gauges and reaches the cantilever of the specimen. A part of the compressive pulse is transmitted to specimen that propagates the crack. Remaining pulse is reflected back as tensile pulse that again is recorded through the gauges of the load bar. The oscilloscope records strain pulses in the load bar, which are analyzed using one dimensional elastic wave analysis to obtain the displacement history of the cantilever end. Responses of the strain gauges on cantilever face, recorded by the same oscilloscope in other channels, yield the initiation time of the crack growth and crack velocity.

This whole set up was initially developed by Verma at.al (1995) for investigating fracture toughness of bonded steel plates. It has now been modified to determine interlaminar toughness of fabric glass fibers reinforced epoxy laminate under impact loading conditions.

2.4 Closure

The experimental set up measures the parameters:

1. Displacement vs. time relation of the cantilever end
2. Interlaminar crack velocity and
3. Initiation time of crack growth.

The experimental data are supplied to the finite element simulation to determine toughness required to initiate the crack (J_{ini}) and toughness of propagating crack (J_{prop}).The details of FEM simulation are discussed in Chapter3.

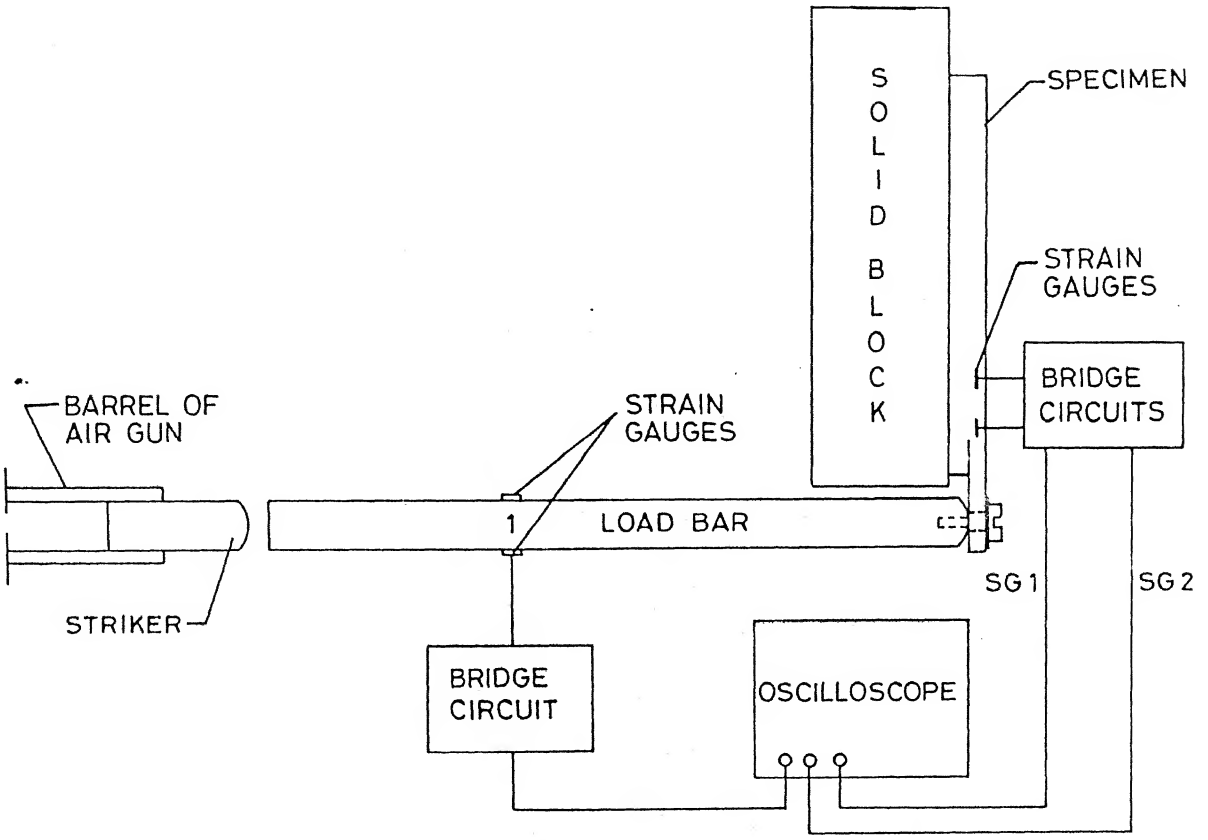

Fig. 2.1 Schematic diagram of the Impact loading setup.

Fig.2.2 A photograph of overall experimental setup

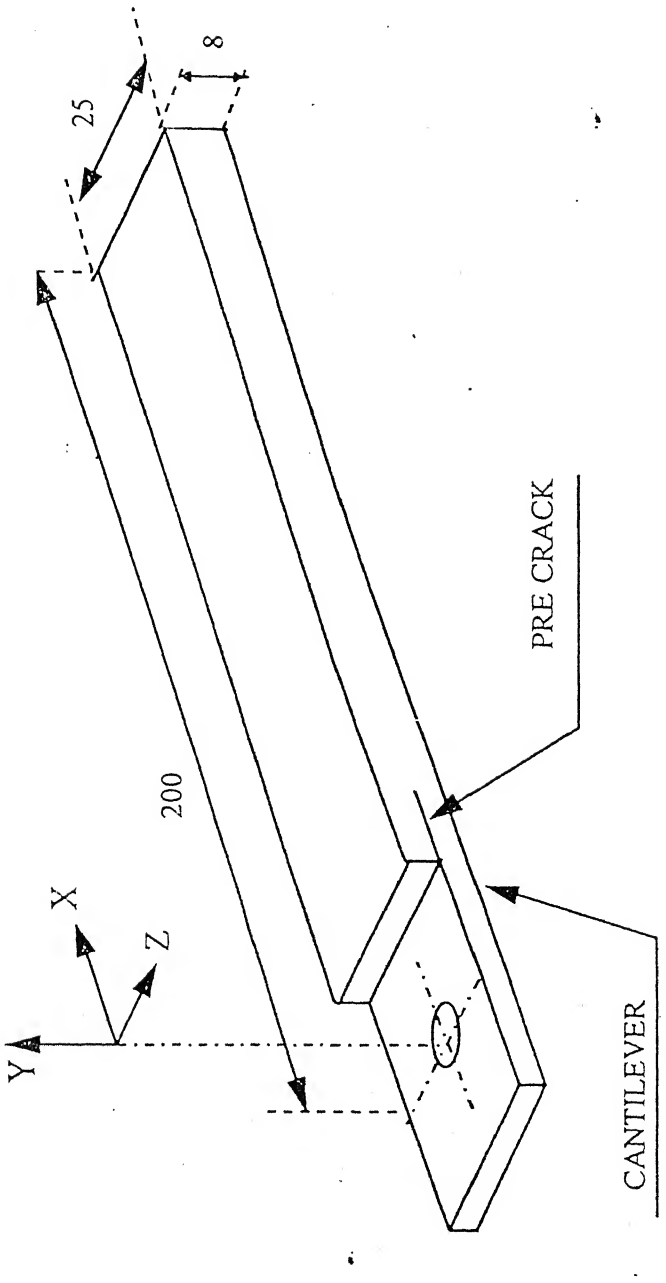

Fig.2.3 Isometric view of specimen

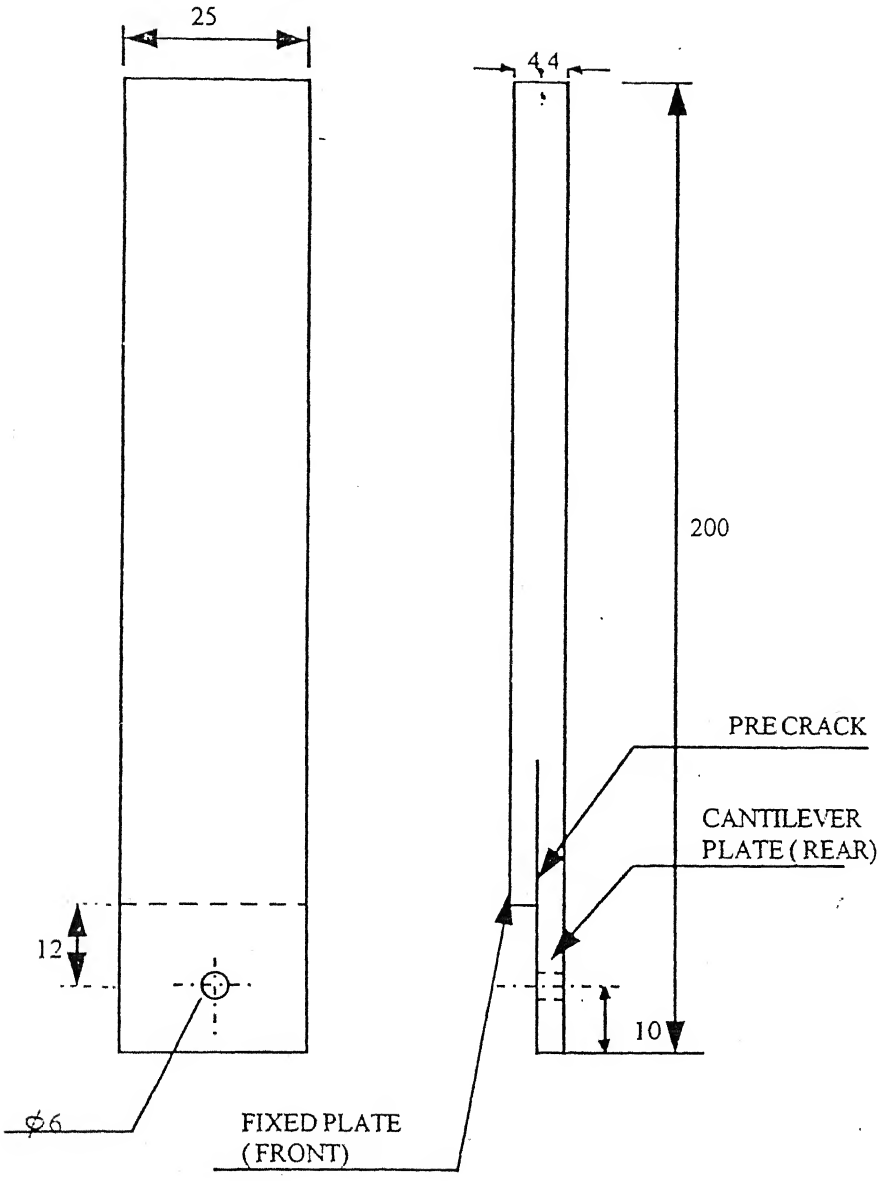

Fig.2.4 Orthographic views of the specimen

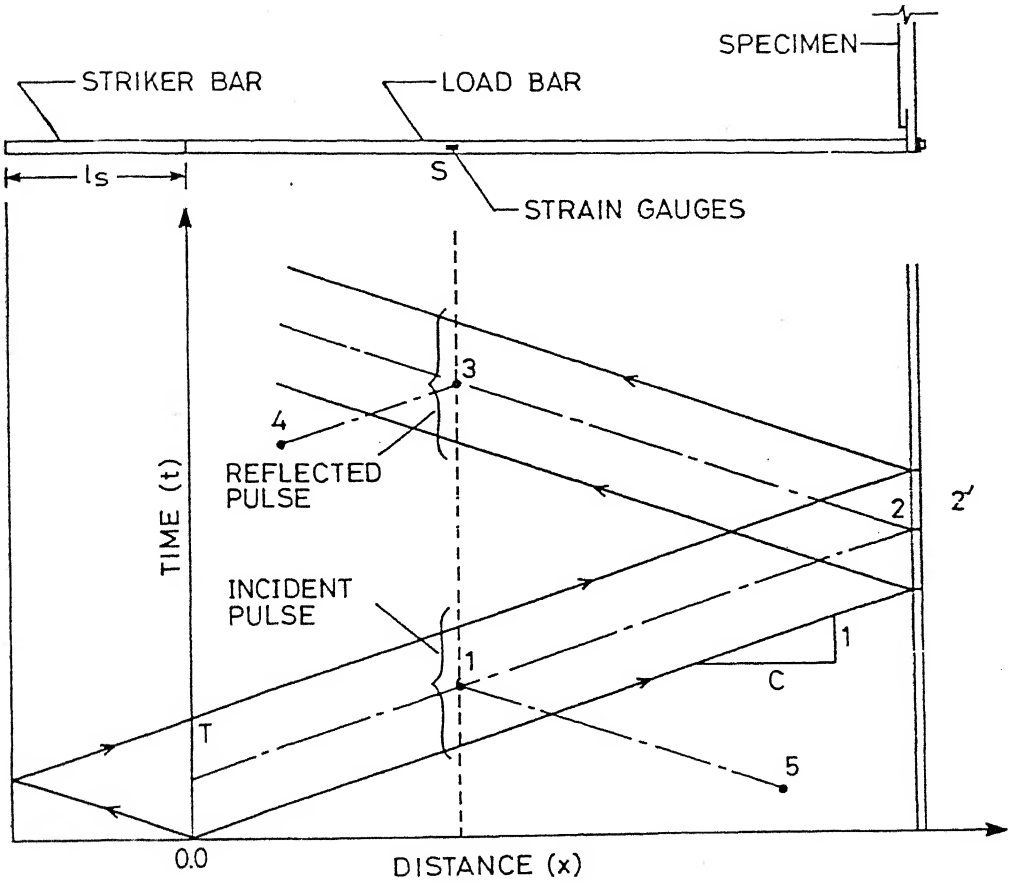

Fig. 2.5 Time-distance (t-x) diagram.

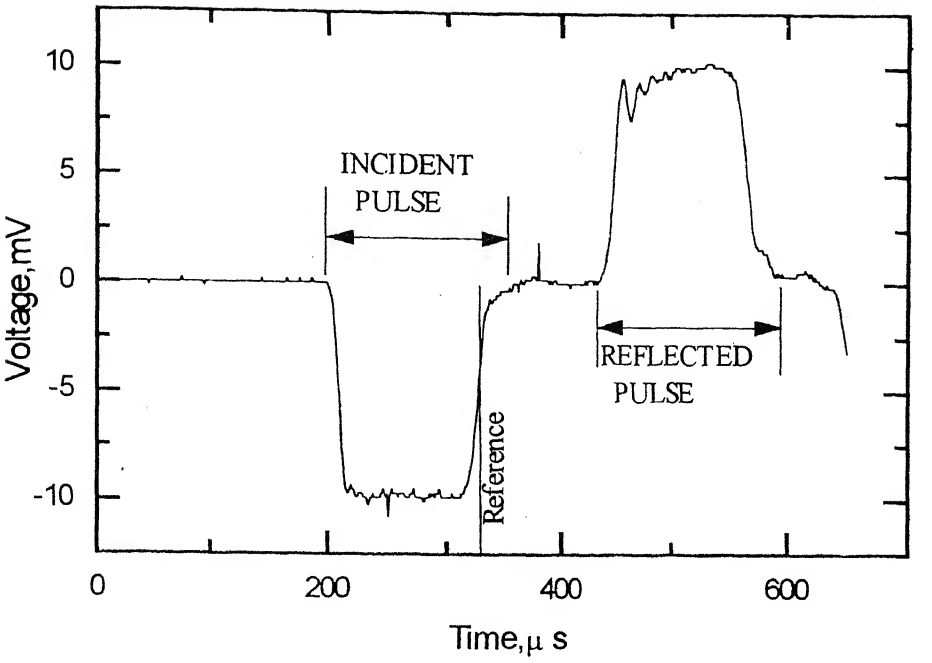

Fig.2.6 A typical record of stress pulses in load bar

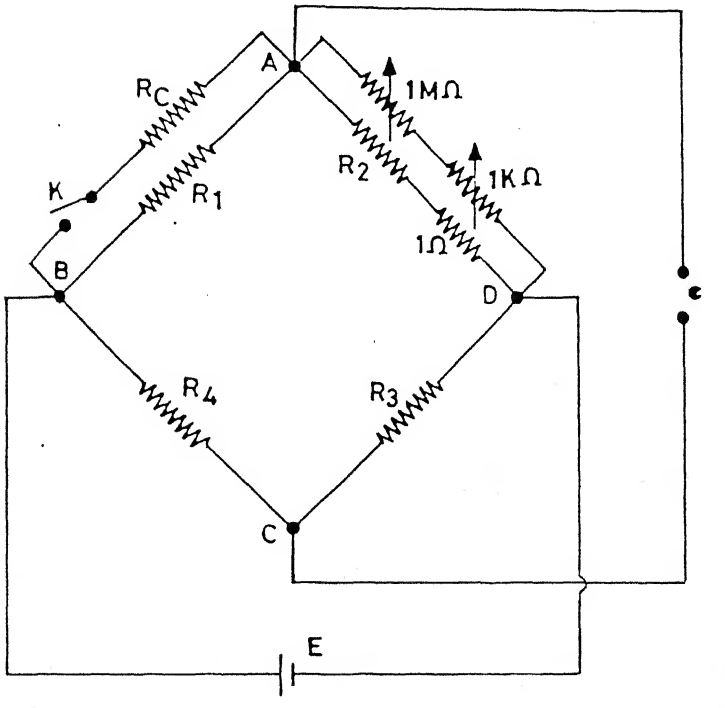

Fig.2.7 Configuration of bridge circuit

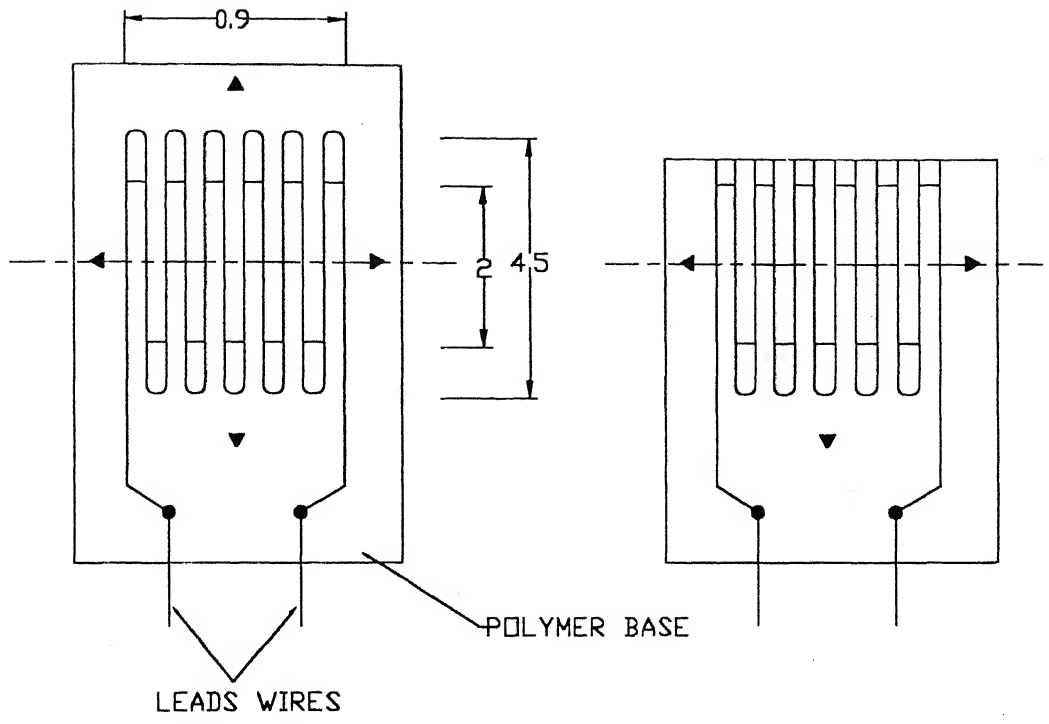

Fig.2.8 Schematic diagram of strain gauge (not to scale)

Fig.2.9 Schematic diagram of strain gauge after cutting

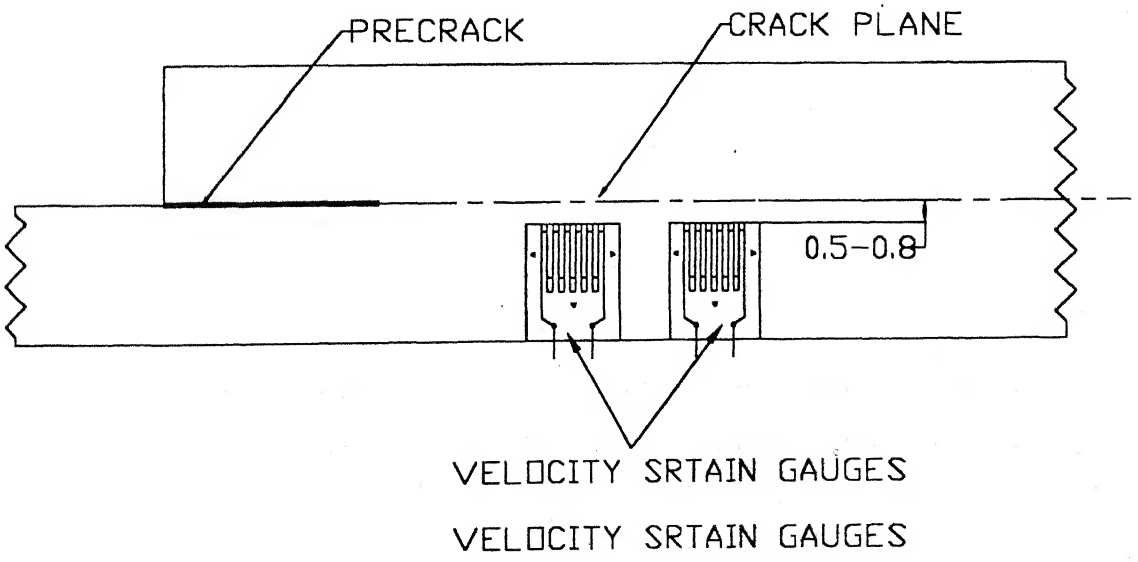

Fig.2.10 Locations of velocity strain gauges with reference to the crack plane

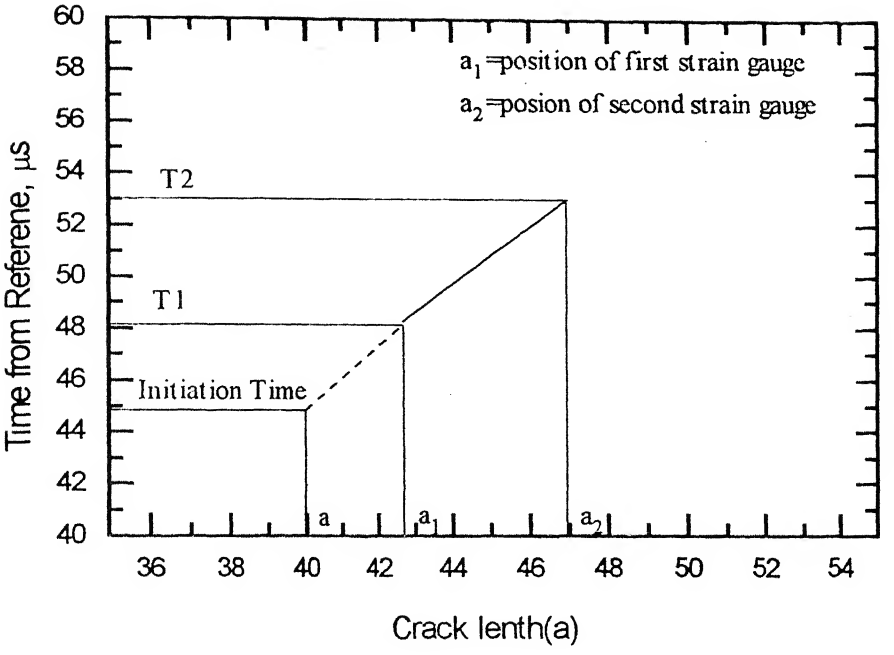

Fig.2.11 Extrapolation of Initiation time

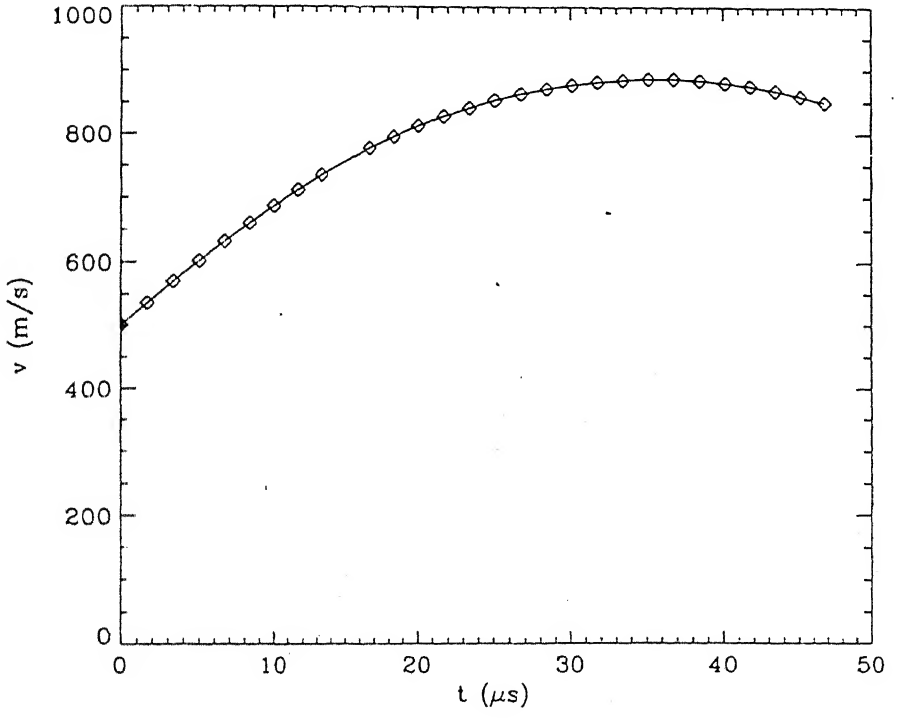

Fig.2.12 Crack tip speed history in a 4×6 inch unidirectional graphite/epoxy Composite plate containing a sharp starter crack.(Ref:Rosakis et at.(1996))

Chapter 3

Numerical Analysis

The experimental measurements gives the profile of the displacement applied at the cantilever end, the time initiation of crack propagation and crack propagation history. These data are used in a finite element code to simulate the dynamic fracture behavior of the DCB specimen. Dynamic fracture phenomena has several important features. As the crack extends and the boundaries of the body change with time, mathematical models are more complex than those of the static case. From experimental point of view, parameters are transient and they have to be measured at high speed accurately.

Keeping all these points in mind, Verma at.al (1995) developed a FE code for finding J-integral variation with time for interlaminar growth crack between two bonded thin plates made of isotropic steel. This FE code is modified by Babu (1998) for evaluating initiation and propagation toughness of unidirectional FRP laminates. Further the program is modified, in the present study, for fabric reinforced polymer composite material.

This chapter briefly describes the finite element formulation, path independent integral, the crack opening scheme and the flow chart of the code.

3.1 Finite Element Formulation

3.1.1 Formulation

The governing system of finite element equations for the linear dynamic response of an elastic body is given in the matrix form as

$$[M]\{\ddot{U}\} + [K]\{U\} = \{R\} \tag{3.1}$$

where [M] and [K] are the mass and stiffness matrices respectively and {R} is the external load vector, and {U}, {Ü} are the displacement and acceleration vectors of the finite element assemblage respectively. Damping forces have been neglected in the formulation. In the above equation global matrices may be obtained as

$$[M] = \Sigma[M]^e$$

$$[K] = \Sigma[K]^e$$

$$[R] = \Sigma[R]^e$$

where element mass, stiffness and traction matrices are given by

$$[M]^e = \int_v \rho\, [N]^T [N]\, dV$$
$$[K]^e = \int_v [B]^T [D] [B]\, dV$$
$$\{R\}^e = \int_s [N] [T]\, dS\,.$$

In these equations [N] is shape function, [B] derivative of shape functions, [D] elastic constitutive relation matrices and [T] traction vector.

3.1.2 Mode Superposition Method

Equation 3.1 can be solved either by time integration or by mode superposition; the former is preferred for simulating wave propagation problem in the specimen. In this integration scheme there are many different methods, which can be classified as "explicit" or "implicit". Relative advantages and disadvantages of each method are given in Bathe (1990). Verma at al. (1997) developed a FE code for 2-D finite element discretization in space analysis using the Newmark integration method for the time variable (Bathe, 1990). Since width of the specimen is large in comparison to the thickness of the specimen, this is a plane strain problem.

Specimen front face that is bonded to a rigid block (Fig.1.1) remains straight. It is therefore expected that effect of this portion on J-integral is negligible in fact,

Verma (1995) simulated FE analysis in the entire specimen and showed that the effect was insignificant. Later, Mallikharjuna (1998) also verified this. Consequently, only cantilever plate of the specimen is analysed to avoid unnecessary computations.

3.1.3 J-Integral

Nishioka and Atluri (1983) studied the use of path independent J-integral using finite element method for dynamic crack propagation. In this present work, $\hat{J}_I$ given by Kishimoto, Aoki and Sakata (1980) is used which is defined as (Fig. 3.1)

$$J_I = \lim_{\varepsilon \to 0} \int_{\Gamma_c^- + \Gamma + \Gamma_c^+} [Wn_i - T_i u_{i,1}] ds + \int_{V-V_\varepsilon} \rho u_i u_{i,1} dV.$$

where W is the strain energy density, u_i is the displacement, n_i is the direction cosine of the unit outward normal, T_i is the traction, Γ_c^-, Γ, Γ_c^+ are defined paths and V, V_ε are volumes.

J-integral is independent of the choice of the path Γ (Fig. 3.1) under steady state crack growth conditions. In many cases, though these conditions are obviously not met fully, the path independence of J –integral can still be established within certain allowable errors. To minimize errors, the integral is evaluated over a path far away from the crack tip. Then the analysis is relatively insensitive to the finer details of the crack tip region. The path is held stationary as crack tip extends in a self-similar manner.

3.1.4 Constitutive Relations for Composites

From the mechanics point of view fibre composites are among the class of material called orthotropic materials. Generalized Hook's Law for two-dimensional orthotropic laminate is given by (Agarwal, B.D., 1990)

$$\sigma_i = Q_{ij}\, \varepsilon_j$$

where σ_I are the stress components, Q_{ij} is the stiffness matrix, ε_j are the engineering strain components and i.j = 1,2,....,6.

$$\begin{Bmatrix}\sigma_1\\ \sigma_2\\ \tau_{12}\end{Bmatrix}=\begin{bmatrix}Q_{11} & Q_{12} & 0\\ Q_{12} & Q_{22} & 0\\ 0 & 0 & Q_{66}\end{bmatrix}\begin{Bmatrix}\varepsilon_1\\ \varepsilon_2\\ \gamma_{12}\end{Bmatrix}$$

Constitutive relations for polymer composites are expressed for three-dimensional cases with nine independent elastic constants. However, only four elastic constants are needed for two-dimensional orthotropy (Agarwal, B.D., 1990).

Consider an orthotropic lamina (Fig. 3.2) with the reference axes coinciding with axes of symmetry and designed as the longitudinal direction, L and the transverse direction, T. Engineering constants for this lamina are elastic module in longitudinal and transverse directions, E_L and E_T respectively, the shearing modulus associated with the axes of symmetry, G_{LT}, the major Poisson ration ν_{LT}, giving transverse strain caused by a longitudinal stress, and the minor Poisson ν_{TL}, giving the longitudinal strain resulting from a transverse stress.

$$Q_{22}=\frac{E_T}{1-\nu_{LT}\nu_{TL}}$$

$$Q_{22}=\frac{\nu_{TL}E_L}{1-\nu_{LT}\nu_{TL}}=\frac{\nu_{LT}E_T}{1-\nu_{LT}\nu_{TL}}$$

Relation between the five engineering constants and four independent elastic modulus are expressed as follows (Agarwal, B.D., 1990).

$$Q_{11}=\frac{E_L}{1-\upsilon_{LT}\upsilon_{TL}}$$

$$Q_{16}=G_{LT}$$

In these equations, a relationship exist between four of the five constants

$$\frac{\nu_{LT}}{E_L}=\frac{\nu_{TL}}{E_T}.$$

In the present study fibre glass fabric is used as reinforcing material (Fig. 3.3). Since number of yarns per cm in each principal direction is approximately same, one can assume

$$E_L = E_T$$

$$\nu_{LT} = \nu_{TL}$$

Modulus of elasticity and Poisson ratio are directly obtained from tensile tests conducted in Experimental Stress Analysis Laboratory and ACMS of IIT Kanpur. The G_{LT} is obtained from expression (Agarwal, B.D., 1990).

$$\frac{1}{E_{45}} = \frac{1}{4}\left\{\frac{1}{E_L} + \frac{1}{E_T} + \frac{1}{G_{LT}} - \frac{2\nu_{LT}}{E_T}\right\}$$

As elastic modulus in longitudinal and transfers (E_L & E_T) are equal, therefore G_{LT} is given by

$$\frac{1}{E_{45}} = \frac{1}{4}\left\{\frac{2(1-\nu_{LT})}{E_L} + \frac{1}{G_{LT}}\right\}$$

where E_{45} is elastic modulus for a 45° ply laminate.

Experimental values for the fibre glass fabric composite obtained from experiments are as follows (Appendix A):

$$E_L = E_T = 26.00 \text{ GPa}$$

$$\nu_{LT} = \nu_{TL} = 0.21$$

$$G_{LT} = 3.5 \text{ Gpa}.$$

These values are used in all experiments of the present study.

3.2 The FE Code

3.2.1 Flow Chart

The flow chart of the finite element code developed by Verma et.al (1995) is shown in Fig. 3.3. This programs evaluates J-integral with time for specified input of

material properties (engineering constants), crack propagation history, cantilever end deflection, mesh size, time step and the path of J-integral.

3.2.2 Mesh Size

Seron et.al (1990) showed that higher order elements are not required in the analysis of determining J-integral of dynamic problems. Four noded isoparametric elements are used in the present study. To take into the consideration of bending as well, fine mesh is used. To avoid nonuniformity of mass distribution, which leads to reflection of waves, uniform mesh is used through out the specimen. In the present work 0.1hx0.1125h mm mesh is used where h is thickness of cantilever (Fig.3.4).

3.2.3 Crack Opening Scheme

In order to simulate the crack propagation, a gradual nodal release method was used. The actual crack (Fig. 3.5) is located at C between the nodes B, D and the holding force F at node B is gradually reduced as the crack is advanced to point D. In most of the studies reported in literature the force F reduces to zero when the crack reaches the next node D. However, it was found that at very high crack speeds, close to the Rayleigh wave speeds, a better model is required. For obtaining a gradual and smooth opening of crack, Verma et.al (1995) employed an alternative method. The holding back force F at the node B is linearly decreased to zero when the crack reaches the end of the next element, point E, in Fig.3.5. When the crack tip is in between nodes B and D, the holding force F_B at node B given by

$$\frac{F_B}{F_{BC}} = \left[1 - \frac{b_1}{2d}\right]$$

where F_{BC} is the force at node B when the crack tip was at point B, b_1 is the crack extension beyond node B and d is the element length as shown in Fig. 3.5. When crack propagates beyond the node D to point D_1, the holding force at node B is given by

$$\frac{F_B}{F_{BC}} = \left[1 - \frac{d + b_2}{2d}\right]$$

3.2.4 Time Step

Time step influences the analysis if not chosen properly. The choice of time step (Δt) for time integration is important for an accurate solution. An optimum choice of time step is $\Delta t = d/c$, where d is smallest mesh size and c is the fastest wave velocity (Verma et.al., 1995)

It is observed that upto initiation time, J-integral does not vary much on time step. Fig. 3.7 shows the variation of J-integral for three different time steps, 0.2, 0.05, 0.02 μs. It is observed that upto initiation time, J-integral does not vary much on time step. Fig.3.7 shows that amplitude of oscillations in propagating phase varies with time step. The amplitude is more for higher value of time step. Therefore a coarse time step of 0.2 μs is selected prior to the growth of the crack to reduce number of iteration and fine time of step of 0.02 μs is used after the crack growth is initiated. By choosing two time steps, overall iterations number used for running program are reduced reasonably

3.2.5 Initiation and Propagation Toughness

Impact energy, imparted at the end of the rear cantilever, propagates within the specimen and reaches the crack tip. J-integral starts building up to initiation time and the crack does not advance (stationary crack). Fig.3.8 shows the variation of J-integral with time for stationary crack. J-integral builds up sharply, attain a peak and then decrease to a low value. However, a stage reaches when the crack tip cannot withstand the loading at the crack tip and the crack starts propagating. The value of J-integral at which the crack starts moving is known as initiation toughness ($\hat{J}_{ini}$). As soon as the crack starts propagating J is reduced drastically to a much lower value and after some time, it stabilizes (Fig. 3.9). This stabilized value of the J-integral is treated as the propagation toughness ($\hat{J}_{prop}$).

3.3 Closure

The aim of this Chapter was to describe the finite element formulation, the path independent integral, the crack opening scheme, the initiation and propagation toughness and the summary of the program.

Initiation and propagation toughness are determined through the technique that combines experimental results with numerical simulation, discussed and tabulated at length in chapter 4.

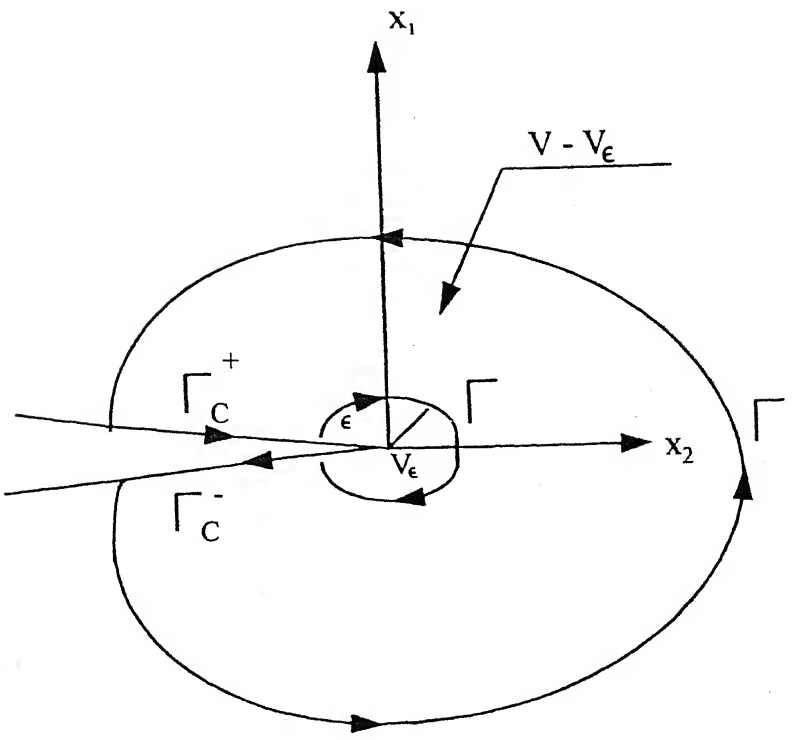

Fig.3.1 Contour for J-integral

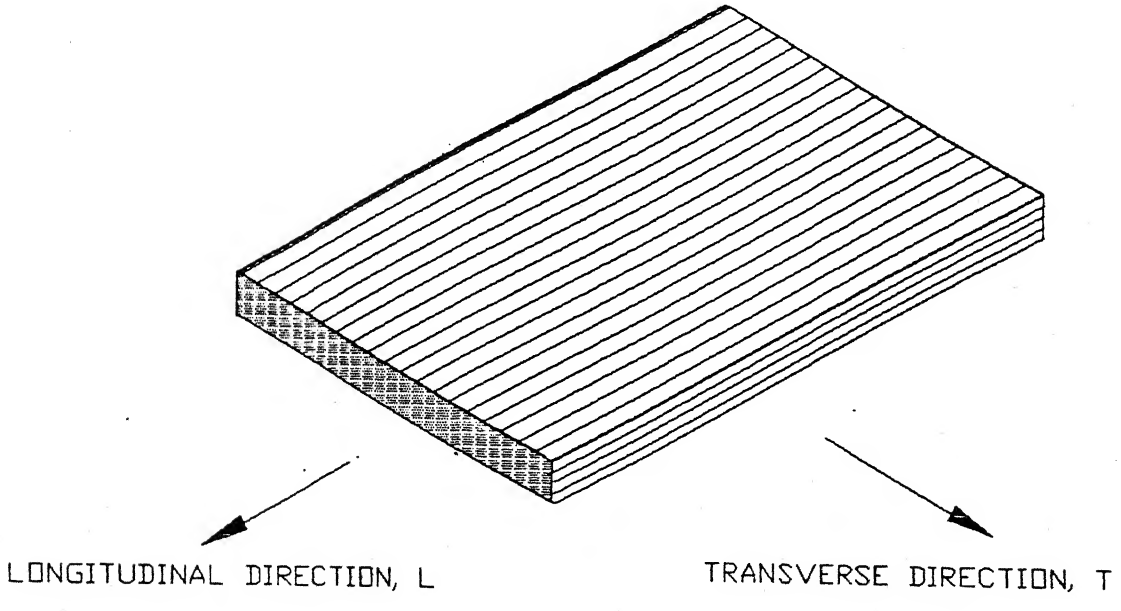

Fig.3.2 Principal material axes for orthographic composite lamina

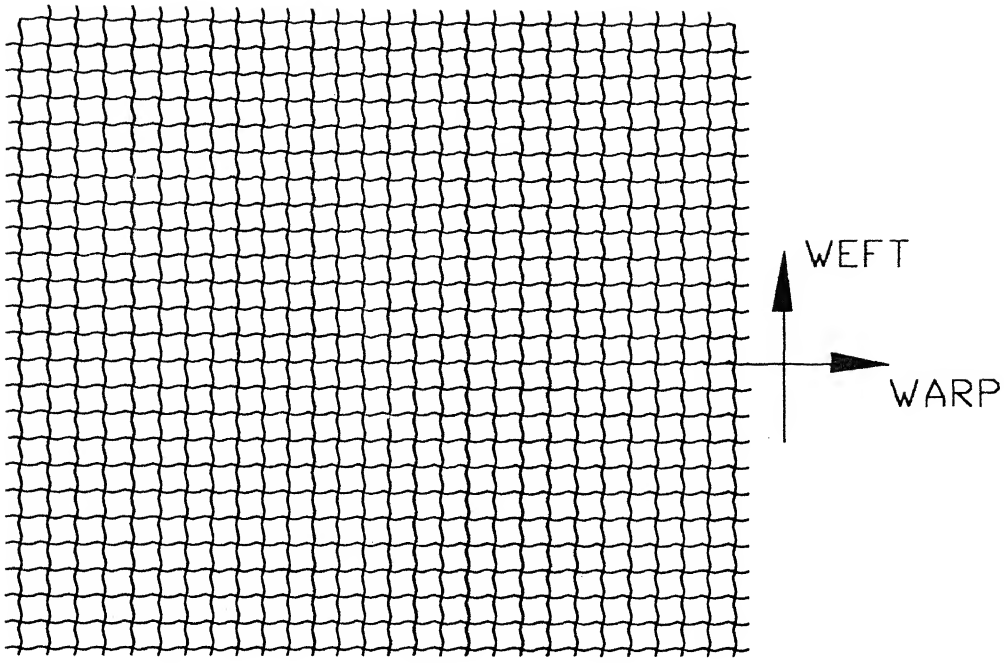

No of Yarn per inch WARP = 40
WEFT= 36

Area Density = 146 gm/m^2

Fig. 3.3 Glass fabric

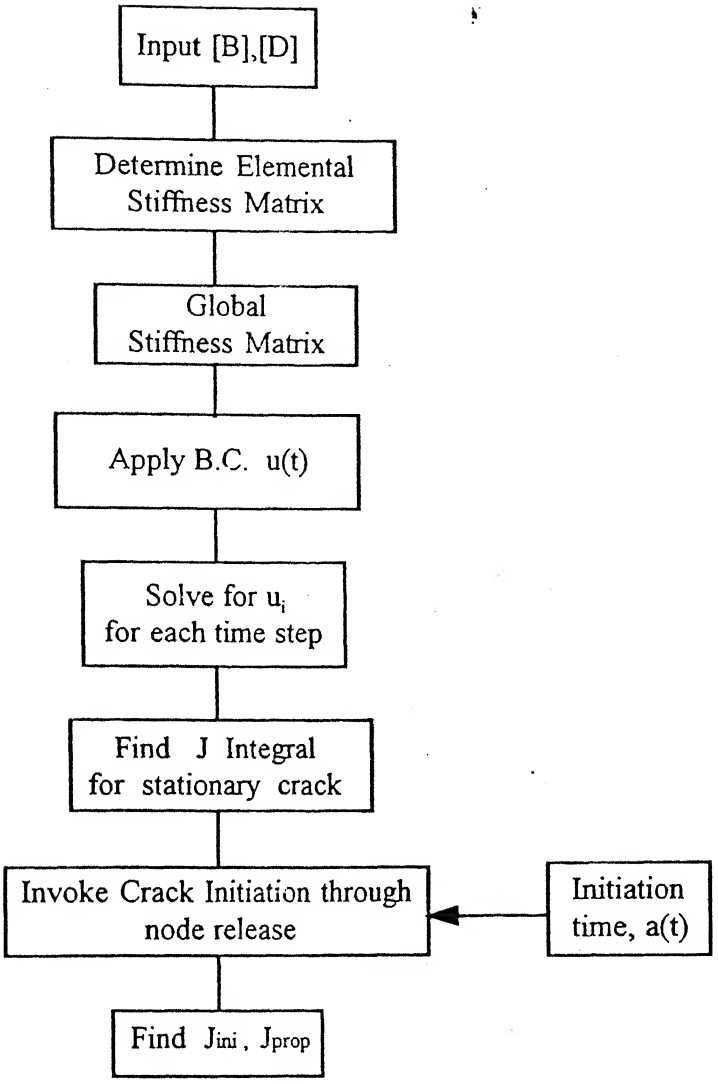

Fig. 3.4 Flow chart of the FE code

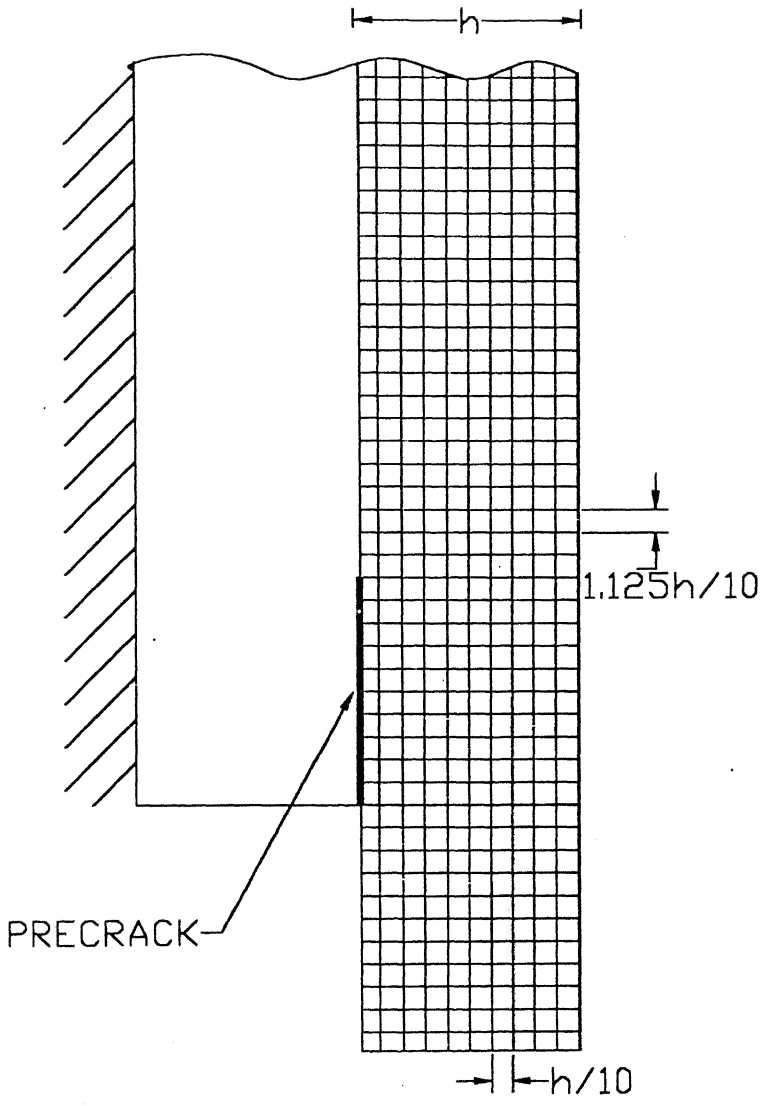

Fig.3.5 Mesh generated for the simulation

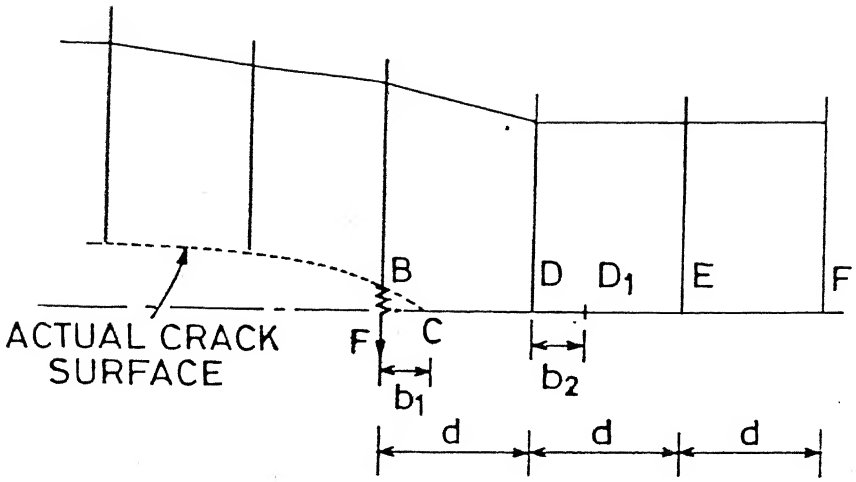

Fig.3.6 Crack opening scheme

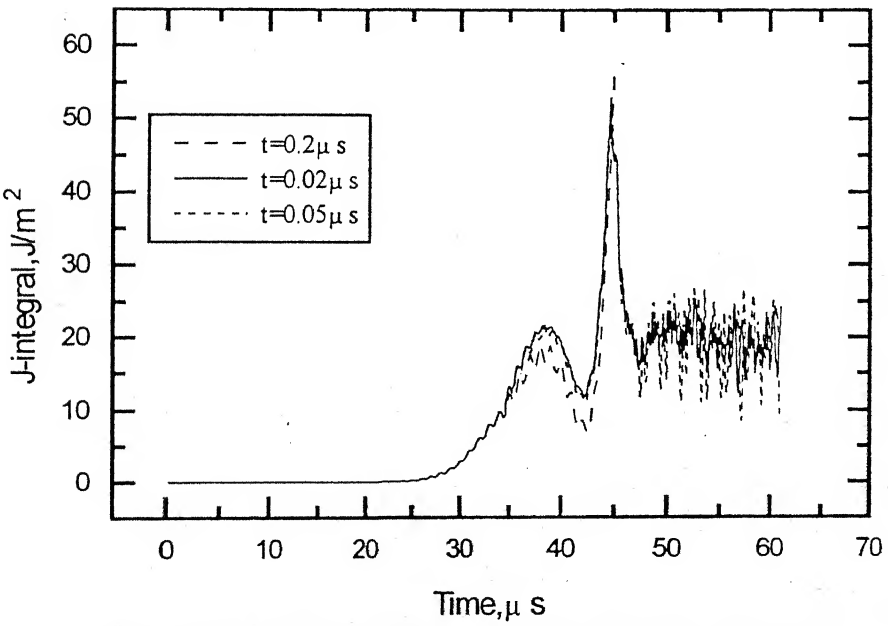

Fig.3.7 Variation of J-integral for different time steps

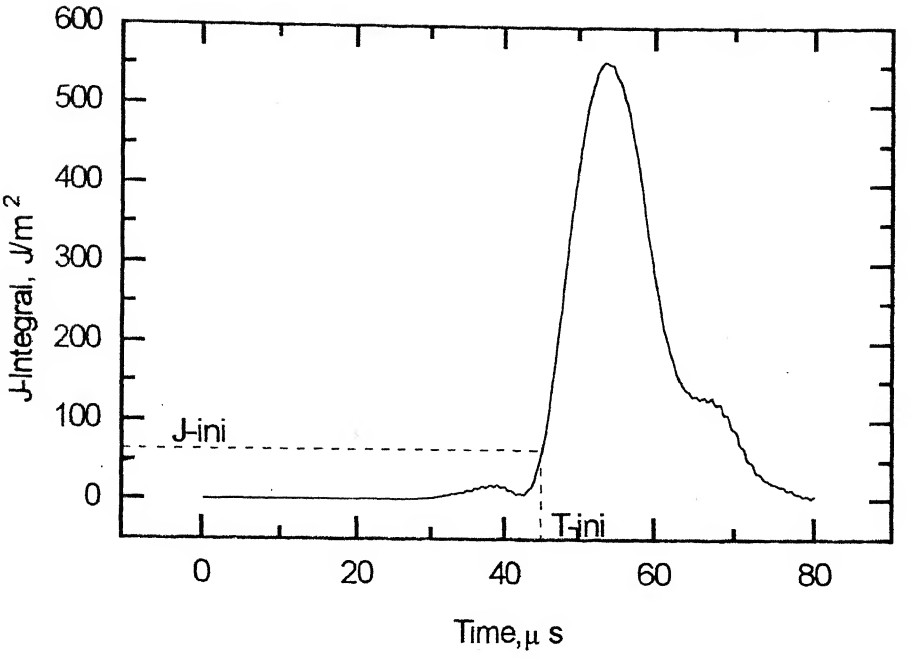

Fig.3.8 A typical variation of J-integral for stationary crack

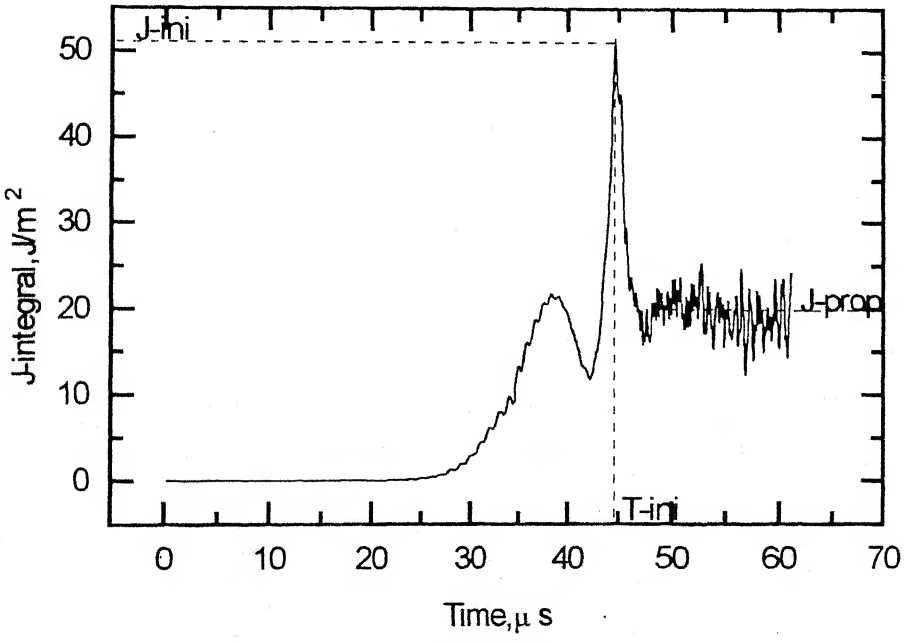

Fig.3.9 A Typical variation of J-integral for propagating crack

Chapter 4

Results and Discussions

4.1 Introduction

Experiments are conducted to determine the deflection of the cantilever end, crack velocity and initiation time. These are the inputs along with the material properties to the FE code as discussed in Chapter 3. The numerical simulation determines variation of J-integral with time for stationary and propagating crack. The chapter briefly describes the results of initiation toughness, propagation toughness and their comparison with the dynamic toughness of interlaminar crack investigated by others.

4.2 Details Procedure of Analysis

In this section, a detail analysis of Experiment S-1 is discussed. When the specimen is impacted by the load bar, a part of the energy is transmitted to the specimen. This energy deflects the cantilever. The remaining energy of the load bar returns back as a compressive pulse. Strain gauges bonded on the load bar monitor the stress pulses. The response of the load bar strain gauges and the velocity strain gauges bonded on the side face of cantilever as recorded in the oscilloscope are shown in Fig. 4.1(a). A zoomed view in horizontal direction of the oscilloscope records is shown in Fig 4.1(b).

The velocity of the load bar end v_2 is evaluated by one dimensional wave propagation theory as discussed in Sec.2.2.2 given by the formula.

$$v_2(t) = \frac{\sigma_3 - \sigma_1}{\rho c}$$

where σ_1 = compressive incident pulse

σ_3 = tensile reflected pulse

ρ = density of material

c = longitudinal wave velocity

The variation of velocity with time is shown in Fig. 4.2. The end displacement u_2 of the load bar is obtained by integrating the velocity history (Sec.2.2.2) using

$$u_2(t) = \int_0^t \left(\frac{\sigma_3 - \sigma_1}{\rho c} \right) dt.$$

Displacement of the load-bar-end is equal to the deflection of the cantilever end because load bar is screwed to the specimen. The variation of deflection of the cantilever end with time is shown in Fig. 4.3. The loading of cantilever starts at the time corresponding to midpoint of the head of the incident pulse and head of the reflected pulse. This is denoted as REFERENCE in the Fig. 4.1(b).

When the crack tip passes the velocity strain gauges, the singular strain field gives a strain peak. The magnified view of the response of the velocity strain gauges is shown in Fig. 4.4. The time difference between the peaks of strains and the distance between location of the gauges give average velocity between strain gauges. The crack length as a function of time is plotted in Fig.4.5. The initiation time is obtained by extrapolating the crack velocity upto precrack length.

The experimental data (the deflection of cantilever end, crack velocity and initiation time) are used as input to the FE code as discussed in Chapter 3. The variation of J-integral in stationary and propagating phases are shown in Figs.4.6 and 4.7. The rise of the interlaminar toughness until the initiation is also obtained experimentally by Lambros John & Rosakis A.J. (1997). They investigated the variation of dynamic fracture toughness upto the initiation time on unidirectional Graphite/epoxy composite plates with edge notched under the impact loading (Fig. 4.8).

Once the FE code is executed upto the initiation time, the crack propagation module is called (Verma, 1995). The location of the crack tip in each iteration is known through the experiment; an appropriate factor, as discussed in Sec.3.2.3, is applied to the holding back force for modeling crack propagation. As discussed in Sec. 3.2.4 a time step of 0.02 μs is chosen in the propagation phase. Using the

boundary conditions and the crack propagation data, the dynamic FE analysis determines the stress/strain field in the specimen in successive time steps. Then the variation of J-integral with time is obtained as shown in Fig. 4.7.

In the beginning the crack remain stationary upto the initiation time and J-integral increases. At the initiation time, the crack tip starts growing under known dynamic displacement boundary conditions. The J –integral suddenly decreases at the initiation time and stabilizes after some time; the stabilized value is treated as propagation toughness (J_{prop}).

The oscillatory behavior of J-integral is due to several reasons:

- The free surfaces of specimen are very close to the crack tip. Some stress waves, emanating from the crack tip, return to the crack tip. The superposition of these waves and their effect on J-integral will provide ripples.
- In the finite element modeling the crack tip is moved from one point to another point in discrete steps by linearly decreasing the holding back force. Thus, the FE code may not be simulating the crack propagation behavior very accurately. The nodal release mechanisms can further be modified to have smooth release of the crack to rule out its effect on the oscillatory nature of J_{prop}.

4.3 Compilation of Results for Shorter Crack Length

In this section, the experimental records, their subsequent analysis and the results from the finite element code are presented. Experimental measurements and subsequent finite element analysis for each experiment is shown at the end of the chapter.

Two types of specimen are used in the present study. The first set employs specimen of a short precrack (39.5 to 42.2 mm) and cantilever thickness in the range of 3.5 to 4.2 mm. The second set uses specimen with precrack of longer length (49.6 to 51.0 mm); the range of cantilever thickness is same as that of the first set.

4.3.1 Details of the Crack Lengths and Locations of Strain Gauges

The details of crack length and strain gauge locations for different experiment are tabulated in Table 4.1. The thickness and width of the cantilever end are used in mesh generation in the FE code (Sec. 3.2.2). Taking the axes of the load bar as reference, the crack length and locations of velocity strain gauges are measured accurately with a travelling microscope. The distance between the velocity strain gauges is maintained between 3.0 and 4.7 mm. Also, the first velocity strain gauge is bonded very close to the crack tip, about 2 mm away.

Table 4.1 Details of Specimen and Locations of Strain Gauges for Short Crack.

Expt No.	Specimen Thickness (mm)	Thickness of Cantilever (mm)	Width of Specimen (mm)	Crack length (mm)	Strain gauges locations from reference			
					SG1 (mm)	SG2 (mm)	Distance between two gauges (mm)	SG1 from crack tip (mm)
S-1	7.6	3.8	24.8	40.0	42.7	47.0	4.3	2.7
S-2	7.5	3.8	25.6	40.1	42.1	45.8	3.7	2.0
S-3	7.6	3.8	25.1	40.3	42.4	46.5	4.1	2.1
S-4	8.0	4.2	24.5	39.5	41.7	45.8	4.1	2.2
S-5	7.7	3.9	25.0	40.6	42.6	47.1	4.5	2.0
S-6	7.8	3.8	25.1	40.0	42.8	47.5	4.7	2.7
S-7	7.8	4.0	24.7	40.4	42.2	45.9	3.7	1.8
S-8	7.5	3.7	25.5	40.0	42.0	45.5	3.5	2.0
S-9	7.3	3.8	25.0	40.0	41.9	45.4	3.5	1.9
S-10	6.0	3.5	25.0	40.2	42.6	45.9	3.3	2.4
S-11	7.0	3.5	25.3	40.1	42.1	45.6	3.5	2.0
S-12	7.0	3.5	25.0	40.3	42.2	45.3	3.0	1.9
S-13	7.7	3.5	25.8	42.2	44.1	47.1	3.0	1.9

4.3.2 Crack Velocity and Initiation Time

Table 4.2 presents the records of the velocity strain gauges responses. The responses of the velocity strain gauges lead to the determination of crack velocity. When the crack tip passes near a strain gauge the singular strain field gives a strain

peak that is recorded in the oscilloscope (Fig. 4.4). The crack velocity is determined from the time difference of the peaks and the distance between the two strain gauges. The velocity of crack ranges between 660 to 1850 m/s. The initiation time is obtained by extrapolating the crack velocity upto the precrack length. The initiation time for the first set of experiment with short precrack length (≈ 40 mm) varies between 44.9 and 54.9 μs.

Table-4.2 Crack Velocity and Initiation Time for Short Crack.

Expt. No.	Peak Responses of Strain Gauges			Crack Velocity	Initiation Time
	SG1 T_1 (μs)	SG2 T_2 (μs)	Time diff. $\Delta T = T_1 - T_2$, (μs)	$\dot{a} = \Delta_2/\Delta T$ (m/s)	$T_{ini} = T_1 - \Delta_1/\dot{a}$ (μs)
S-1	48.0	53.0	5.0	860	44.86
S-2	56.0	58.0	2.0	1850	54.92
S-3	47.5	50.5	3.0	1367	45.97
S-4	50.5	53.0	2.5	1640	49.16
S-5	54.0	57.5	3.5	1286	52.44
S-6	54.0	58.0	4.0	1175	51.66
S-7	55.5	58.5	3.0	1233	54.04
S-8	52.5	55.5	3.0	1167	50.71
S-9	49.5	53.5	4.0	875	47.33
S-10	54.5	59.5	5.0	660	50.86
S-11	51.5	55.5	4.0	875	49.20
S-12	52.5	56.5	4.0	750	49.97
S-13	52.5	57.0	4.5	667	49.65

4.3.3 Interlaminar Fracture Toughness

Experimental data of the Expt. S-1 as discussed in Sec. 4.2 are summarized as follows :

Voltage drop of incident pulse (Fig.4.1b) = 10 mV

Stress level in load bar corresponding to voltage drop = 259.84 MPa

Duration of incident pulse = 125 μs

Velocity of the load bar end (Fig.4.2) = 12.5 m/s

(between 40 μs and 120 μs)

Maximum deflection of cantilever end (Fig.4.3) = 1.4 mm

Initiation time (Fig.4.5) = 44.86 μs

Crack tip velocity (Fig.4.5) = 860 m/s

Experimental data along with material properties (F_L, E_T, G_{LT}, ν_{LT}, ρ) are used to evaluate J-integral (Appendix 3). Variation of the J-integral for the stationary crack Expt. S-1 is shown in Figs. 4.6. The crack propagation is invoked after the initiation time (44.86 μs) and then the J-Integral is shown in Figs. 4.7(a) and 4.7(b). J-Integral for initiation and propagation is directly obtained from the figures; which are 82 and 18 J/m^2 respectively. Oscilloscope records, variation of velocity of load bar end, variation of deflection of cantilever end and variation of J-integral for stationary – propagating phase for other experiments are presented in Appendix 2. Zoomed views of propagating phase for all experiments are shown in Figs. 4.9 and 4.10. Crack tip velocity, initiation and propagation toughness are presented in Table 4.3. J-initiation varies from 52 to 536 J/m^2 and propagation toughness 6.0 to 18 J/m^2.

Table 4.3 J – initiation and J-propagation Toughness for Short Crack.

Expt. No.	Crack Velocity å (m/s)	Initiation Toughness J_{ini} (J/m^2)	Propagation Toughness J_{prop} (J/m^2)
S-1	860	52	18
S-2	1850	118	7.5
S-3	1367	116.	9
S-4	1640	321	7.5
S-5	1286	275	6.0
S-6	1175	418	7.5
S-7	1233	418	11
S-8	1167	384	10
S-9	875	466	10
S-10	660	414	15
S-11	875	536	15
S-12	750	535	20
S-13	667	210	8

4.4 Compilation of Results for Longer Crack Length

The details of crack length and location of strain gauges for longer crack are tabulated in Table 4.4. The records of velocity strain gauges are tabulated in Table 4.5 and J_{ini} and J_{prop} are presented in Table 4.6. J_{ini} and J_{prop} were found 62 to 400 J/m^2 and 3.0 to 20 J/m^2 for crack velocity ranging 633 to 2150 m/s. Zoomed views of propagating phases are shown in Fig.4.11 and 4.12. The oscilloscope records, variation of velocity of load bar end and deflection of cantilever end; variation of J-integral for stationary and propagating phases are presented in Appendix 2.

Table 4.4 Details of Specimen and Locations of Strain Gauges for Long Crack.

Expt No.	Specimen Thickness (mm)	Thickness of Cantilever (mm)	Width of Specimen (mm)	Crack length (mm)	Strain gauges locations from reference			
					SG1 (mm)	SG2 (mm)	Distance between two gauges (mm)	SG1 from crack tip (mm)
L-1	8.5	4.2	25.3	50.2	52.4	56.7	4.3	2.2
L-2	7.8	4.0	25.0	49.8	52.0	56.2	4.2	2.2
L-3	7.8	3.8	25.2	49.6	52.0	56.1	4.1	2.1
L-4	8.0	3.9	25.0	50.6	53.0	56.9	3.9	2.4
L-5	7.8	4.0	25.3	50.1	52.4	56.9	4.5	2.3
L-6	8.3	4.3	25.4	50.6	52.8	56.6	3.6	2.2
L-7	8.4	4.2	25.4	50.2	52.4	56.6	4.2	2.2
L-8	7.9	4.1	25.3	51.0	53.3	57.1	3.8	2.3
L-9	8.4	3.7	20.9	49.7	52.2	56.2	4.0	2.5
L-10	7.4	3.8	24.9	50.2	52.1	56.6	4.5	1.9
L-11	7.0	3.6	24.9	50.1	51.8	56.0	4.2	1.7
L-12	7.1	3.8	25.1	50.8	52.4	56.5	4.1	1.6

Table-4.5 Crack Velocity and Initiation Time for Long Crack.

Expt. No.	Peak Responses of Strain Gauges			Crack Velocity $\dot{a} = \Delta_2/\Delta T$ (m/s)	Initiation Time $T_{ini} = T_1 - \Delta_1/\dot{a}$ (μs)
	SG1 T_1 (μs)	SG2 T_2 (μs)	Time diff. $\Delta T = T_1 - T_2$, (μs)		
L-1	61.5	63.5	2.0	2150	60.48
L-2	58.5	62.5	4.0	1050	56.40
L-3	62.0	64.0	2.0	2050	60.98
L-4	61.5	65.5	4.0	975	59.04
L-5	58.5	62.5	4.0	1125	56.46
L-6	60.0	63.0	3.0	1267	58.26
L-7	61.0	64.0	3.0	1400	59.43
L-8	69.5	75.5	6.0	633	65.87
L-9	64.0	66.0	2.0	2000	62.75
L-10	61.5	65.5	4.0	1125	59.81
L-11	59.0	62.0	3.0	1400	57.79
L-12	68.0	70.5	2.5	1640	67.02

Table 4.6 J – initiation and J-propagation Toughness for Long Crack.

Expt. No.	Crack Velocity $\dot{a}$ (m/s)	Initiation Toughness J_{ini} (J/m^2)	Propagation Toughness J_{prop} (J/m^2)
L-1	2150	253	10
L-2	1050	125	12.5
L-3	2050	400	10
L-4	975	69	10
L-5	1125	72	15
L-6	1267	301	10
L-7	1400	242	12
L-8	633	386	20
L-9	2000	393	10
L-10	1125	38	7
L-11	1400	72	3
L-12	1640	343	15

4.5 Discussion

4.5.1 Initiation toughness of short crack

The initiation toughness of 13 experiments with short crack is shown in Fig. 4.13 with a best-fit linear curve. It shows that the initiation toughness decreases with crack tip velocity. The best-fit curve shows that J_{ini} at crack velocity of 660 m/s is 410 J/m^2 which decreases to 200 J/m^2 at crack velocity of 1850 m/s.

Results of other investigators on glass fabric reinforced epoxy laminates donot exist to the best knowledge of this investigator and therefore direct comparison of initiation toughness under impact conditions cannot be made. However, Ramakhrishna (1997), Babu & Mallikharjuna (1998) and Pandey (2000) have conducted similar experiments on glass fibre unidirectional laminates.

Ramakhrishna used specimen whose dimensions and precrack length were almost same as those of this study. Initiation toughness reported by him was varying between 91 and 230 J/m^2. Comparison of the initiation toughness with that of the present study is shown in Fig. 4.14.

While comparing these two sets of results, following differences are worth noting:

- Ramakhrishna work was on unidirectional glass fibre laminates whereas this study is made on glass fabric reinforced polymer composites.
- Ramakhrishna's laminates were prepared from prepregs, which were cured at usual temperature of 120°C. The quasistatic toughness of these laminates reported by him is 415 J/m^2. This toughness is of the same order of laminates prepared by prepregs of well-known international suppliers. The prepregs used in the present study were made through a modified technique in which prepregs are cured with a cold technology using curing temperature substantially smaller than 120°C. Consequently, the plies are bonded better with each other when a laminate is made. The quasistatic toughness of this laminate is experimentally determined to be 924 J/m^2 (Appendix 3).

- Ramakhrishna sharpened the tip of interlaminar crack of his specimen by extending the precrack with a wedged chisel before conducting the experiments. In ideal conditions, the crack front should remain normal to the axis of the specimen. However, some inclination from the ideal case is always present but efforts are made to keep the inclination minimum. It was realized, after conducting many experiments that in a specimen with a sharpened crack tip with the chisel, the probability of low inclination of the crack front is poor and therefore the success rate was low (<25%). Specimens used for the present study are as cast introduced by a thin sheet of Teflon (0.12 mm thickness). Therefore, the probability that crack front is normal to specimen axis is high. This leads to a high success rate of repeatability of experiments better than 85%.

As expected due to low quasistatic toughness and reasons just mentioned above, initiation toughness reported by Ramakhrishna is small in comparison of the results obtained in the present study.

The work of Babu & Mallikharjuna (1998) was similar to the work of Ramakhrishna. However, they used laminates of unidirectional glass fibre reinforced epoxy which were prepared from prepregs produced through the cold technology. The quasistatic interlaminar toughness was 1055 J/m^2, which was much higher than quasistatic toughness (415 J/m^2) of laminates used by Ramakrishna. Their specimen dimensions and precrack length were same as those of the present work. The specimens used by them were sharpened with a sharp nose chisel. Therefore, their success rate was also poor (<25%).

Further, they used velocity strain gauges of smaller length (0.2 mm gauge length). Although this length of the gauges was found appropriate for experiments with steel (Verma, 1995) but these strain gauges are not suitable for heterogeneous material like polymer composites. In the present work larger strain gauge with length of 2 mm and width 0.9 mm and specially designed for composites are used. They are purchased from Tokyo Sokki Kenkyijo Co. Ltd., Japan.

Figure 4.15 shows the comparison of initiation toughness reported by Babu and Mallikharjuna and that of the present work. Following observations are worth noting:

- Babu & Mallikharjuna conducted experiments at relatively low crack tip velocities in comparison of the present study. Their crack tip velocity range is from 472 to 933 m/s; experiments of the present work are conducted in the range of 667 to 1850 m/s. Average initiation toughness of the Babu and Mallikharjuna is 343 J/m^2 and the present study is 369 J/m^2 for the same range of crack velocity of 472 to 933 m/s. Since the results match well, crack sharpening does not seem to make a difference. Also the dynamic toughness of the unidirectional laminates and the fabric based laminates is not significantly different. The as cast crack tip certainly improves the reliability of success.
- Quasistatic toughness reported by them is 1055 J/m^2 is also almost same as determined in the present work, which is 924 J/m^2.

Pandey (2000) also worked on unidirectional glass fibre composites laminates made from prepregs manufacturer by the cold technology. He also used specimen as cast precrack introduced by a thin sheet of Teflon (0.12 mm thickness). Velocity strain gauges of 2 mm length and 0.9 mm width and specially designed for composites are used to get strain peaks in the specimen. Therefore, Pandey used almost same procedure for specimen preparation and velocity strain gauges that adopted in the present work. His results are worth comparable to the present study although his specimen is made of unidirectional glass fiber reinforced polymers.

The comparison of results reported by him and the present work for initiation toughness of short crack is shown in Fig. 4.16. In both cases, J-initiation decreases with interlaminar crack velocity and the results are similar although the laminate material was different.

4.5.2 J- Propagation of short crack

The propagation toughness of 13 experiments with short crack is shown in Fig. 4.17 with a best-fit linear curve. It shows that the propagation toughness decreases with crack tip velocity. From the fit curve J_{prop} at crack velocity of 660 m/s is 14.5 J/m^2 which decreases to 6 J/m^2 at crack velocity of 1850 m/s.

As stated in the previous subsection, the results of other investigators on glass fabric reinforced epoxy laminates are not available therefore direct comparison of propagation toughness can not be made. However, results reported by Babu & Mallikharjuna (1998) and Pandey (2000) for unidirectional glass fibre polymer laminates are used to compare the results of the present study.

Babu and Mallikharjuna (1998) investigated with specimen geometry and precrack length same as of the present work. The average value of the results reported by Babu and Mallikharjuna is 65 J/m^2 for crack velocity between from 422 to 933 m/s. Comparison of propagation toughness reported by Babu and Mallikharjuna with that of the present work is shown in Fig. 4.18. The J_{prop} of the study is substantially lower than J_{prop} Babu & Mallikharjuna. The nature of interface between two like plies of unidirectional laminate is quite different from the interface between two plies of fabric reinforced laminate. In the unidirectional case, fibers of adjacent like plies tend to dig into each other. On the other hand, fibers of a fabric ply are well constrained. The lower J_{prop} of fabric laminate is probably due to this difference.

Further, Pandey (2000) did work on unidirectional glass fiber composites for same geometry and precrack length. His specimens are also prepared through the cold technology. Comparison of propagation toughness reported by him and the present work shown in Fig. 4.19. It is worth noting that Pandey reported low values of propagation toughness with average of 20.5 J/m^2 whereas Babu and mallikharjuna reported 65 J/m^2. The J_{prop} of Panday's investigation on unidirectional laminate is slightly higher than J_{prop} of this study on fabric laminates.

4.5.3 Initiation and propagation toughness of long crack

The initiation toughness of 12 experiments with long crack is shown in Fig. 4.20. Unlike in the case of short crack where J_{ini} decreases with the crack velocity, J_{ini} of long crack does not show any trend. The average value of the initiation toughness of long crack specimen is found 224.5 J/m^2. The average value of the initiation toughness of short crack is 328 J/m^2, which is higher than that of long crack. Because of the high scatter, the difference is not significant.

The propagation toughness of these 12 experiments is shown fig. 4.21 with that of short crack. The values of J_{prop} and their variation with crack velocity are similar to the J_{prop} of short crack; that is, J_{prop} decreases with crack velocity.

4.6 Closure

In this Chapter, the initiation toughness of 13 experiments with short crack and 12 experiments of long crack was tabulated and compared with other investigators. These 25 experiments are conducted on fabric glass reinforced epoxy laminates. Specimens used for the present study are as cast introduced by a thin sheet of Teflon. Also velocity strain guages specially made for composites are used to get strain peaks.

The variation of J_{ini} of short crack decreases with crack velocity whereas it does not show any trend for long crack. However, the variation of J_{prop} decreases with crack velocity for both short and long crack lengths. The effect of crack length variation on J_{ini} and J_{prop} is not significant.

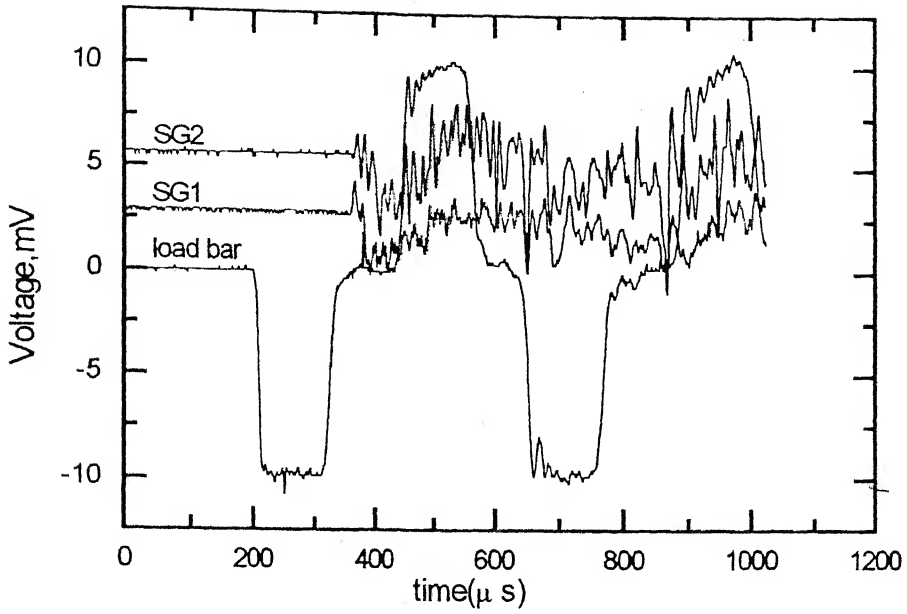

Fig:4.1(a) Oscilloscope records of Expt. S-1

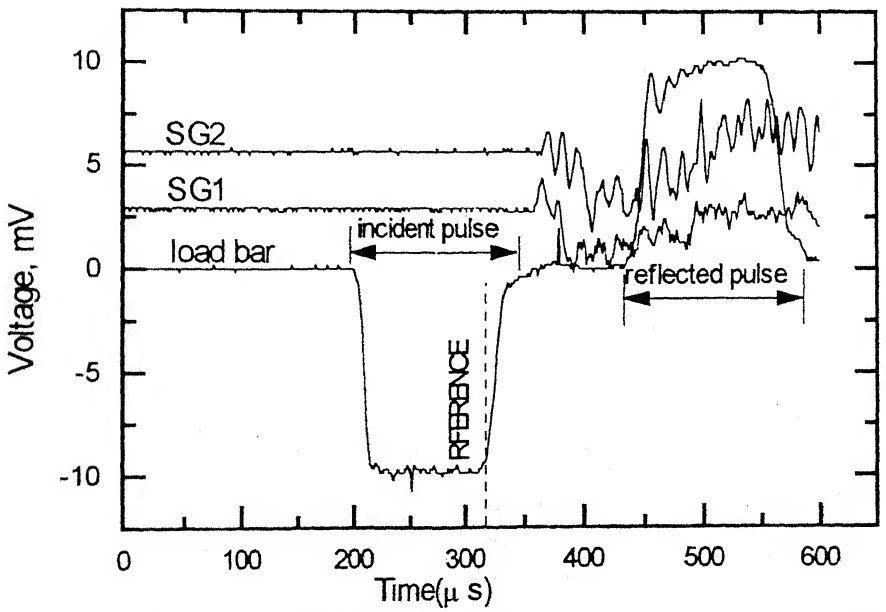

Fig.4.1(b) Zoomed view of oscilloscope records of Expt. S-1

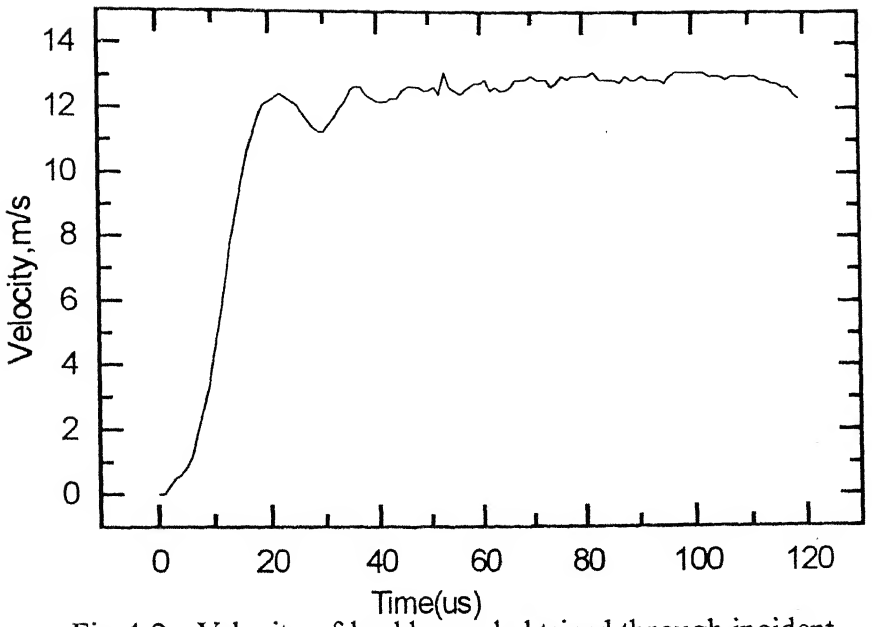

Fig.4.2 Velocity of load bar end obtained through incident -reflected pulses of the load bar for Expt. S-1

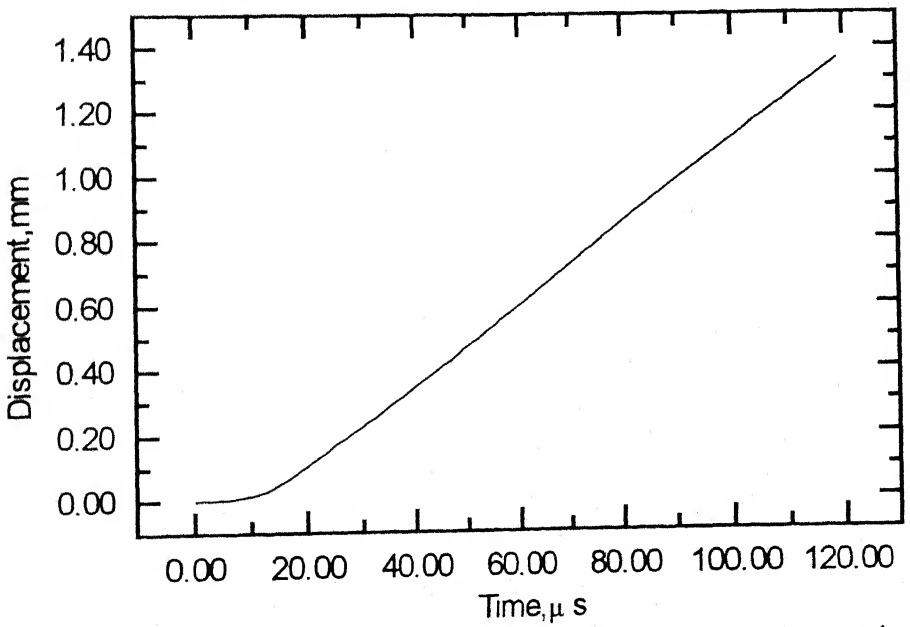

Fig4.3 Displacement of cantilever end obtained by integrating the velocity input curve for Expt. S-1

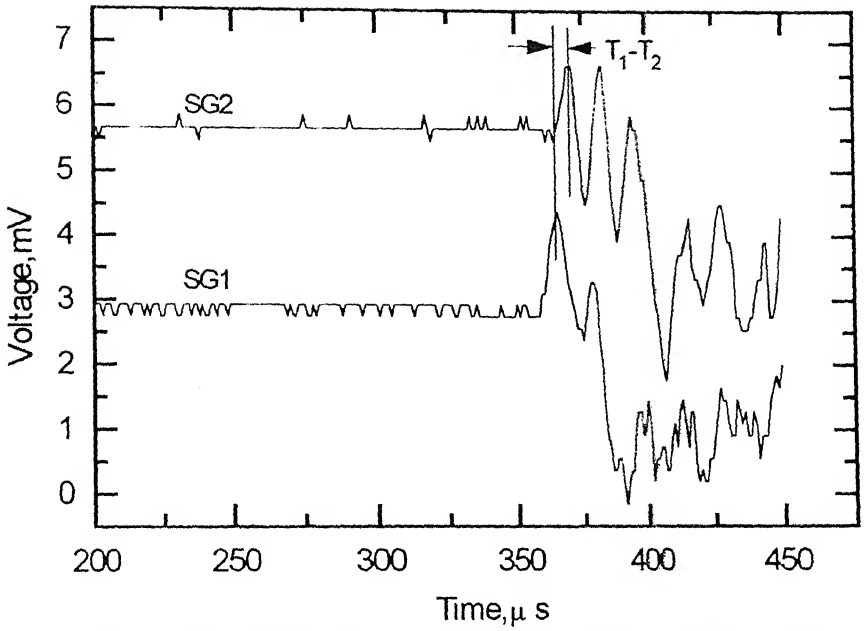

Fig.4.4 Magnified view of responses of the velocity strain gauges for Expt. S-1

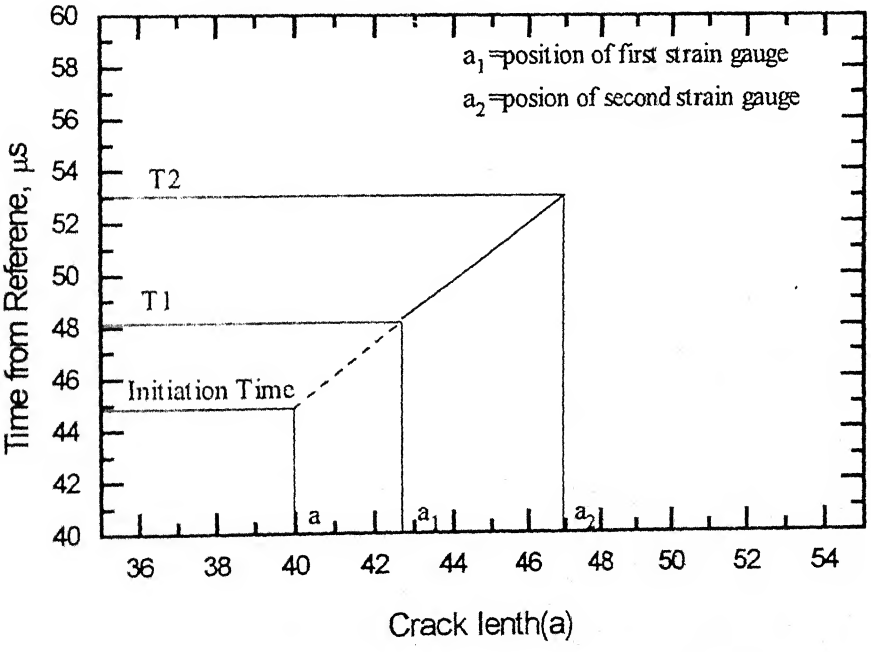

Fig.4.5 Extrapolation of Initiation time

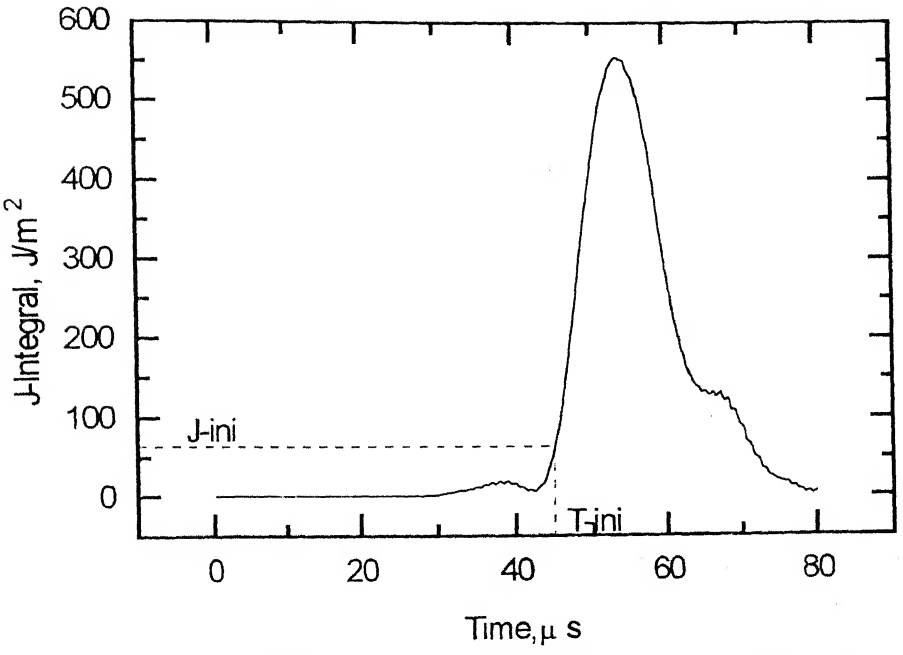

Fig.4.6 Variation of J-integral for stationary crack for Expt. S-1

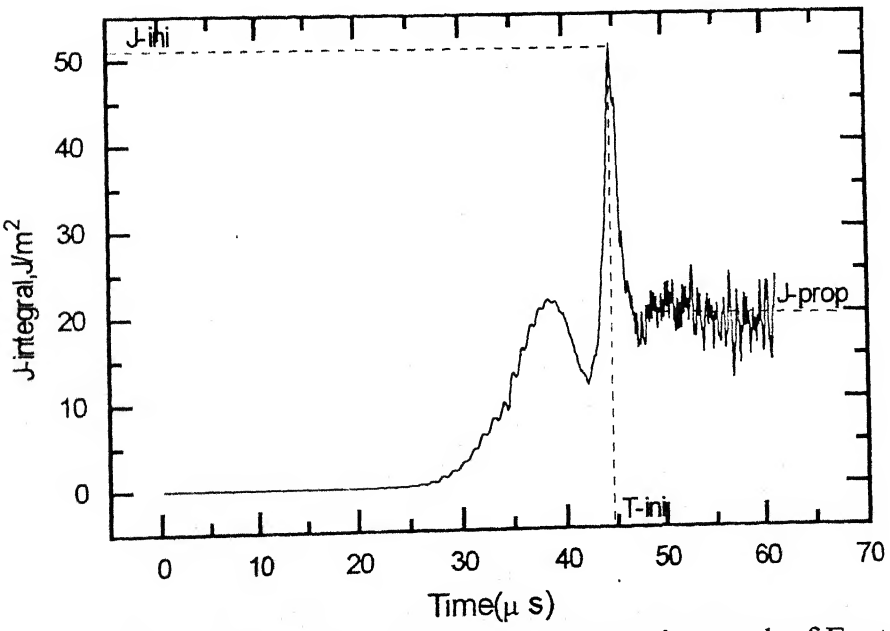

Fig.4.7(a) Variation of J-integral for propagating crack of Expt. S-1

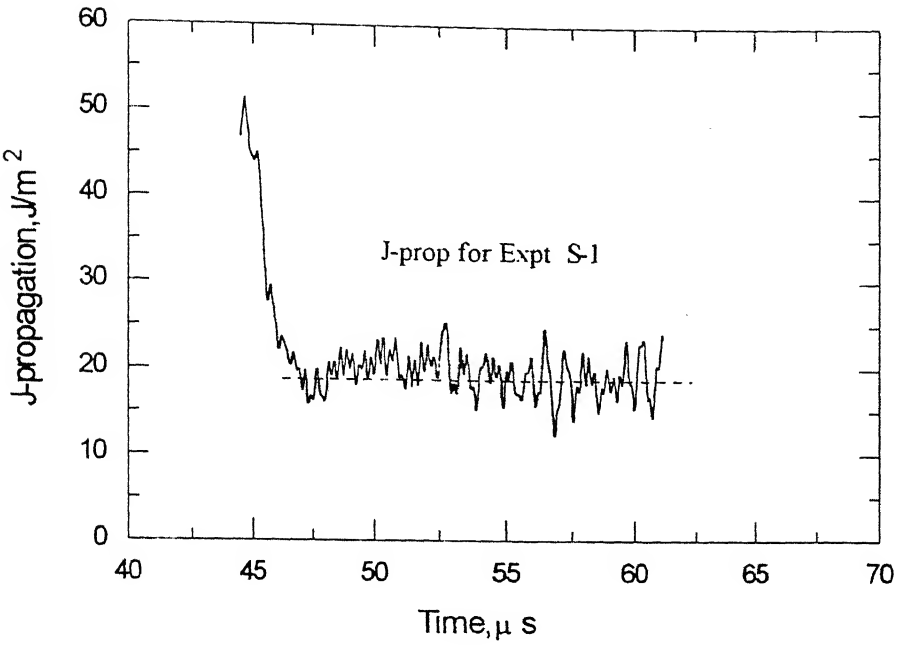

Fig.4.7(b) Zoomed view J-propagation for Expt. S-1

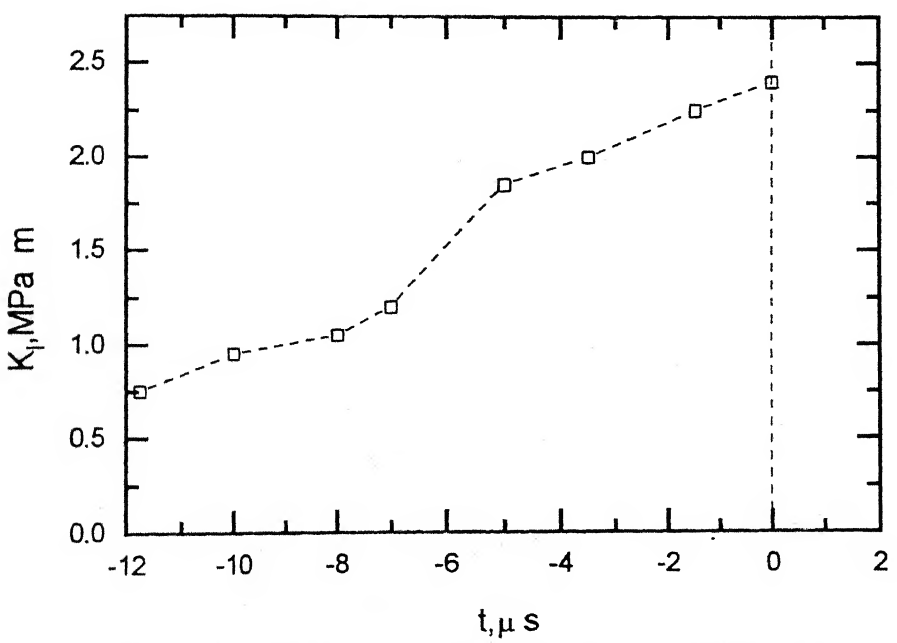

Fig.4.8 Dynamic fracture toughness variation upto initiation time
[John and Rosakis(1997(a)]

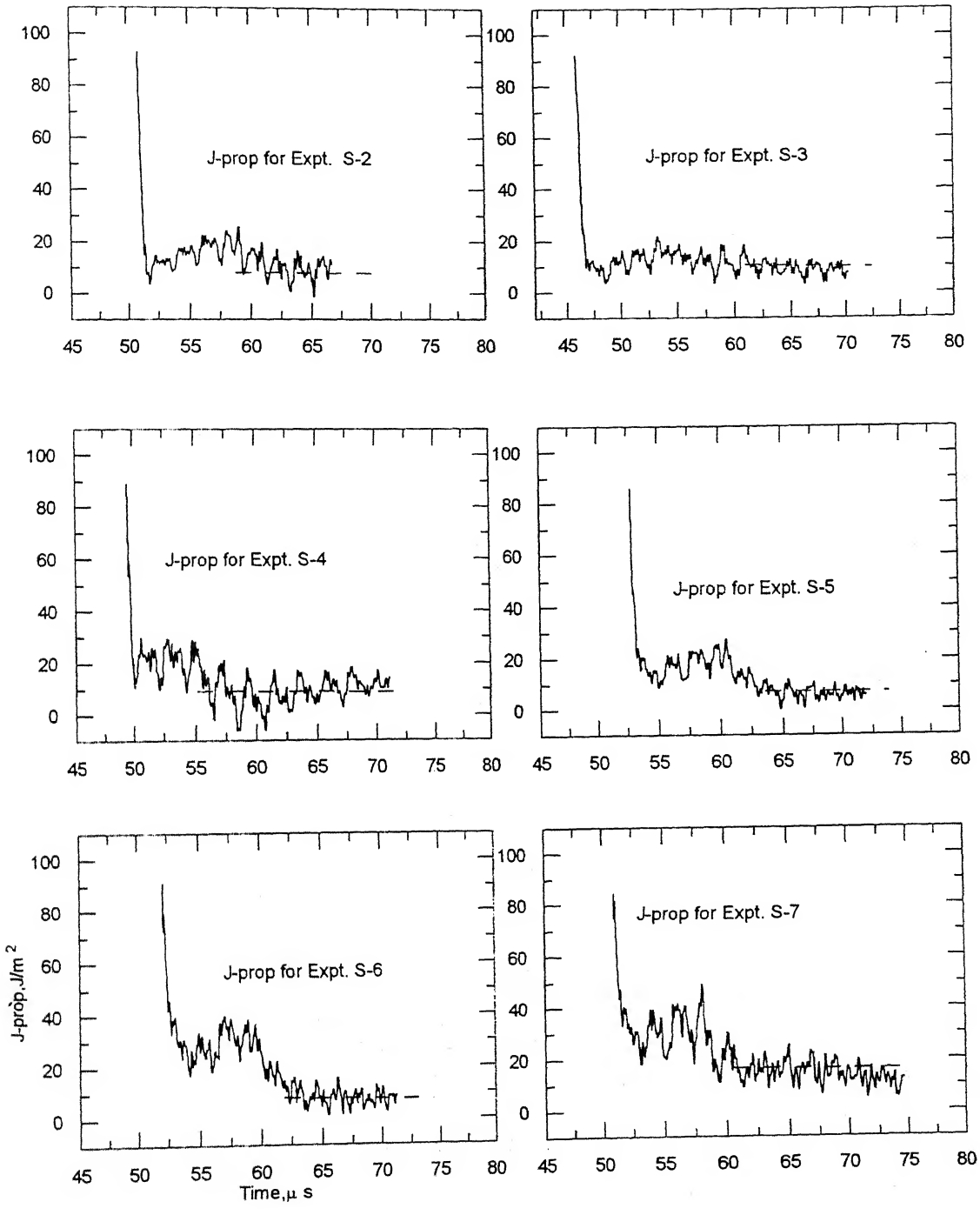

Fig.4.9 Zoomed views of J-propagation [Expts. S-2 to S-7]

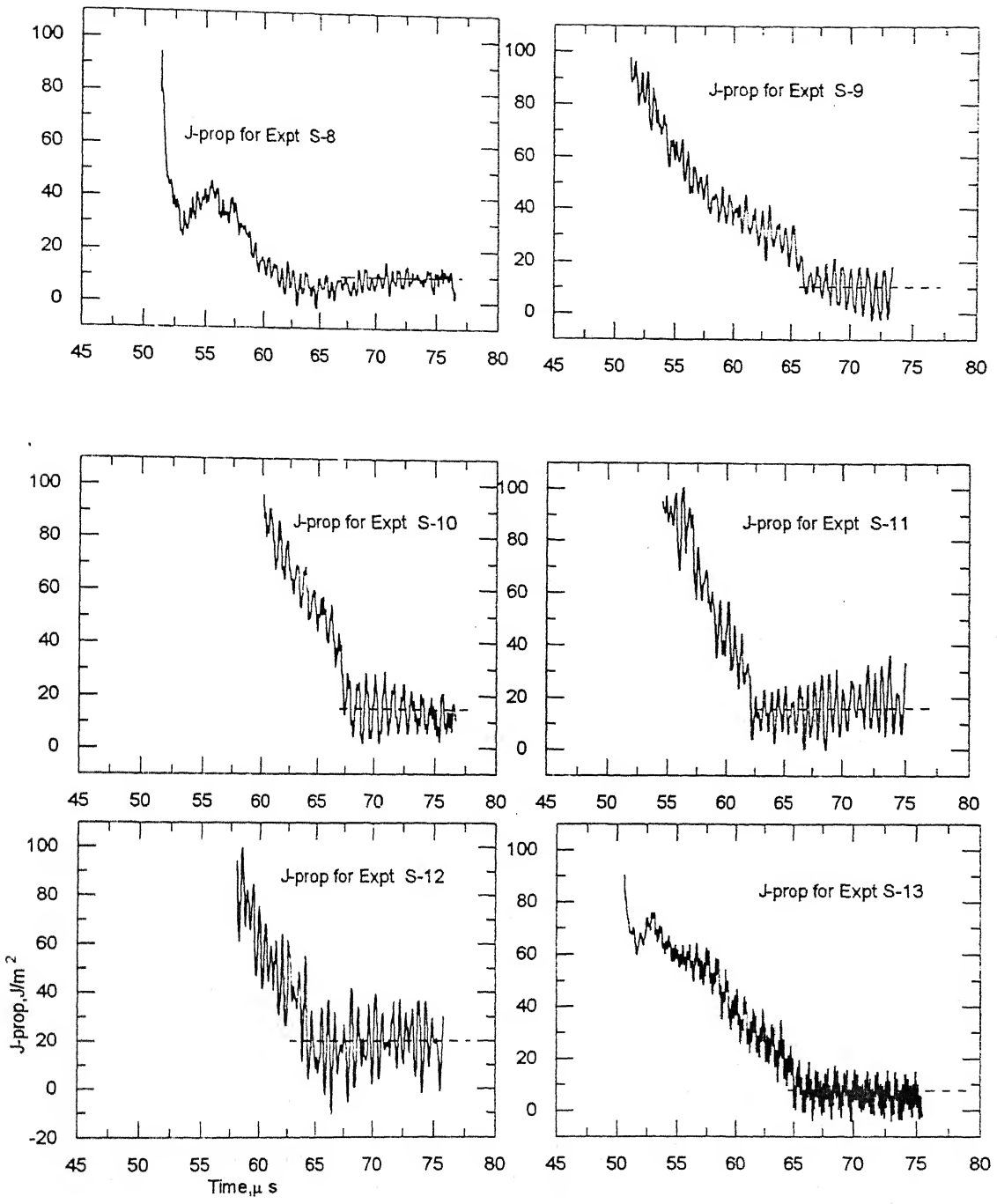

Fig.4.10 Zoomed views of J-propagation [Expts. S-8 to S-13]

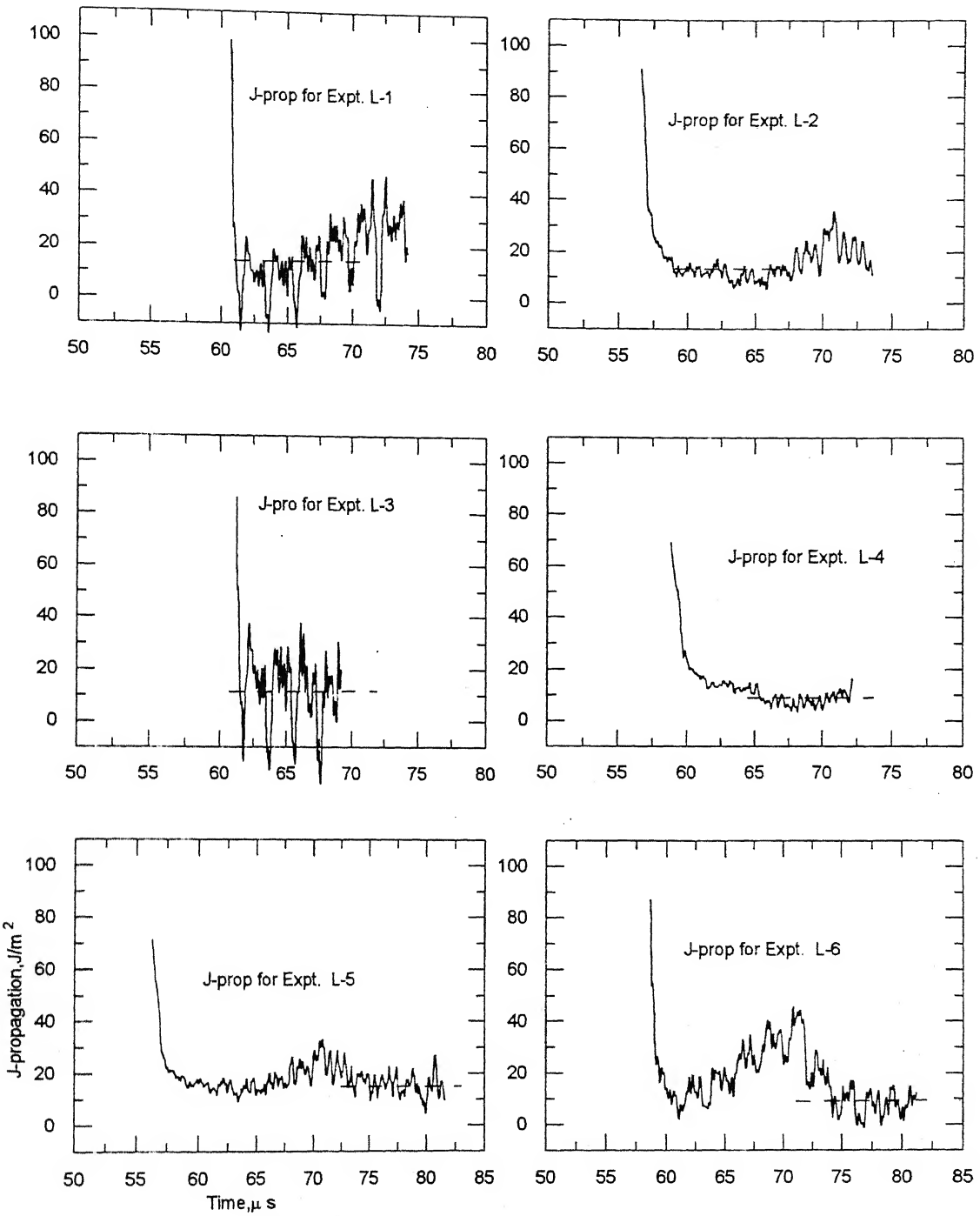

Fig.4.11 Zoomed views of J-propagation [Expts. L-1 to L-6]

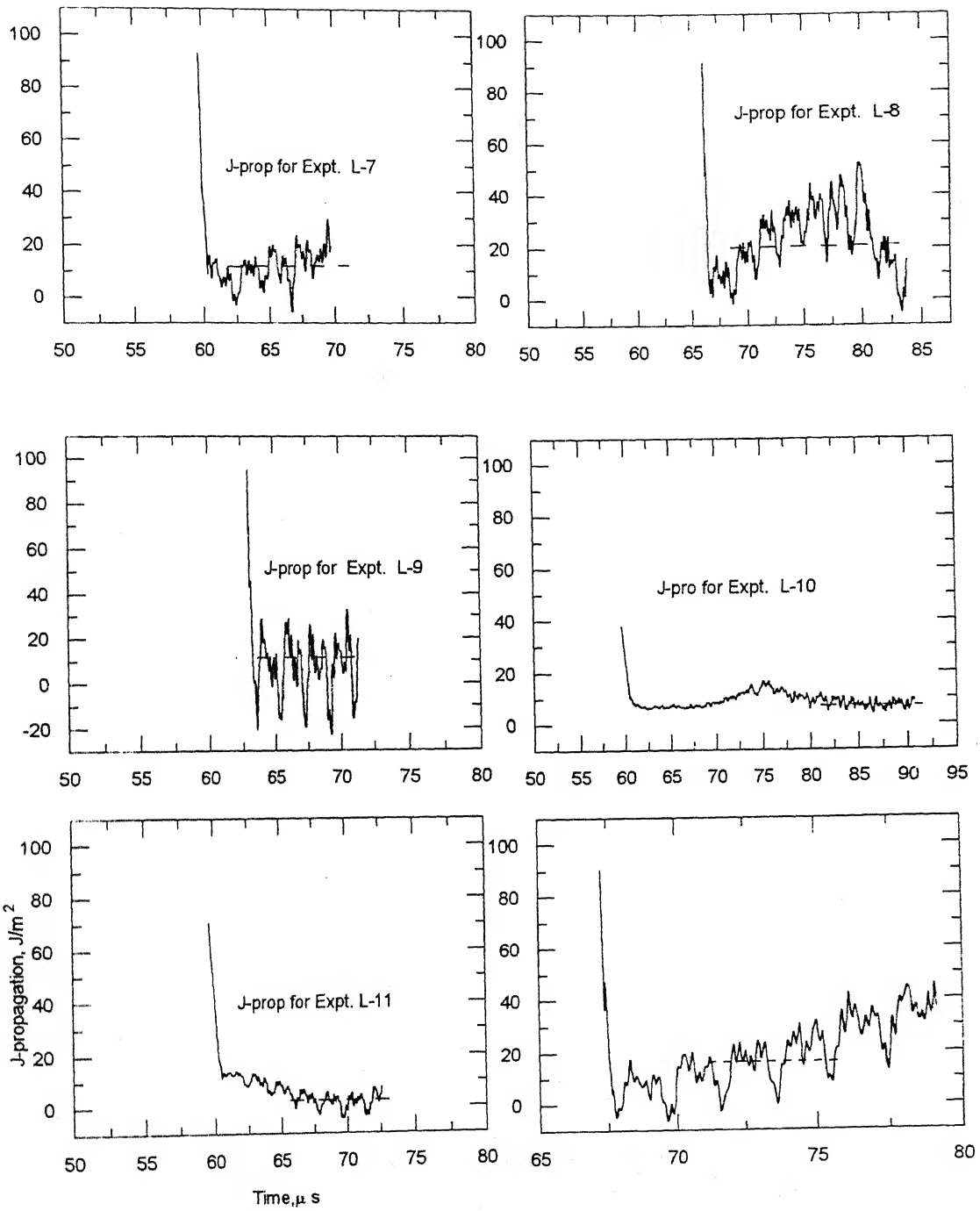

Fig.4.12 Zoomed viwes of J-propagation {Expts. L-7 to L-12]

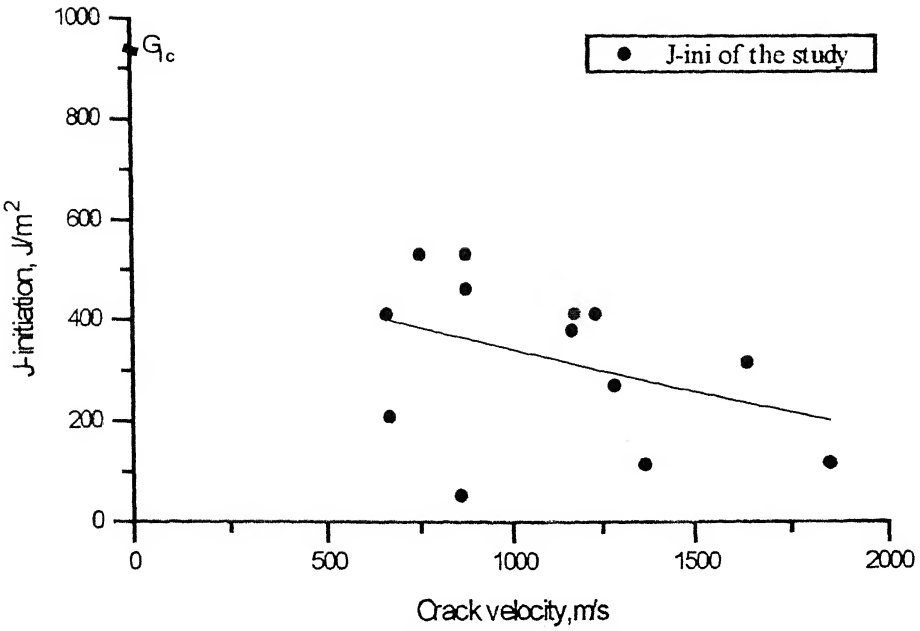

Fig.4.13 Variation of J-initiation with crack velocity for short crack

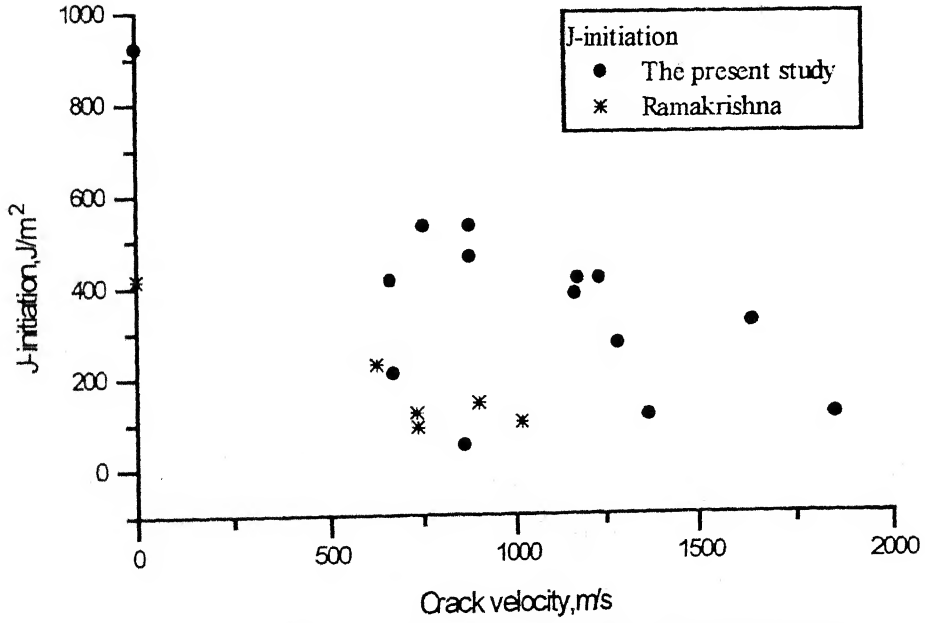

Fig.4.14 Comparison of J-ini with that of Ramakrishana

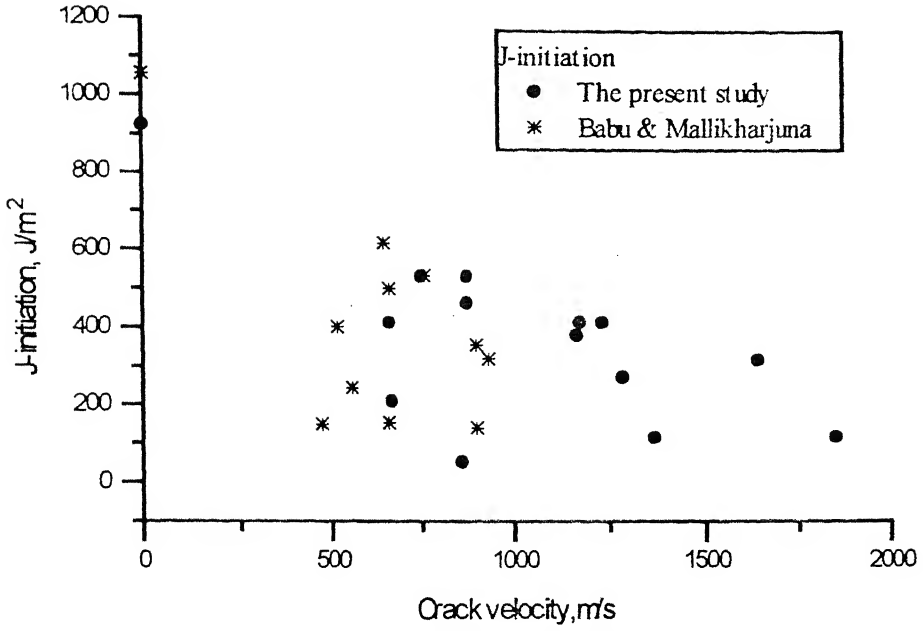

Fig.4.15 Comparison of J-ini with that of Babu & Mallikharjuna

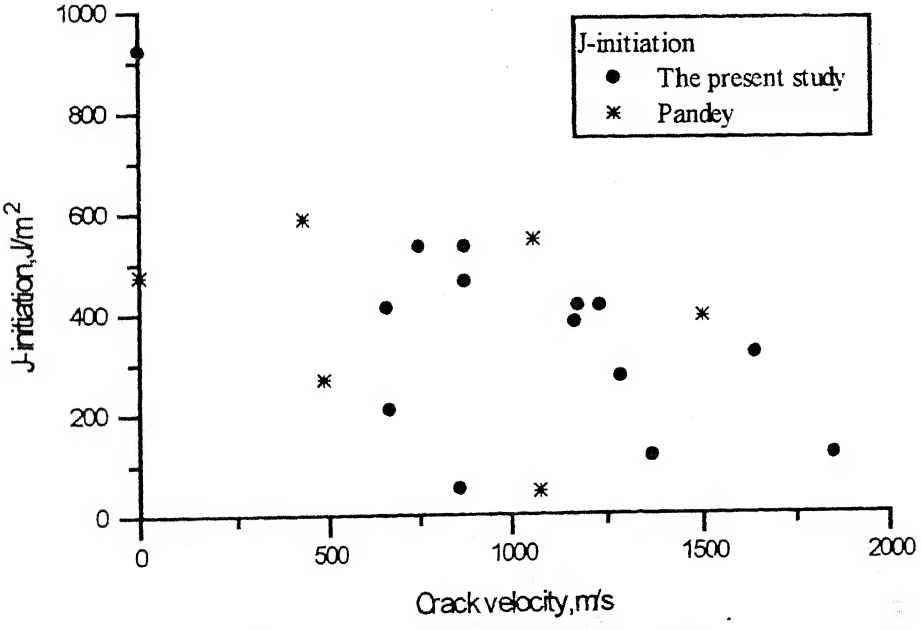

Fig.4.16 Comparison of J-ini with that of Pandy

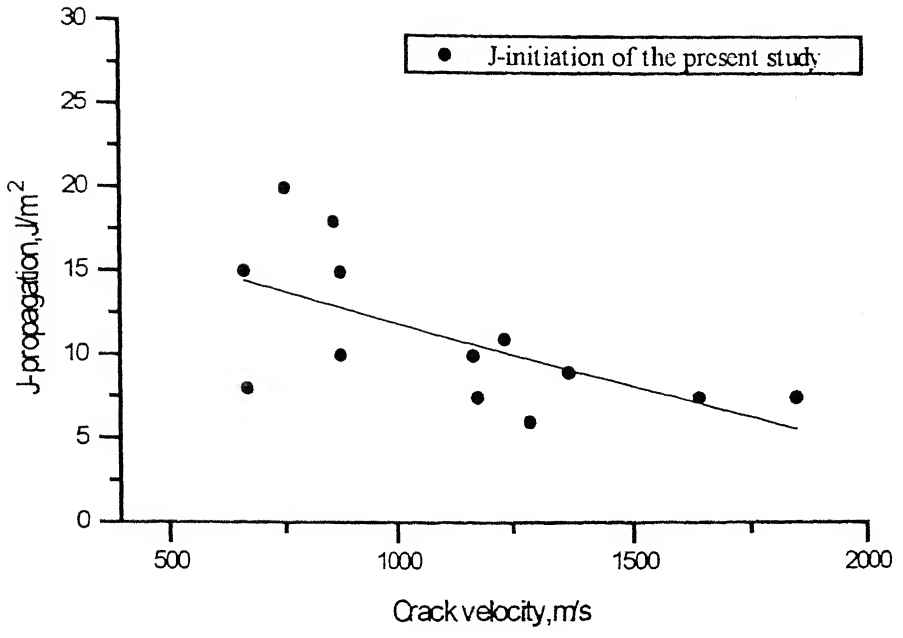

Fig.4.17 Variation of J-prop with crack velocity for short crack

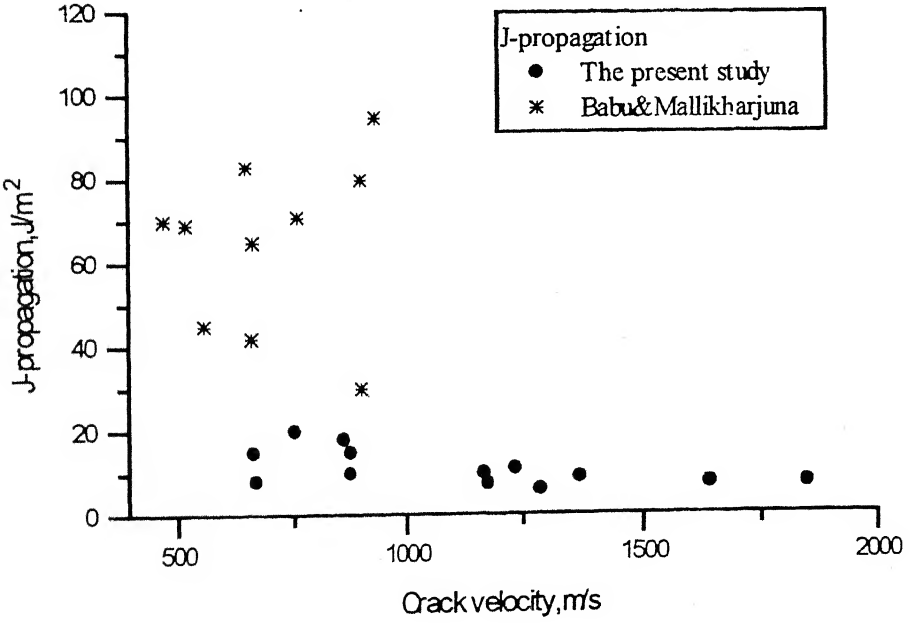

Fig.4.18 Comparison of J-prop with that of Babu & Mallikharjuna

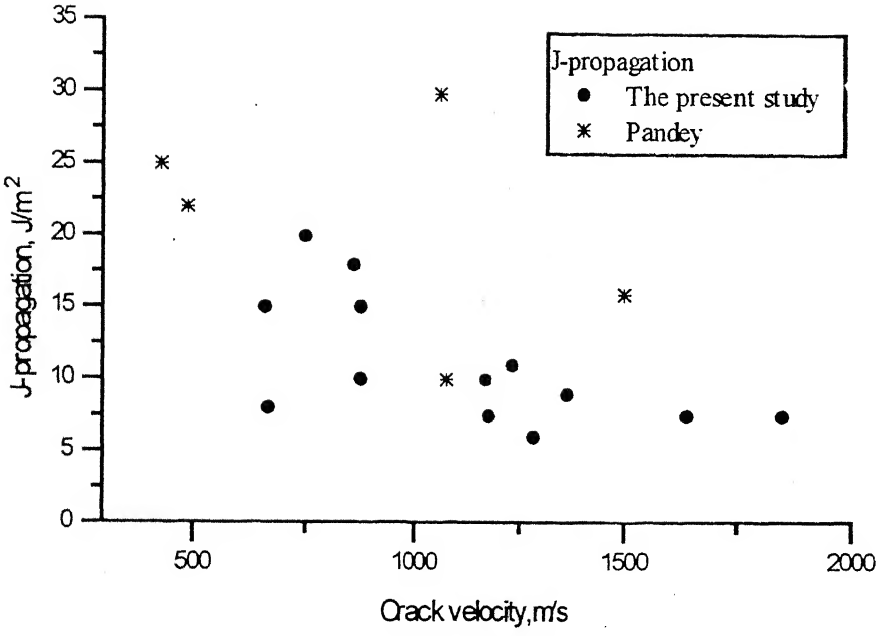

Fig.4.19 Comparison of J-prop with that of Pandey

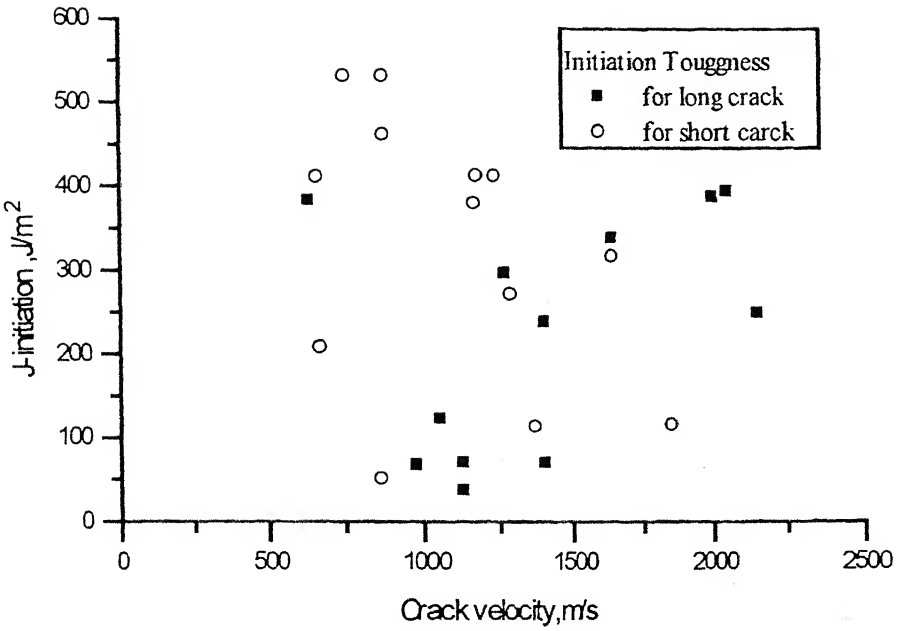

Fig.4.20 Comparision of J-ini of long and short cracks of the study

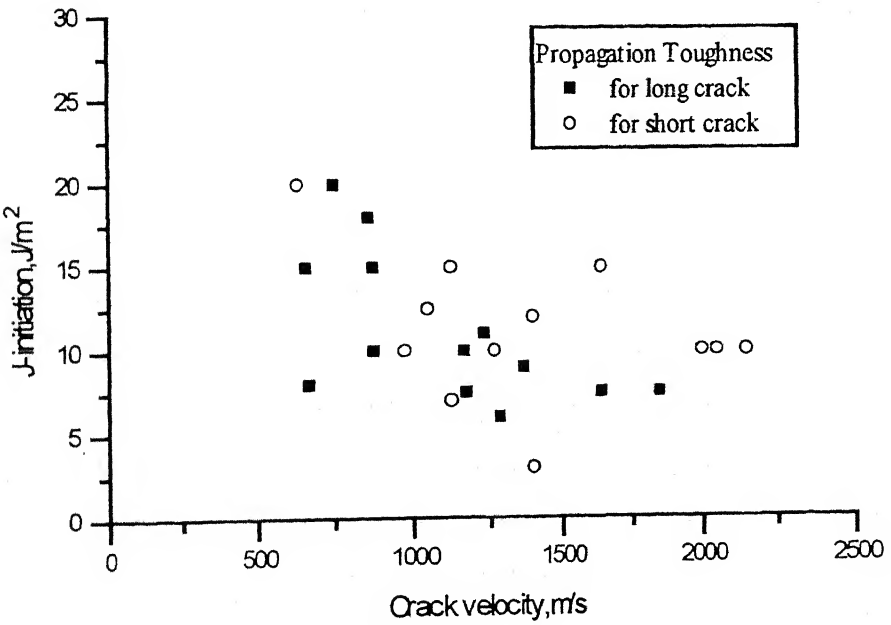

Fig.4.21 Comparision of J-prop for long and short cracks of the study

Chapter 5

Conclusion and Scope for Further Work

5.1 Conclusion

The present work is carried on fiberglass fabric/epoxy laminates for finding dynamic interlaminar toughness under impact loading through a hybrid technique using experimental measurements and finite element analysis to determine the initiation and propagation toughness of DCB specimen.

Experimental technique consists of a specimen; the front face of which is bonded to a rigid block and the other cantilever was loaded through a load bar. The load bar is impacted with a striker accelerated in an air gun. An incident compressive elastic pulse, generated in the load bar, transfers a portion of energy to the specimen; of the energy, the rest is reflected as the reflected pulse. The incident and reflected pulses are monitored by strain gauges bonded on the load bar from which deflection of cantilever end is calculated

The response within specimen after the impact is simulated using the FE code and boundary conditions determined through the experiment. After each successive time step, stress and displacement fields are determined in the entire specimen. An appropriate path is chosen to find J-integral around the crack tip. Initially the crack remains stationary and $\hat{j}$ builds up. At the initiation time, the crack starts propagating; the crack growth is introduced in the numerical simulation by gradual release of nodal forces at the crack front. Further, the crack velocity was measured by monitoring the strain response of the two strain gauges bonded in series ahead of the crack tip.

The initiation toughness (J_{ini}) was found to vary between 52 to 550 J/m^2 for short crack and between 38 and 400 J/m^2 for long crack. The value of the propagation toughness (J_{prop}) lies between 6 to 18 J/m^2 for short crack and between 3 and 20 J/m^2 for long crack. The propagation toughness was measured for crack velocity varying

in the range 660 to 2200 m/s. These results were then compared with quasistatic interlaminar toughness (G_{IC}). It has been observed that dynamic interlaminar toughness of the crack is much smaller than the quasistatic interlaminar toughness.

5.2 Scope of Further Work

- More experiments are needed to study the effect of crack length over the wider range, 25 mm to 65 mm, on dynamic toughness.

- The thickness of the cantilever can be varied to find its effect on the values of J_{ini} and J_{prop}.

- Advance digital storage oscilloscope/high speed photography may be used to record strain gauges responses more accurately.

REFERENCES

Agarwal, B.D. and Broutman, L.J. (1990) *Analysis and Performance of Fibercomposites*,2nd ed., John Wiely Sons. Inc.

Agarwal B.D.,Kumar Prashant and Khanna S.K. (1986) Determination of the fracture toughness of fabric reinforced composites by J-integral approach, *Composites Science and Technology*, 25, 311-323.

Bathe Klauss-jurgen (1990) *Finite element procedure in engineering analysis*, Prentice Hall of India

Babu K.N. (1998) Dynamic interlaminar toughness of unidirectional GFRP laminates, *M.Tech. Thesis*, Mech. Engg., IIT Kanpur

Berger J.R., Dally J.W. and Sanford R.J. (1990b) Determining the dynamic stress intensity factor with strain gages using a crack tip location algorithm, *Engineering Fracture Mechanics*, 36, 145-156.

Broek D. (1984) *Elementary Engineering Fracture Mechanics*, Mortinus Nijhoff Publishers,. The Hague.

Lambros John and Rosakis A.J. (1997a) Dynamic crack initiation and growth in thick unidirectional graphite/epoxy plates, *Composites Science and Technology*, 7(1), 55-65.

Lambros John and Rosakis A.J. (1997b) An Experimental study of Dynamic delamination of thick fiber reinforced polymeric matrix composites, *Journal of Experimental Mechanics*, 37, 360-366.

Kolednik O. (1991) On the physical meaning of the J-a Curves, *Engineering Fracture Mechanics*, 38(6), 403-412.

Kumar Prashant and Rai Badri (1993) Delamination of barely visible impact damage in CFRP laminates, *Composite Structures*, 23, 313-318.

Kumar Prashant and Narayan,M.D. (1993) Energy Dissipation of Projectile impacted panels of glass fabric reinforced composites, *Composite Structures, 15, 75_90.*

Kumar Prashant and Kishore, N.N. (1998) Initiation and propagation toughness of delamination crack under an impact load, *Journal of the Mechanics and Physics of Solids*, 46, 1773-1787.

Kumar Prashant (1999) *Element of Fracture Mechanics*, Wheeler Publishing, New Delhi.

Mallikharjuna R.R. (1998) Determination of interlaminar toughness of GFRP laminates at very high crack velocity *M.Tech. Thesis*, Mech. Engg., IIT Kanpur.

Nishioka T. and Atluri S.N. (1983) Path independent integrals, Energy Release rate and General solution of Near-tip Fields in Mixed Mode Dynamic Fracture Mechanics, Engineering Fracture Mechanics, 18(1), 1-22.

Owen,D.J.R and Shantaram,D. (1986) *Computational methods in mechanics of fracture*, ed. S.N. Alturi. Elservier Science, New York.

Ramakrisha Alluri (1996) Initiation and propagation toughness of interlaminar cracks in FRP laminates under impact loading, *M.Tech. Thesis*, Mech. Engg., IIT Kanpur.

Ravi Chandar K. and Knauss W.G. (1982) Dynamic crack tip stresses under stress wave loading - A comparison of theory and experiment, *International Journal of Fracture*, 20, 202-222.

Ravi Chandar K. and Knauss W.G. (1984a) An experimental investigation into dynamic fracture : I. Crack initiation and arrest, *International Journal of Fracture*, 25, 247-262.

Ravi Chandar K. and Knauss W.G. (1984b) An experimental investigation into dynamic fracture : II. Microstructural aspects, *International Journal of Fracture*, 26, 65-80.

Ravi Chandar K. and Knauss W.G. (1984c) An experimental investigation into dynamic fracture : III. On steady-state crack propagation and crack branching, *International Journal of Fracture*, 26, 141-154.

Ravi Chandar K. and Knauss W.G. (1984d) An experimental investigation into dynamic fracture : IV. On interaction of stress waves with propagating cracks, *International Journal of Fracture*, 26, 189-200.

Ravichandran G. and Clifton R.J. (1989) Dynamic fracture under plane wave loading, *International Journal of Fracture*, 40, 157-201.

Rosakis A.J., Duffy J. and Freund L.B. (1984) The determination of dynamic fracture toughness of AISI 4340 steel by the shadow spot method, *Journal of the Mechanics and Physics of Solids*, 4, 443-460.

Sun C.T. and Grandy J.E. (1986) Dynamic delamination fracture toughness of a Graphite/Epoxy laminate under impact, *Composite Science and Technology*, 31, 55-72.

Takeda N., Sierakowski R.L., Ross C.A. and Malvern L.E. (1982) Delamination crack propagation in ballistically impact glass/epoxy composite laminates, *Experimental Mechanics*, 22, 19-25.

Truss R.W., P.J. Hine and R.A. Duckett (1997) Interlaminar and intralaminar fracture toughness of uniaxial continuous and discontinuous carbon fibre/epoxy composites, *Composites*, 28A, 627-636.

Verma S.K. (1995), Determination of static and dynamic interlaminar fracture toughness - A combined experimental and finite element method, *Ph.D. Thesis*, Mech.Engg., IIT Kanpur.

Verma S.K., Kumar Prashant, Kishore N.N. (1997) An experimental cum numerical technique to determine interlaminar fracture toughness, *Engineering Fracture Mechanics*, 60, 583-596.

Zehnder Alant T. and Rosakis Ares J. (1990) Dynamic fracture initiation and propagation in 4340 steel under impact loading, *International Journal of Fracture*, 43, 271- 285.

APPENDIXES

Appendix –1

Experimental Characterization of Composites

Experimental characterization refers to the determination of the material properties through tests conducted on suitably designed specimens. Elastic constants and strengths are basic mechanical properties of materials. For a unidirectional laminate, there are four independent elastic constants; the elastic module in the longitudinal and transverse directions, the shear modulus, the major Poisson ratio.

For a fabric composite material having equal number of yarns in warp and weft directions, the elastic module in the longitudinal (warp) and transverse (weft) directions are approximately equal. Similarly, major and minor Poisson ratios are also equal. In the present study, the glassfibre fabric having equal number of yarns in warp and weft directions is used. Therefore, only three tests are needed to determine E_L , ν_{LT} and G_{LT} .

DETERMINATION OF E_L AND ν_{LT}

The static unidirectional tension test is conducted to determine elastic modulus and Poisson ratio of the material. Straight specimen with 25.4 width and 153 mm long are employed with end tabs of 38 mm long on each end (Fig.A.1.1). The specimen are cut from a laminate of 16 plies.

The test are performed on Instron 850 at displacement control loading rate of 2 mm/min. Fig. A.1.1 shows dimensioning of the tensile test specimen . Strain gauges BELA-5-8 supplied by Toky Sokki Kankyijo Co. Ltd., Japan are used. The Poisson ratio is measured by placing the two strain gauges at the center of specimen in longitudinal and lateral directions. The responses of the strain gauges is measured through strain indicators. The Poisson ratio is given by

$$\nu_{LT} = -\frac{E_T}{E_L}$$

Table A.1.1 Experimental values of E_L and ν_{LT}

Expt. N	Longitudinal Modulus E_L (GPa)	Major Poisson Ratio ν_{LT}
1	26.72	0.20
2	26.56	0.19
3	25.53	0.21
4	27.79	0.20
5	24.55	0.21

The average value of E_L = 26.23 GPa and average ,ν_{LT} = 0.202 were used in the computer simulation.

DETERMINATION OF ,G_{LT}

In plane shear properties of a fabric glass composite are determined by conducting a tension test on a $[\pm 45]_s$ laminate. G_{LT} is determined for $[\pm 45]_s$ laminate of 16 layers at 6 mm/min displacement by using expression

$$G_{LT} = \frac{E_x}{2(1+\nu_{xy})}$$

Table A.1.2 Modulus of Rigidity

Expt. No	Modulus of Rigidity G_{LT} (GPa)
1	3.573
2	3.582
3	3.500
4	3.500

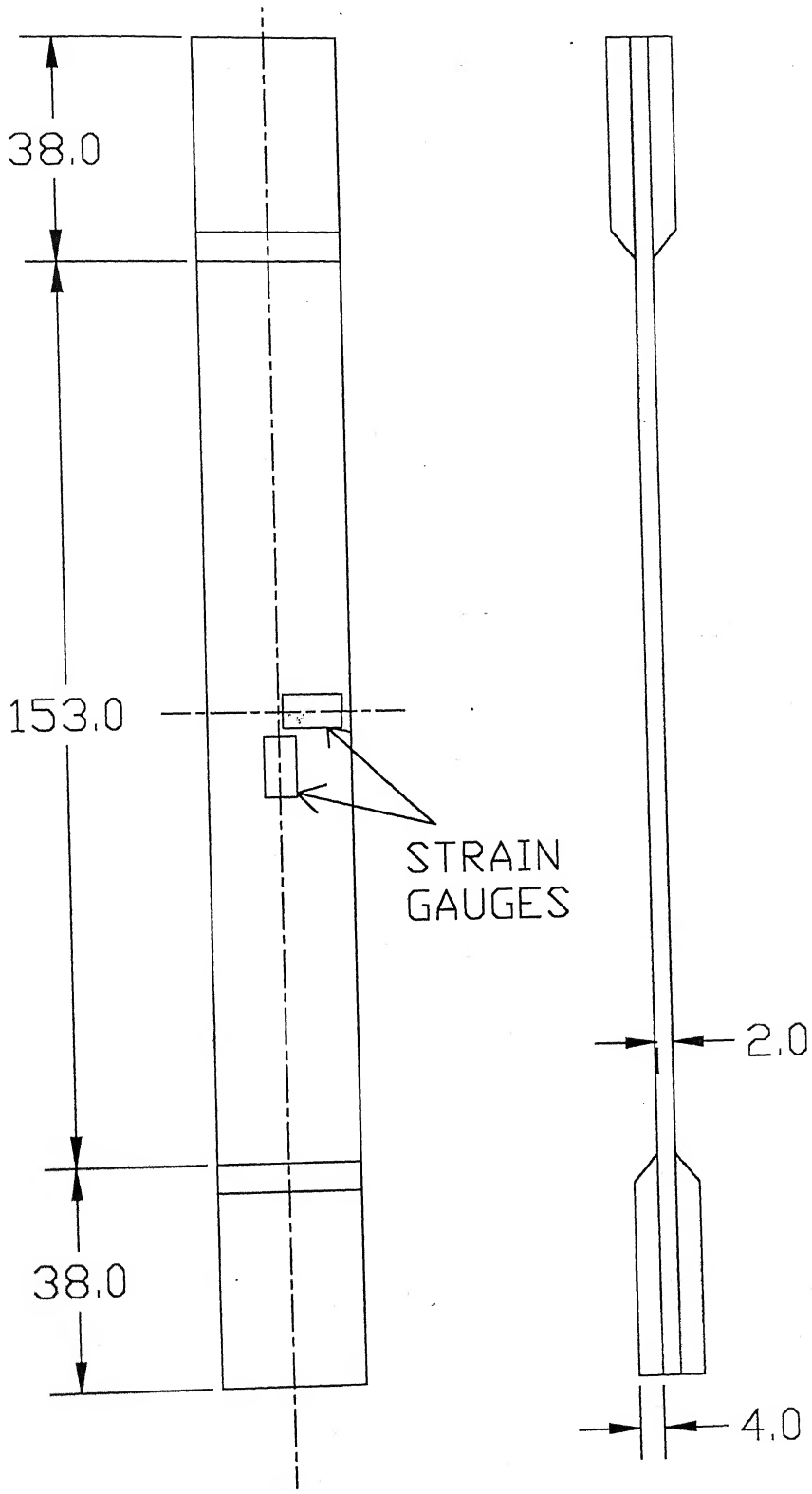

Fig. A.1.1 Tension test specimen

Appendix 2

Details of Experiments

The figures of oscilloscope records, variation of velocity of load bar end, displacement history of cantilever-end, variation of J-integral for stationary crack, and J-integral of propagating crack are shown in this appendix for Expts. No. S-2 to S-13 and L-1 to L-12. Experimental number and concerned figures are tabulated in following Table:

Expt. No.	Concerned Figures
S-2	A.2.1 (a, b, c, d, e)
S-3	A.2.2 (a, b, c, d, e)
S-4	A.2.3 (a, b, c, d, e)
S-5	A.2.4 (a, b, c, d, e)
S-6	A.2.5 (a, b, c, d, e)
S-7	A.2.6 (a, b, c, d, e)
S-8	A.2.7 (a, b, c, d, e)
S-9	A.2.8 (a, b, c, d, e)
S-10	A.2.9 (a, b, c, d, e)
S-11	A.2.10 (a, b, c, d, e)
S-12	A.2.11 (a, b, c, d, e)
S-13	A.2.12 (a, b, c, d, e)
L-1	A.2.13 (a, b, c, d, e)
L-2	A.2.14 (a, b, c, d, e)
L-3	A.2.15 (a, b, c, d, e)
L-4	A.2.16 (a, b, c, d, e)
L-5	A.2.17 (a, b, c, d, e)
L-6	A.2.18 (a, b, c, d, e)
L-7	A.2.19 (a, b, c, d, e)
L-8	A.2.20 (a, b, c, d, e)
L-9	A.2.21 (a, b, c, d, e)
L-10	A.2.22 (a, b, c, d, e)
L-11	A.2.23 (a, b, c, d, e)
L-12	A.2.24 (a, b, c, d, e)

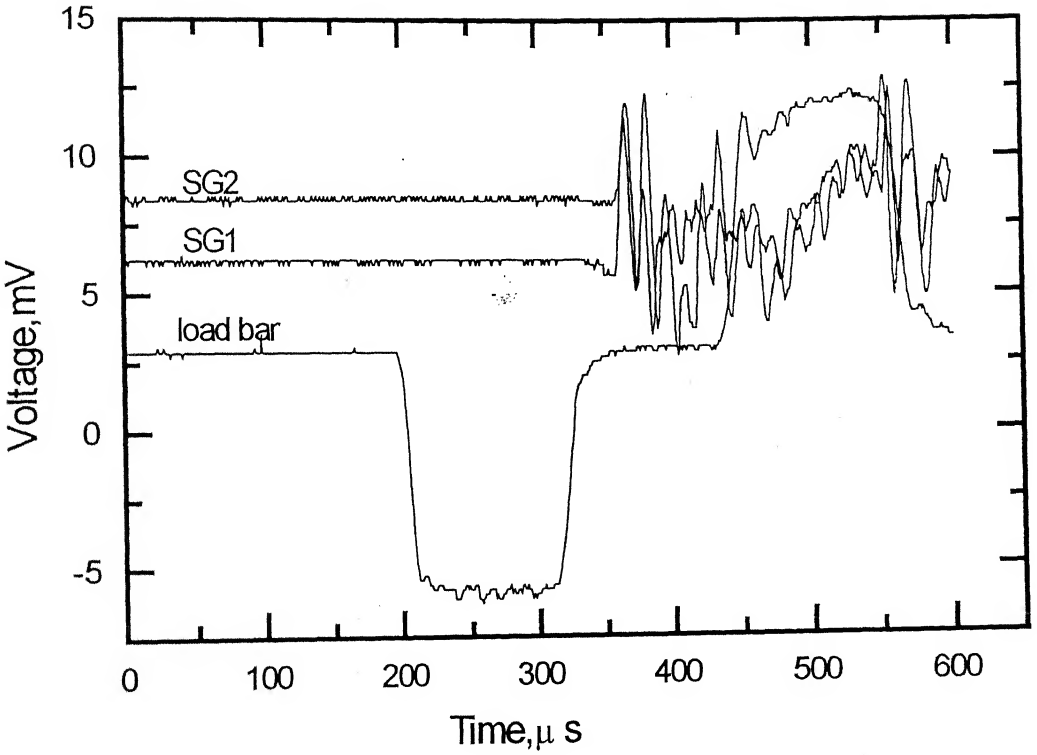

Fig. A.2.1(a) Oscilloscope Records of Expt S-2

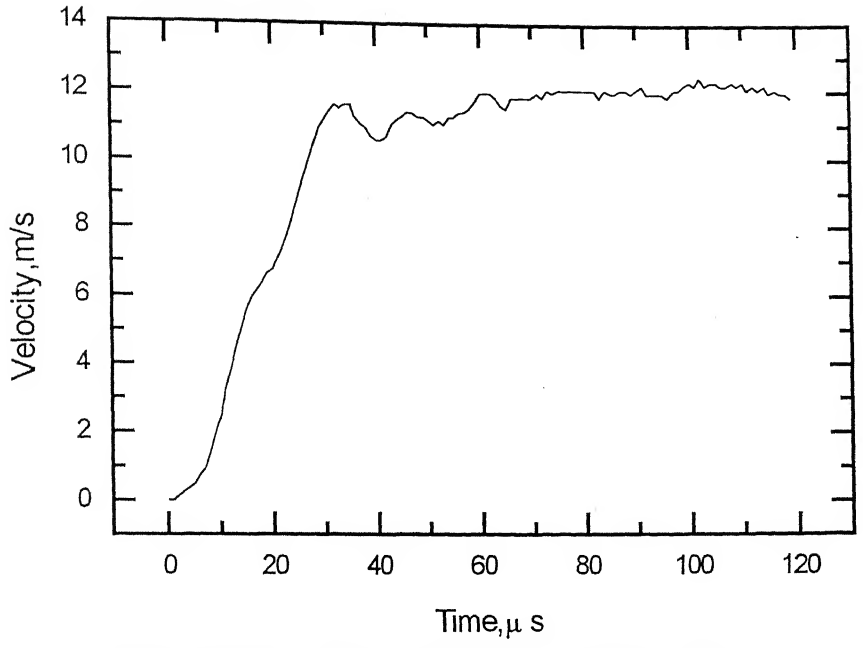

Fig.A.2.1(b) Velocity of load bar end Expt. S-2

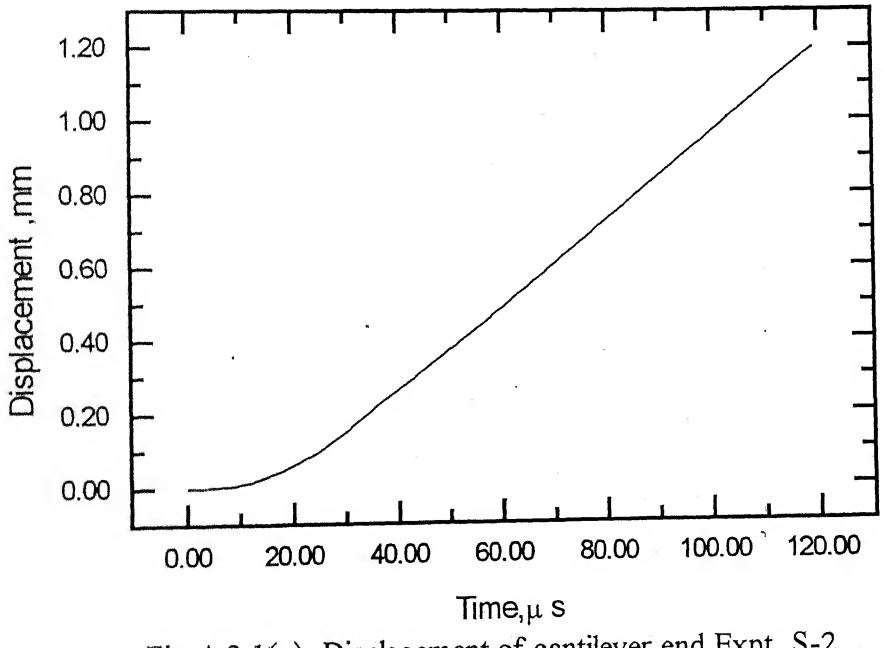

Fig.A.2.1(c) Displacement of cantilever end Expt. S-2

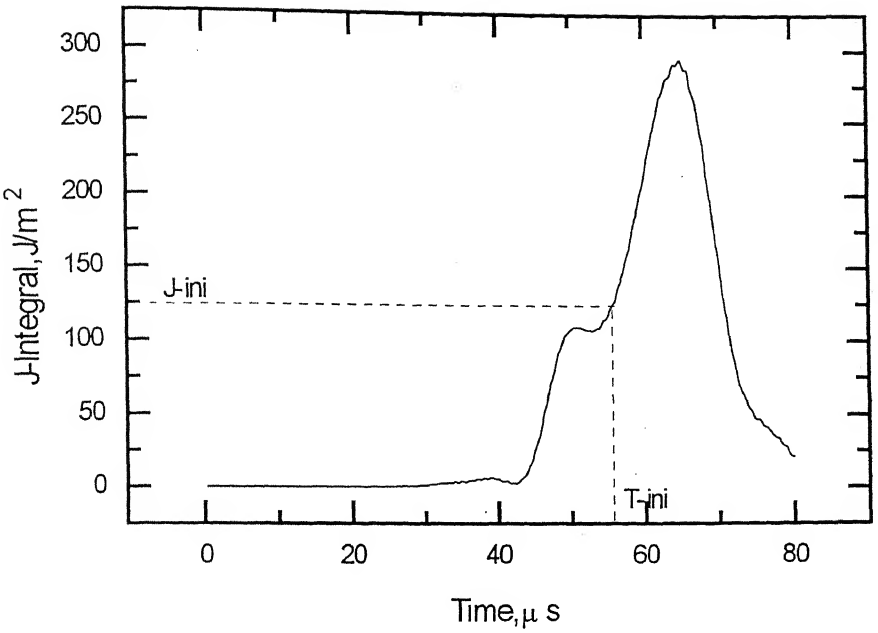

Fig. A.2.1(d) Variation of J-integral for stationary crack Expt. S-2

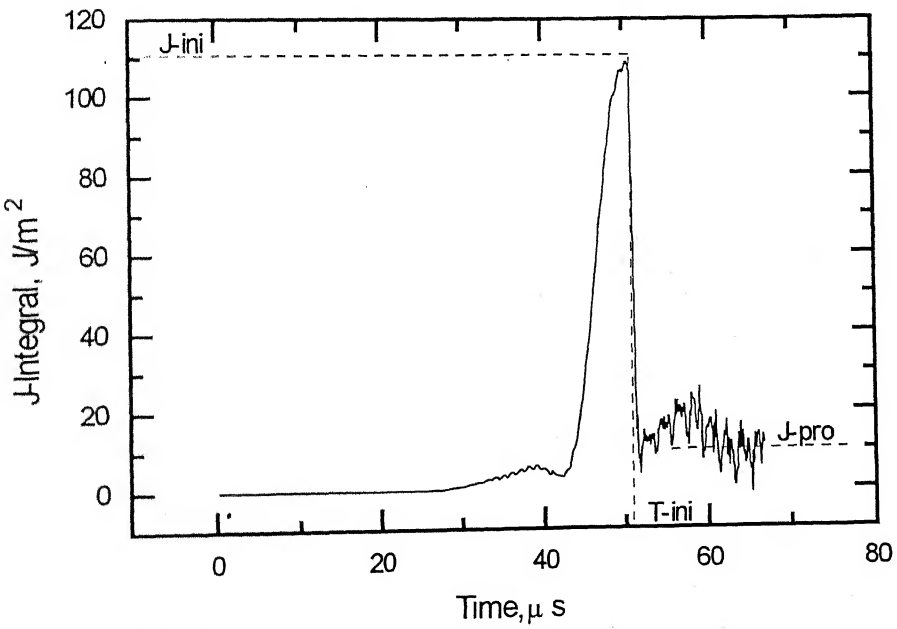

Fig. A.2.1(e) Variation of J-integral for stationary & propagating crack Expt. S-2

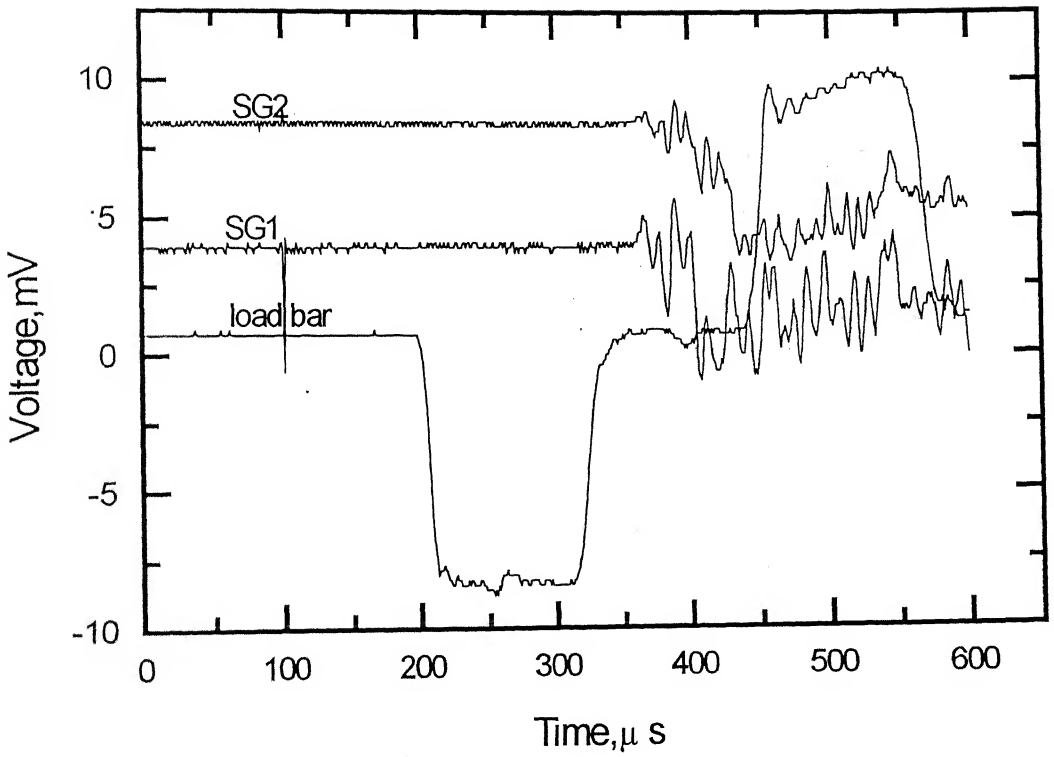

Fig.A.2.2(a) Oscilloscope records of Expt. S-3

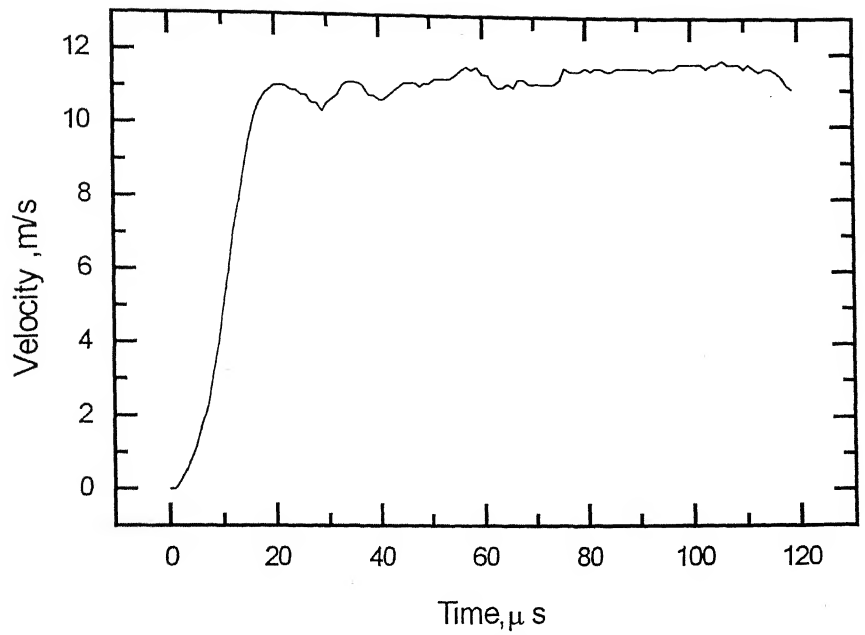

Fig. A.2.2(b) Velocity of load bar end Expt. S-3

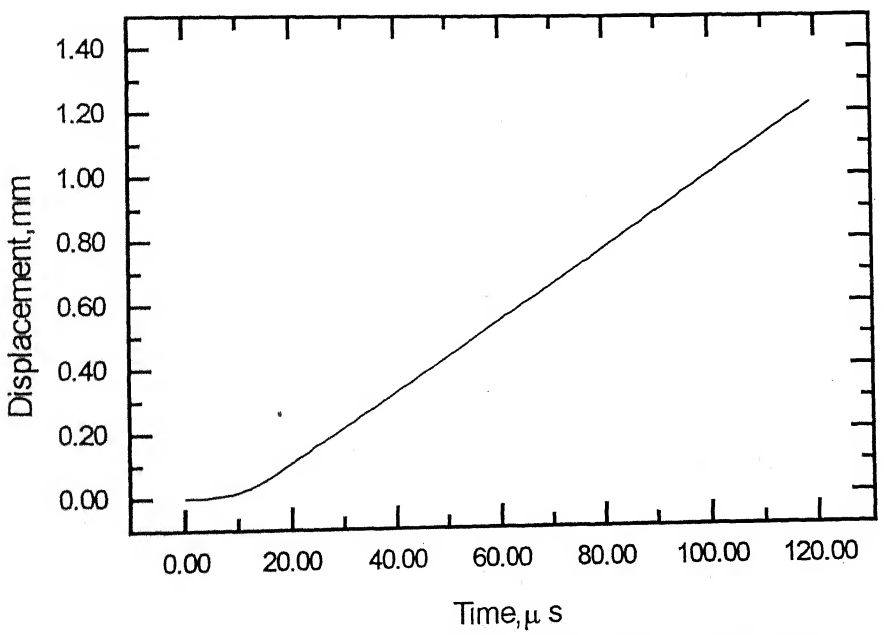

Fig. A.2.2(c) Displacement of cantilever end Expt. S-3

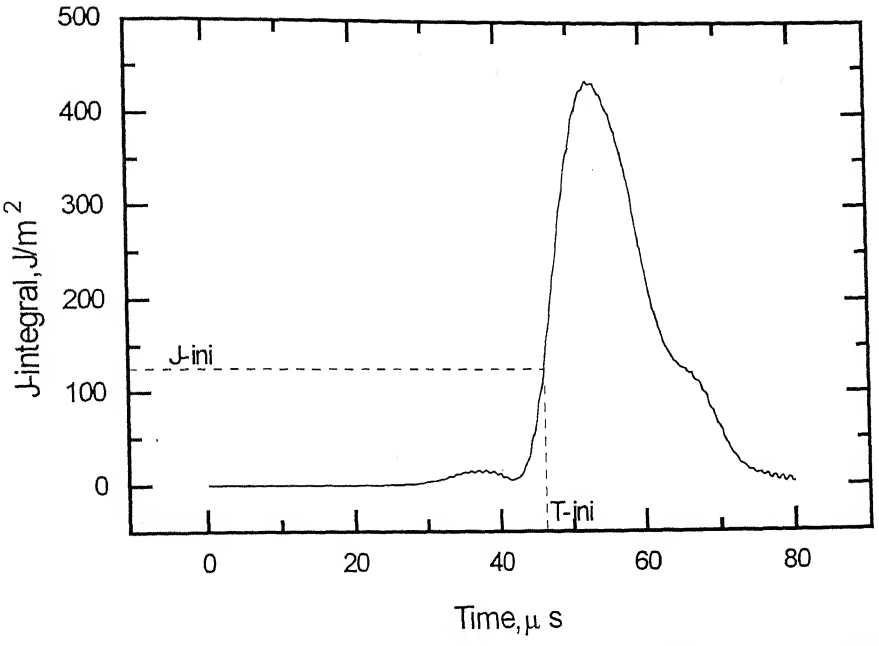

Fig. A.2.2(d) Variation of J-integral for stationary crack Expt. S-3

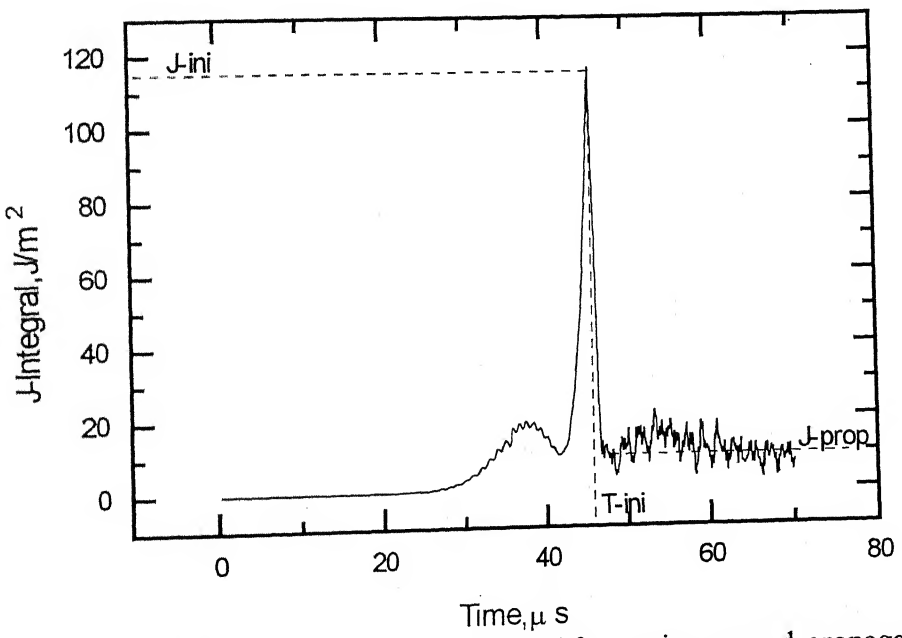

Fig. A.2.2(d) Variation of J-integral for stationary and propagating crack Expt. S-3

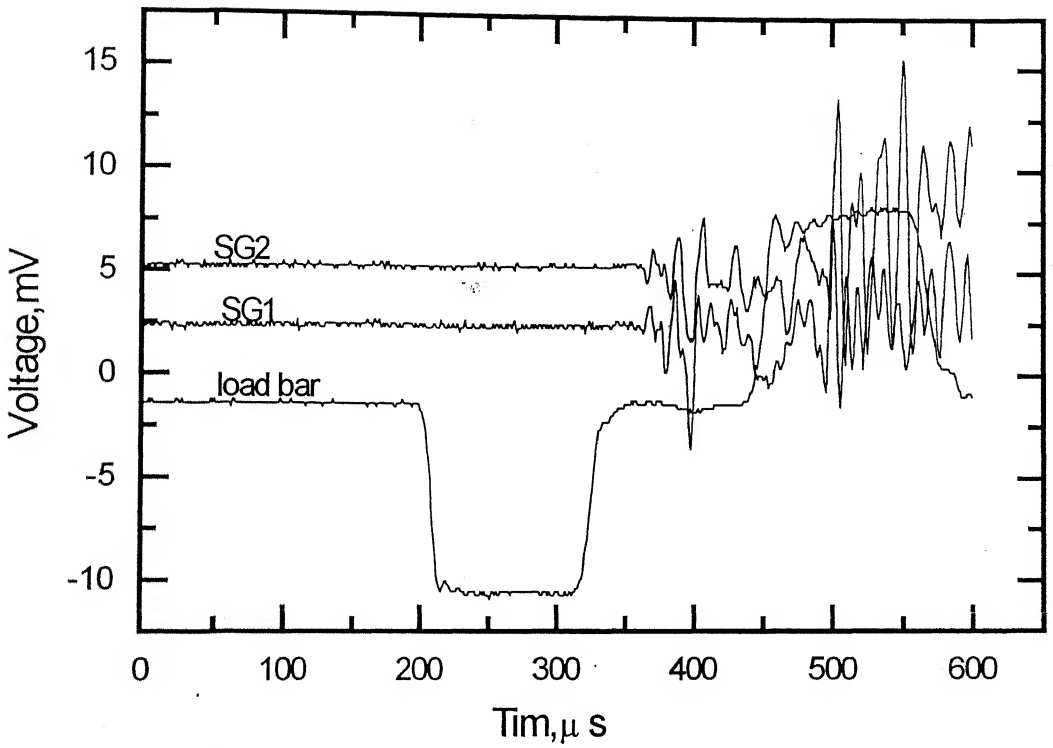

Fig. A.2.3(a) Oscilloscope Records Expt. S-4

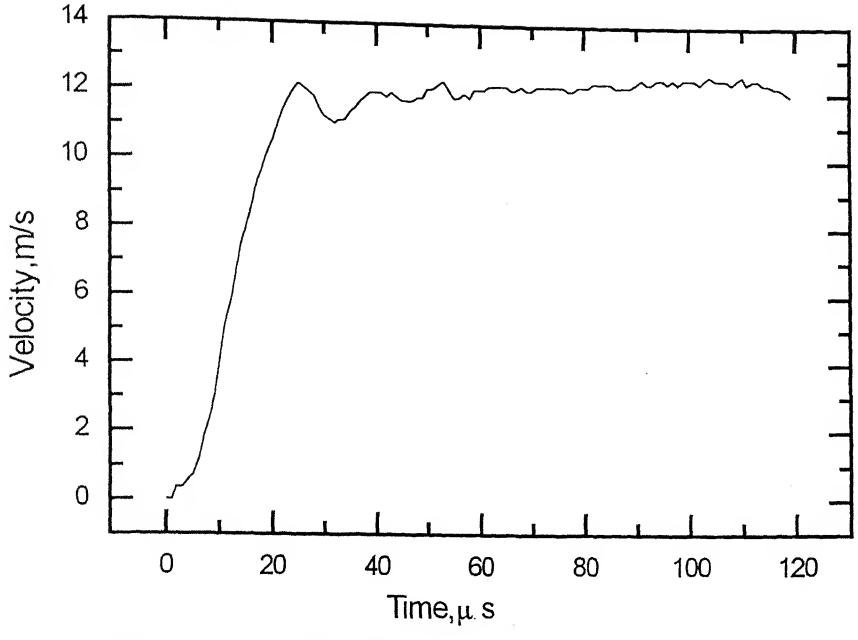

Fig. A.2.3(b) Velocity of load bar end Expt. S-4

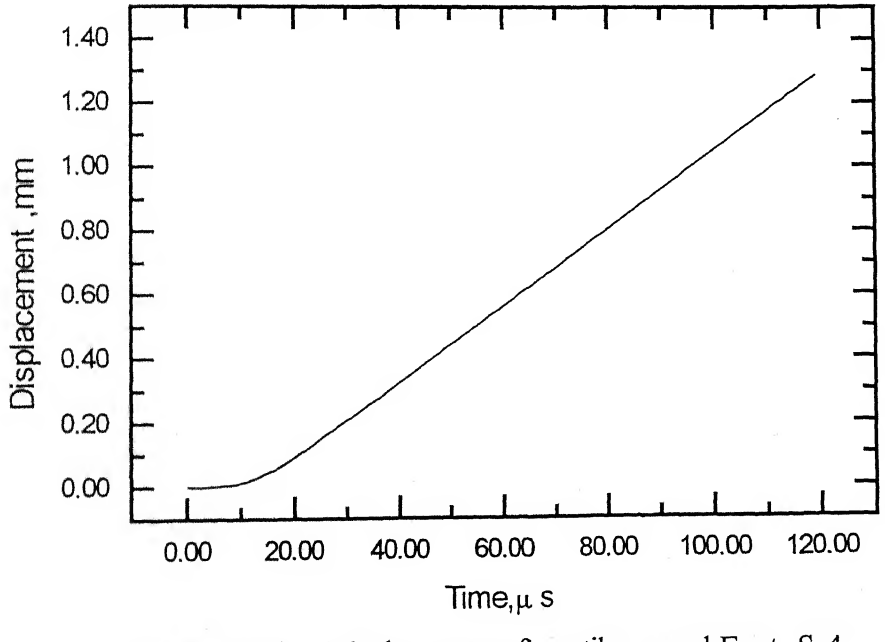

Fig:A.2.3(c) Displacement of cantilever end Expt. S-4

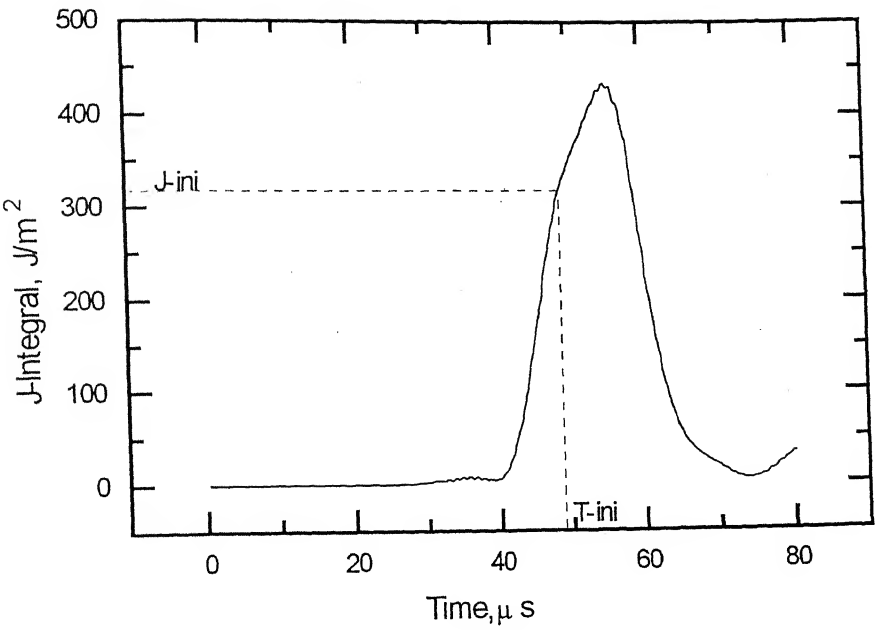

Fig.A.2.3(d) Variation of J-integral for stationary crack Expt. S-4

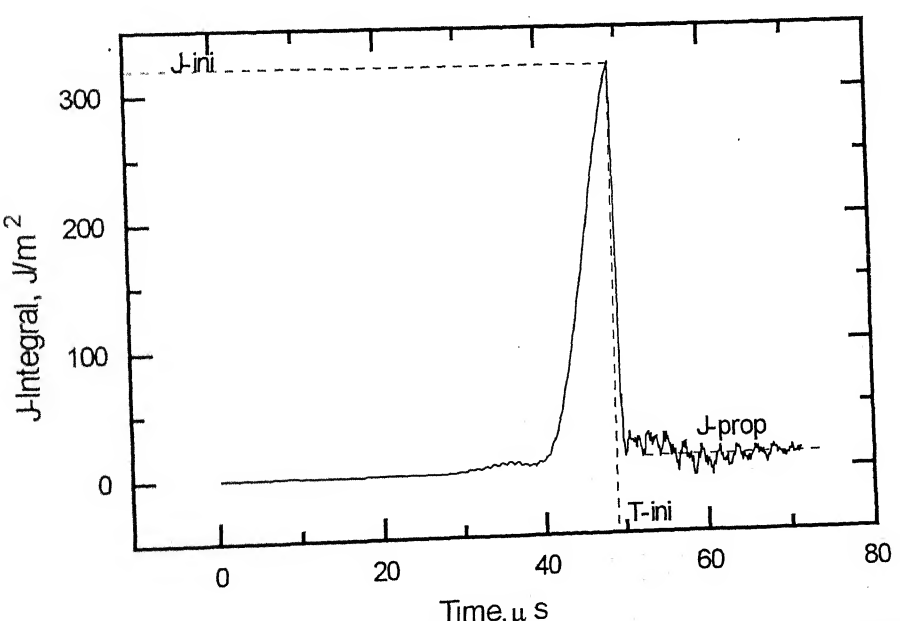

Fig.A.2.3(e) Variation of J-integral for stationary & propagating crack Expt. S-4

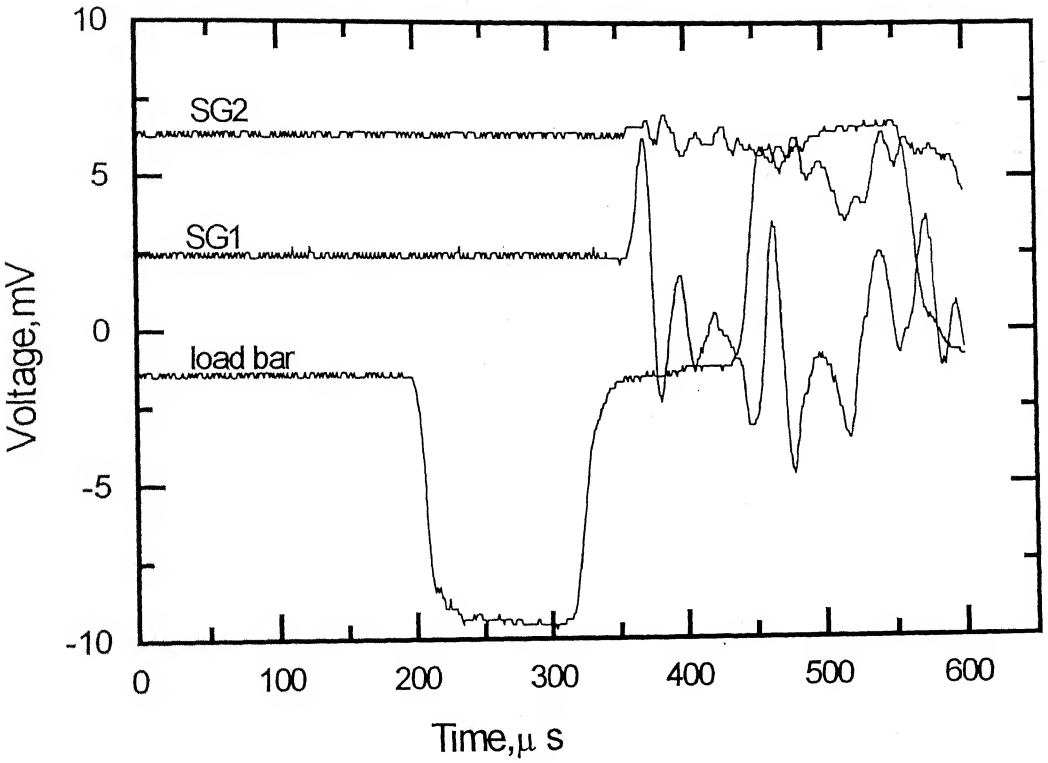

Fig. A.2.4(a) Oscilloscope Records Expt. S-5

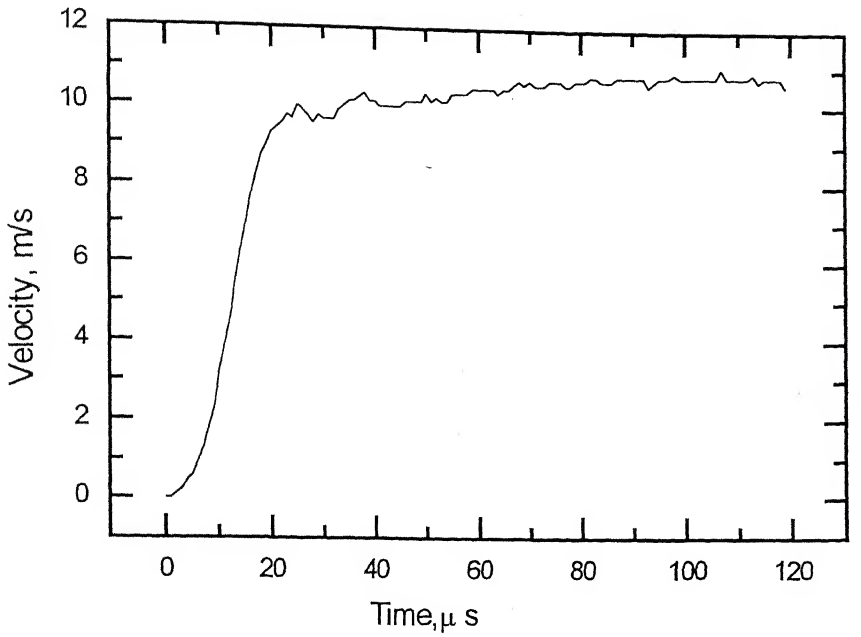

Fig. A.2.4(b) Velocity of load bar end Expt. S-5

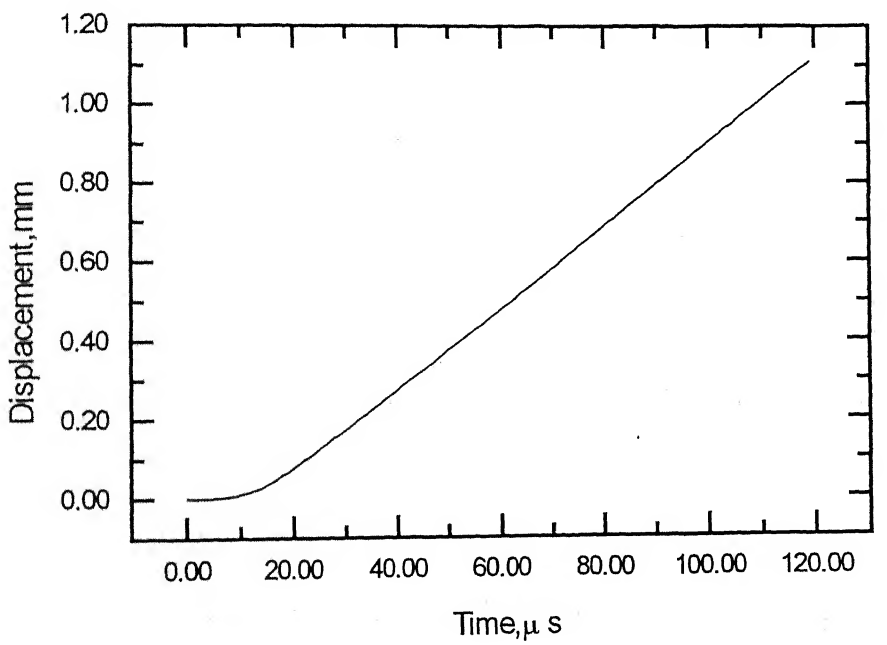

Fig. A.2.4(c) Displacement of cantilever end Expt. S-5

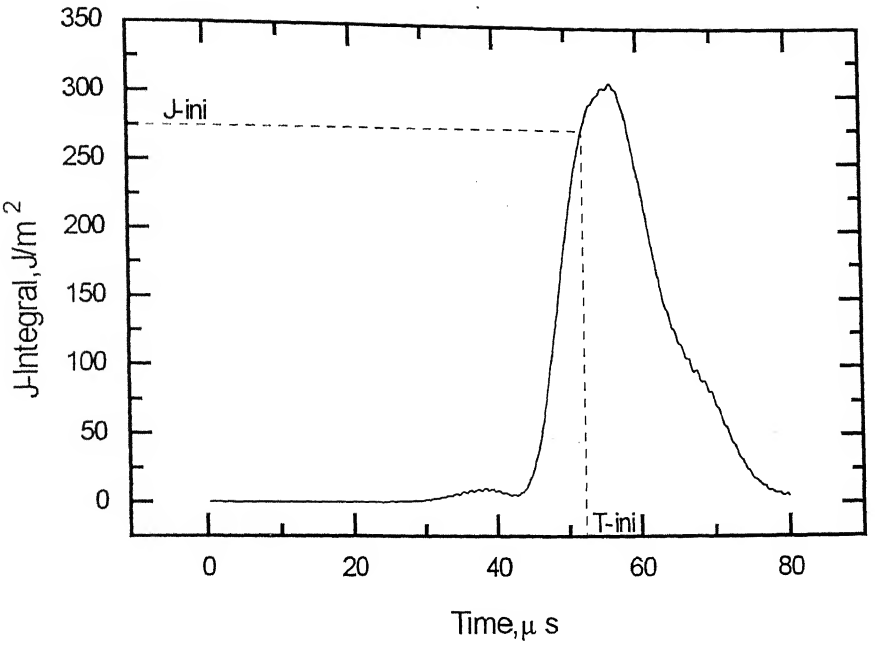

Fig.A.2.4(d) Variation of J-integral for stationary crack Expt. S-5

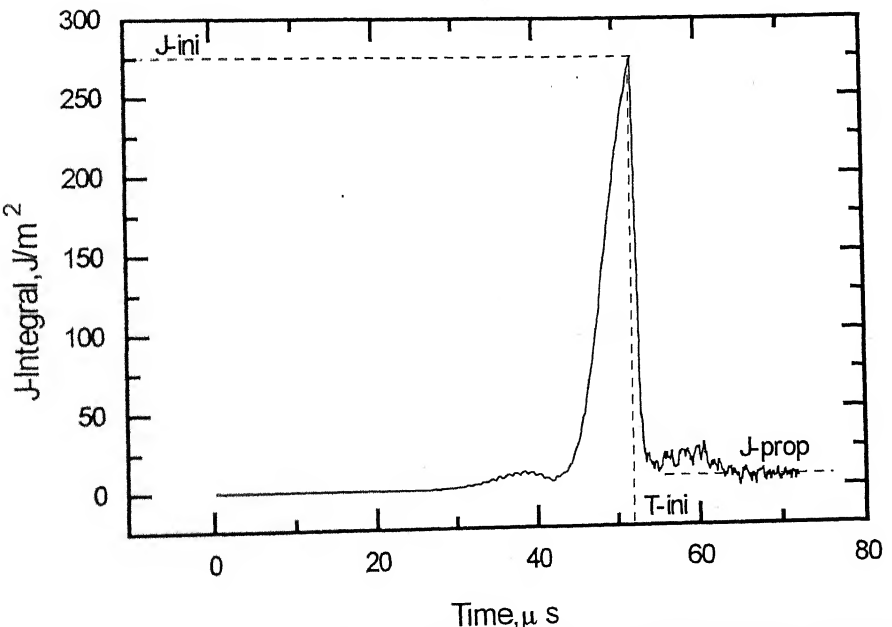

Fig.A.2.4(e) Variation of J-integral for stationary & proppagating crack Expt. S-5

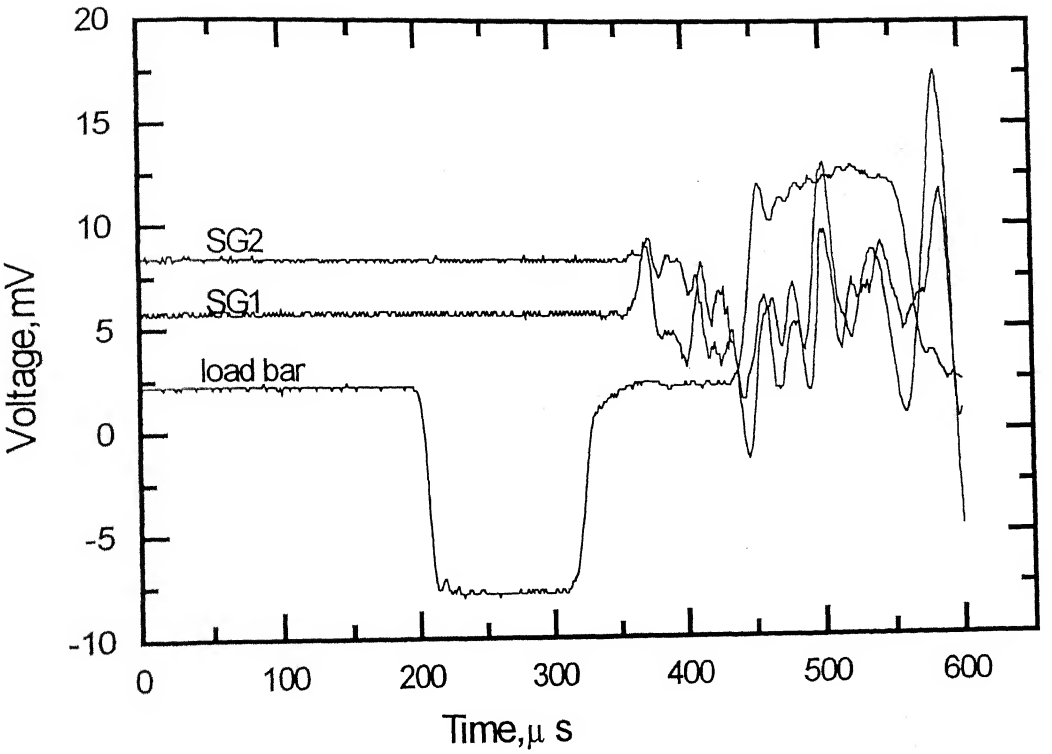

Fig. A.2.5(a) Oscilloscope records Expt. S-6

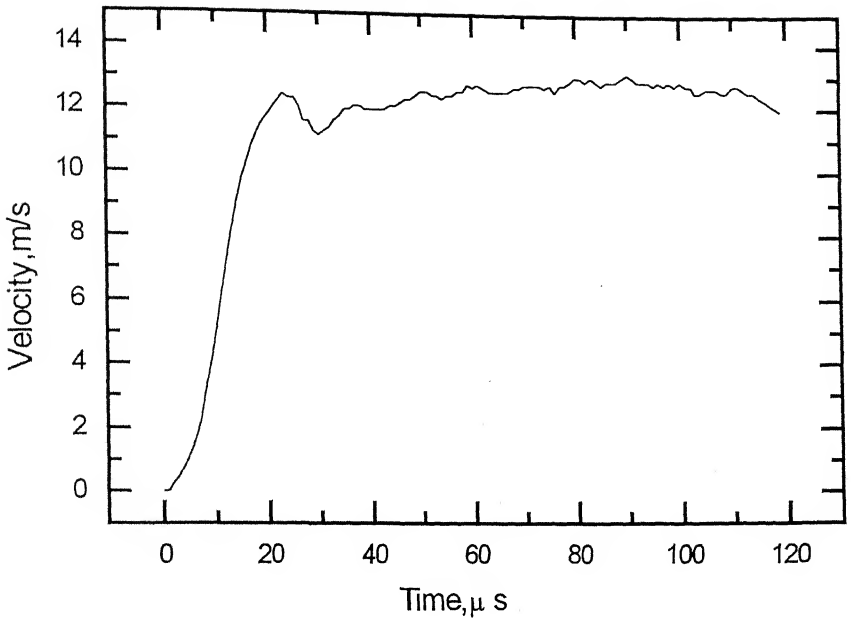

Fig. A.2.5(b) Velocity of load bar end Expt. S-6

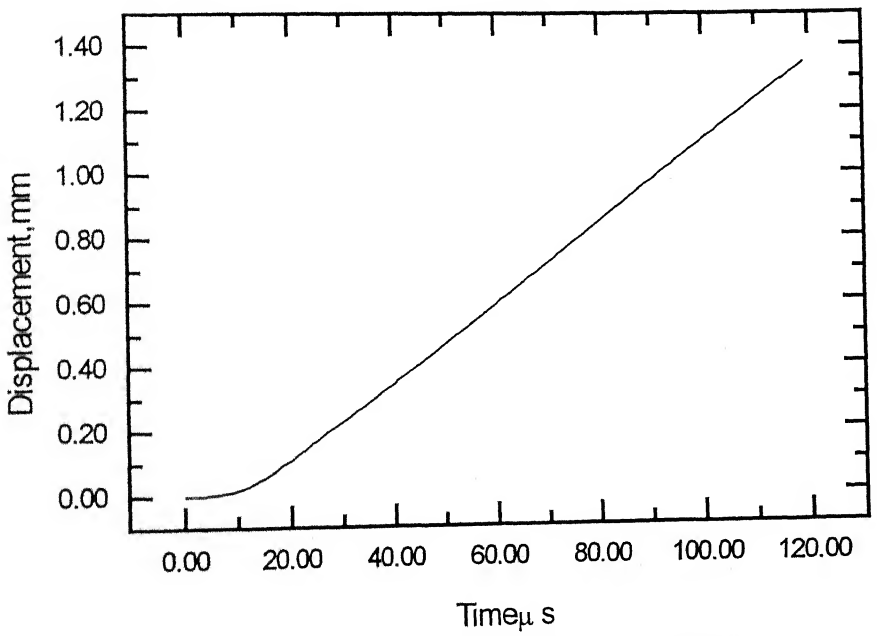

Fig. A.2.5(c) Displacement of cantilever end Expt. S-6

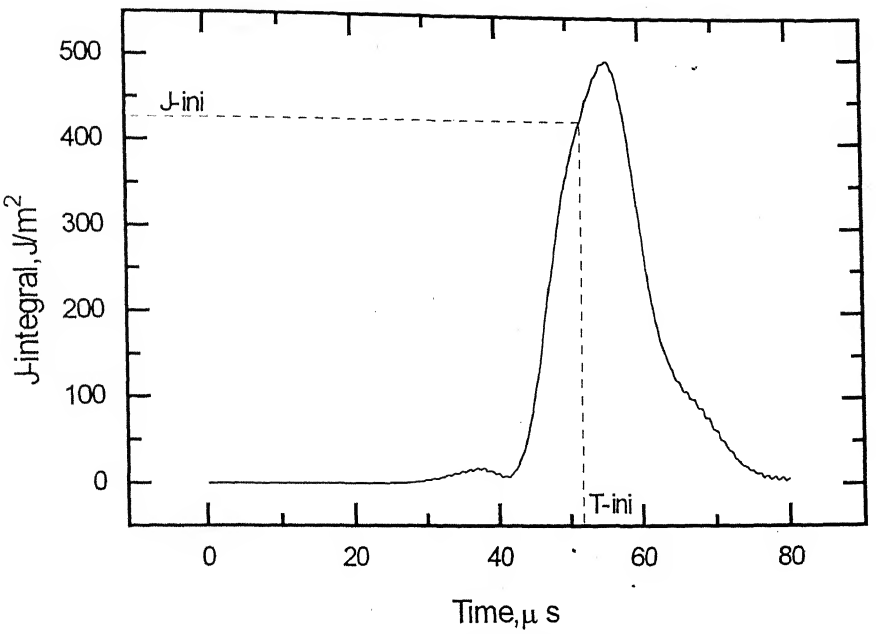

Fig. A.2.5(d) Variation of J-integral for stationary crack Expt. S-6

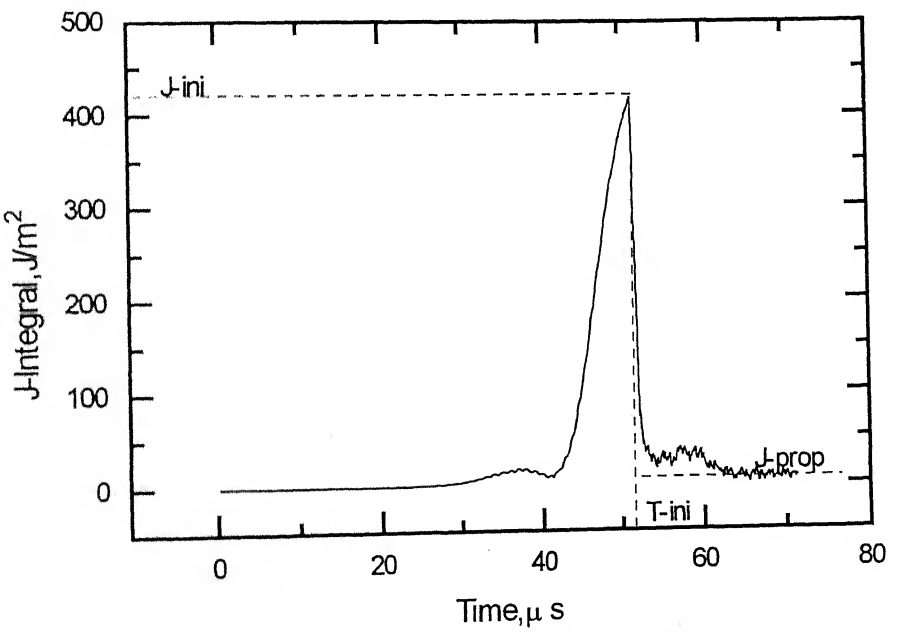

Fig. A.2.5(d) Variation of J-integral for stationary & propagating crack Expt. S-6

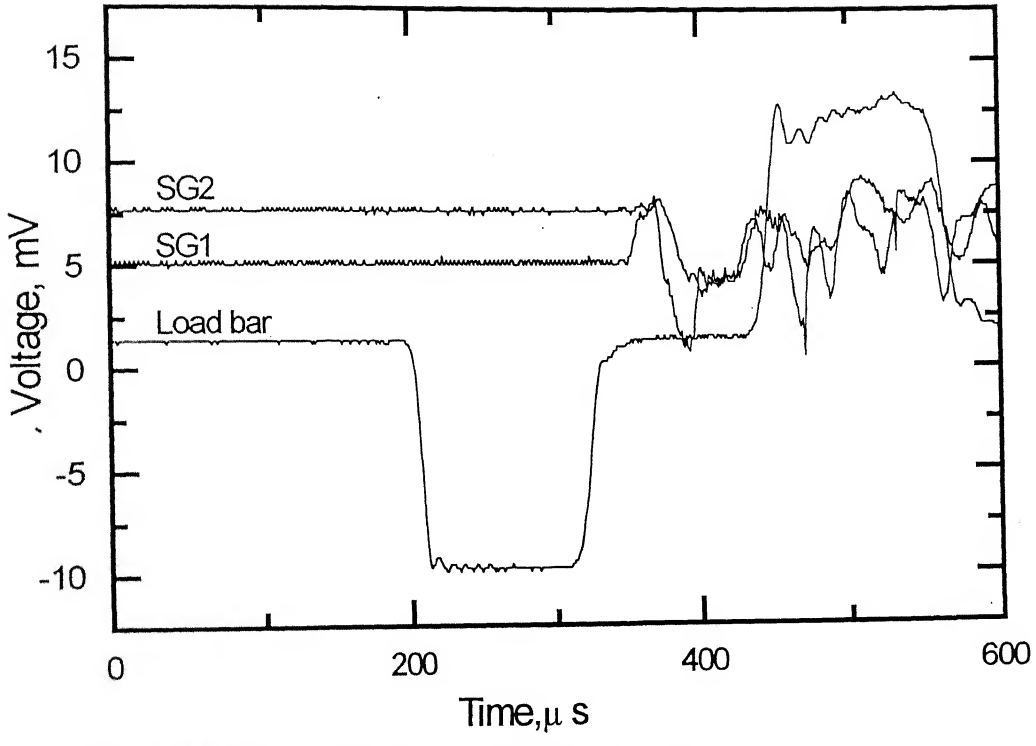

Fig.A.2.6(a) Oscilloscope records Expt. S-7

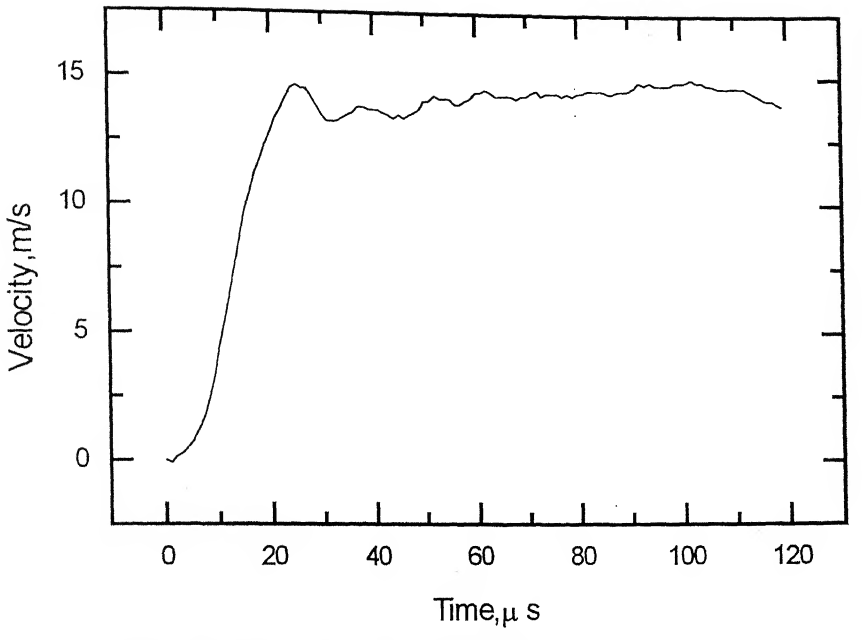

Fig.A.2.6(b) Velocity of load bar end Expt. S-7

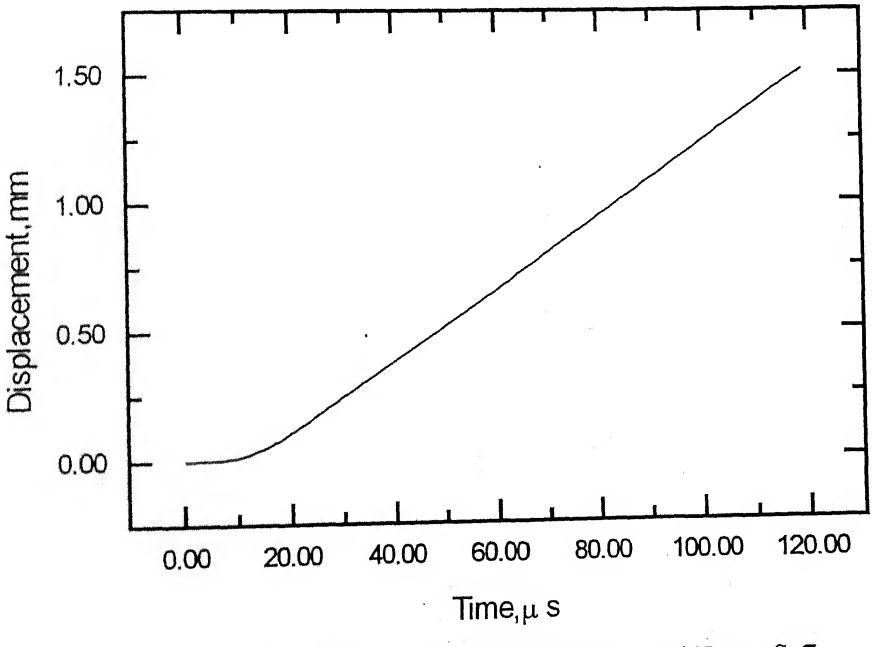

Fig.A.2.6(c) Displacement of cantilever end Expt. S-7

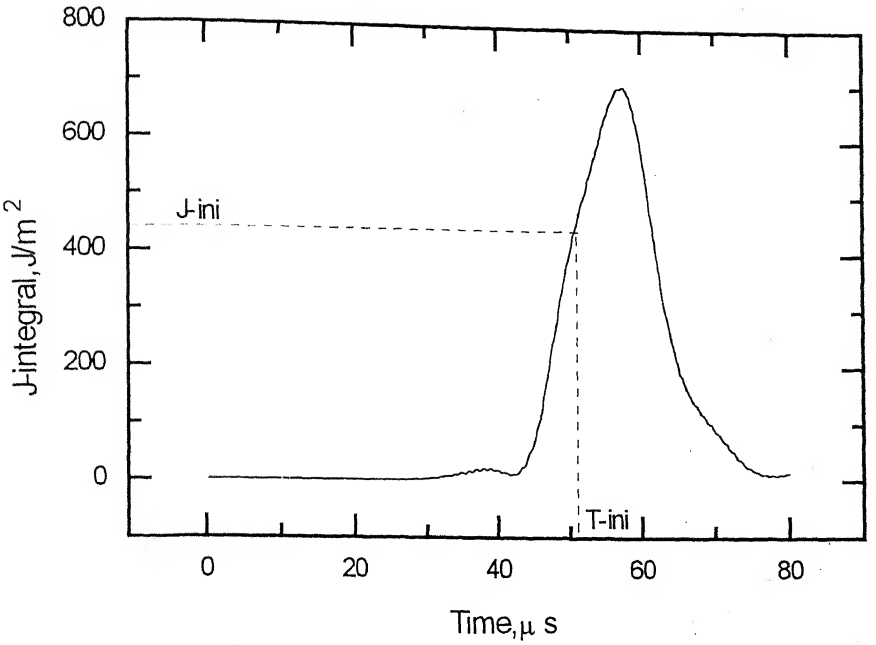

Fig. A.2.6(d) Variation of J-integral for stationary crack Expt. S-7

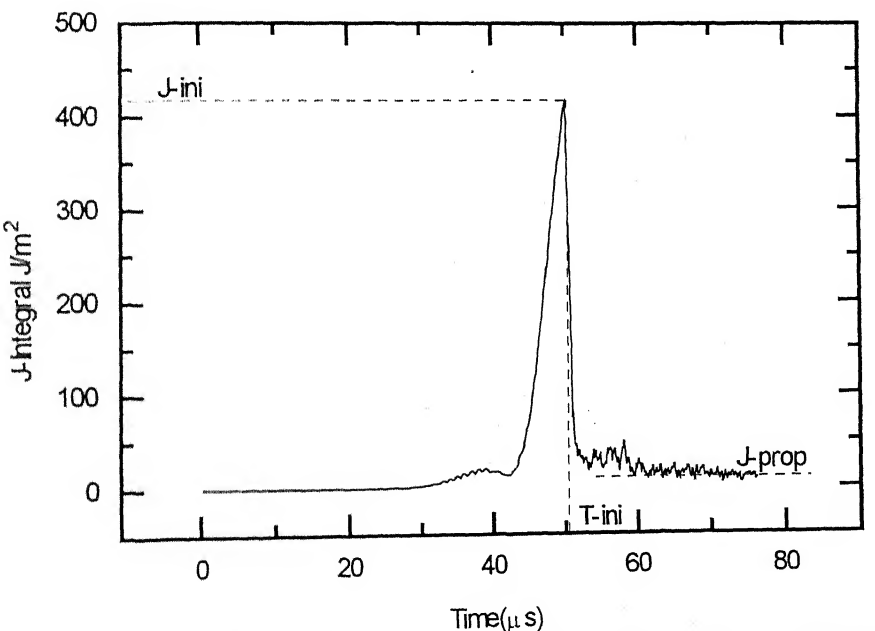

Fig. A.2.6(e) Variation of J-integral for stationary & propagating crack Expt. S-7

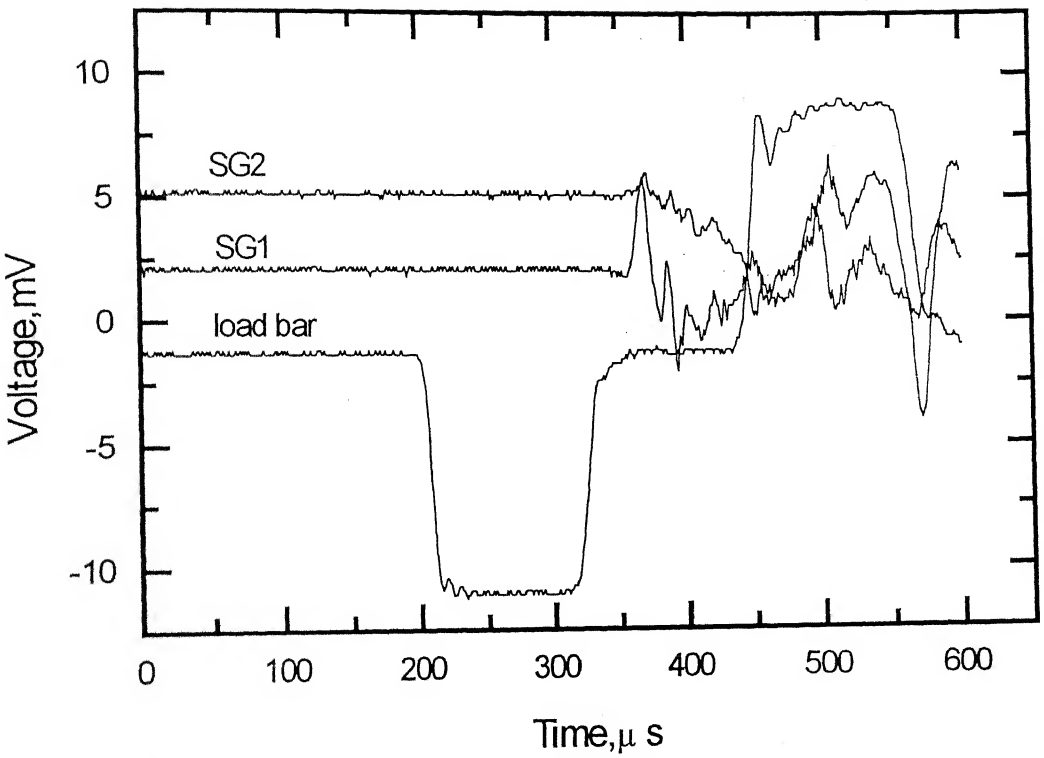

Fig.A.2.7(a) Oscilloscope Records Expt. S-8

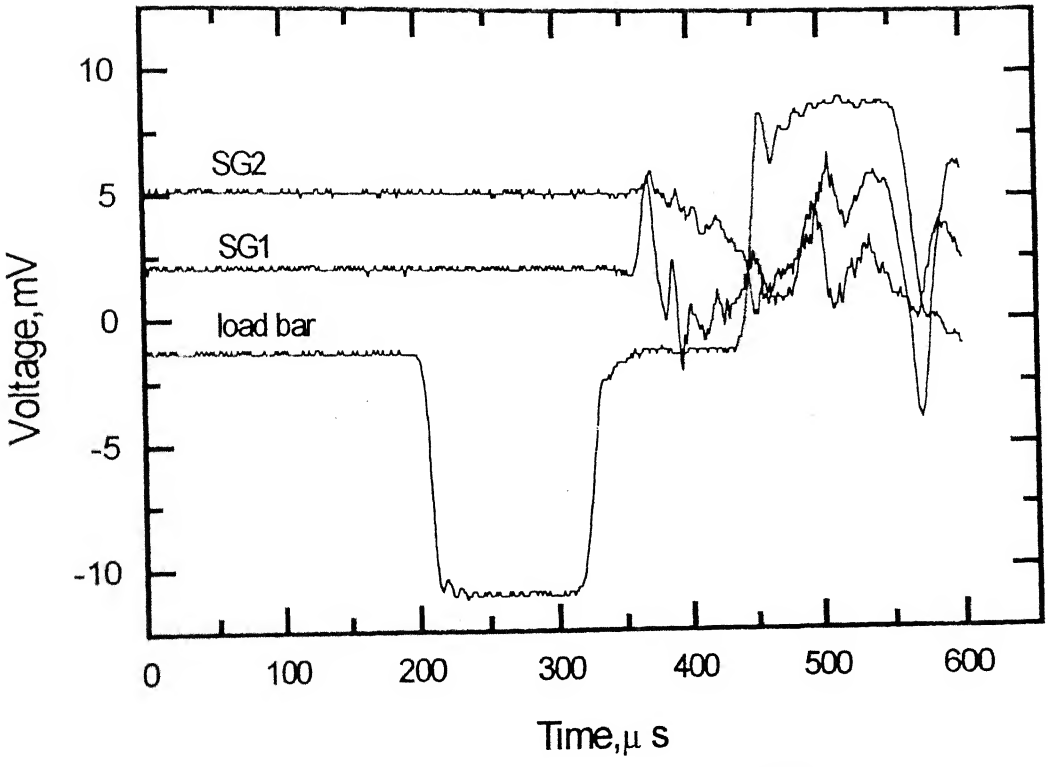

Fig.A.2.7(a) Oscilloscope Records Expt. S-8

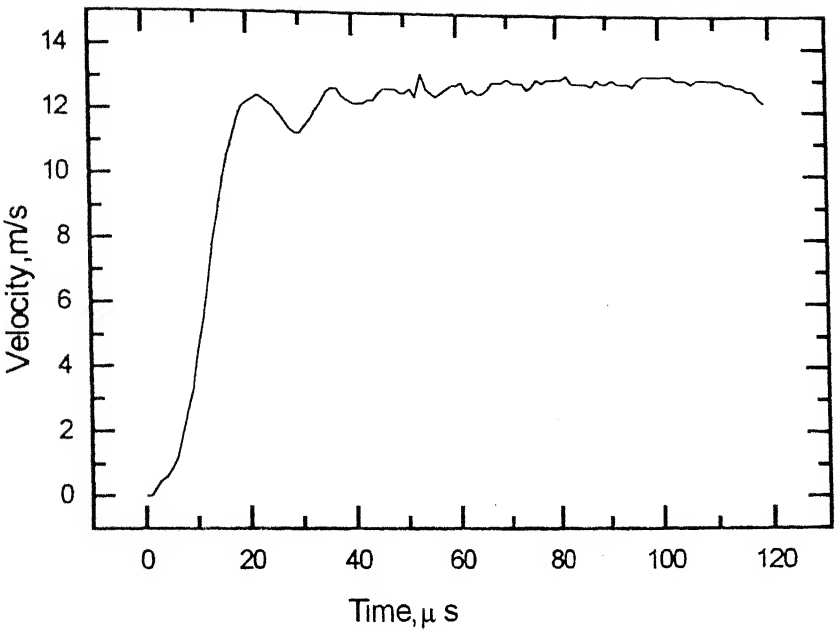

Fig.A.2.7(b) Variation of velocity of load bar end Expt. S-8

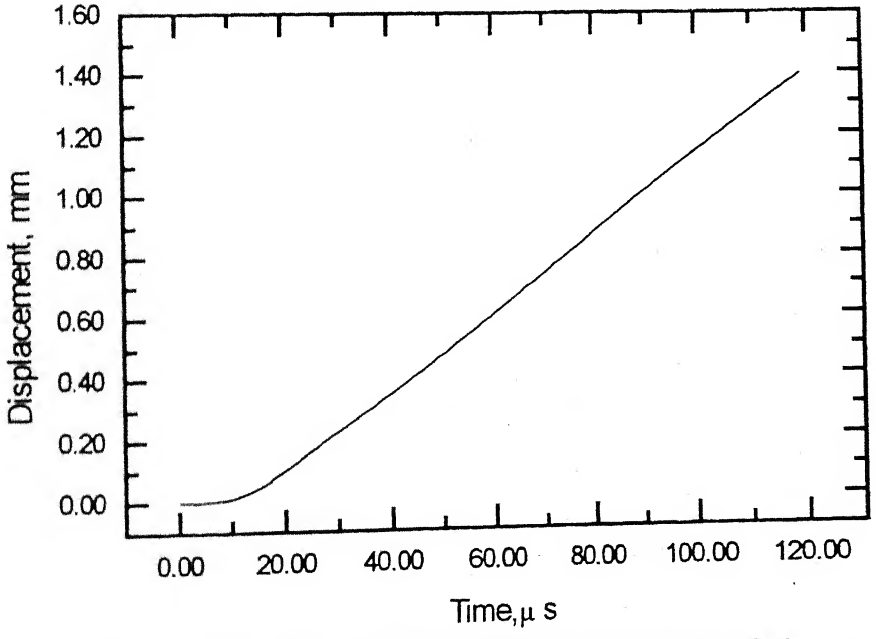

Fig.A.2.7(c) Displacement of cantilever end Expt. S-8

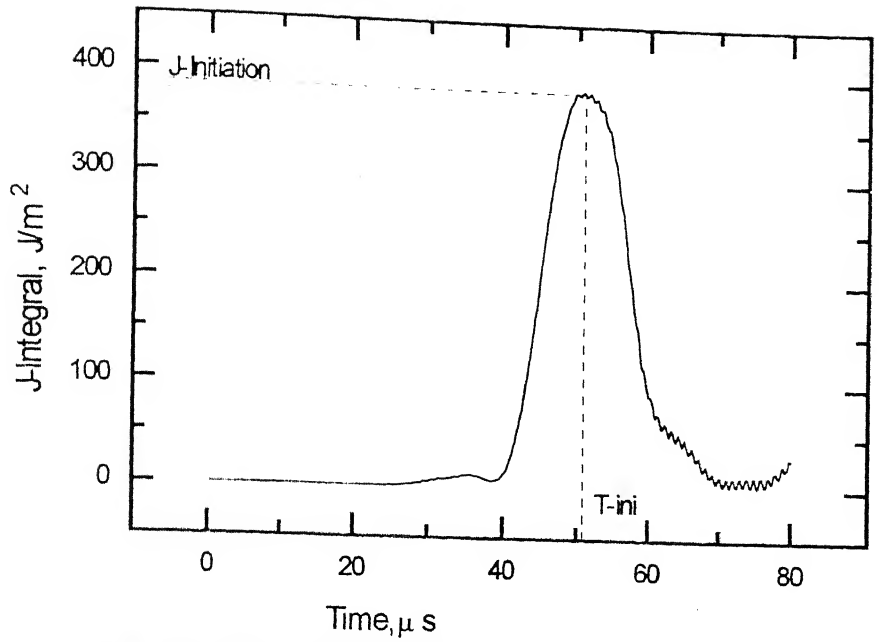

Fig. A.2.7(d) Variation of J-Integral for stationary crack Expt. S-8

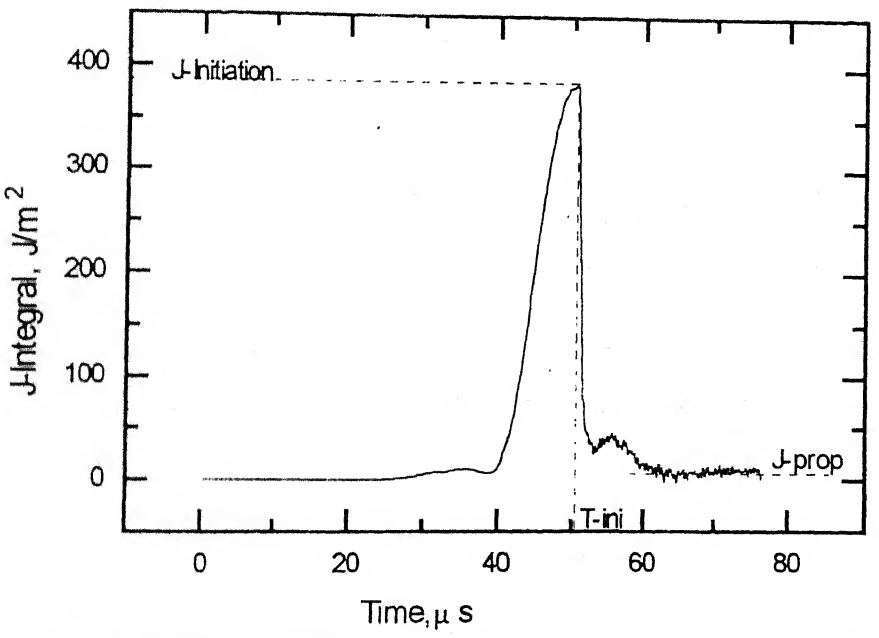

Fig. A.2.7(e) Variation of J-Integral for Stationary & Propagating crack Expt. S-8

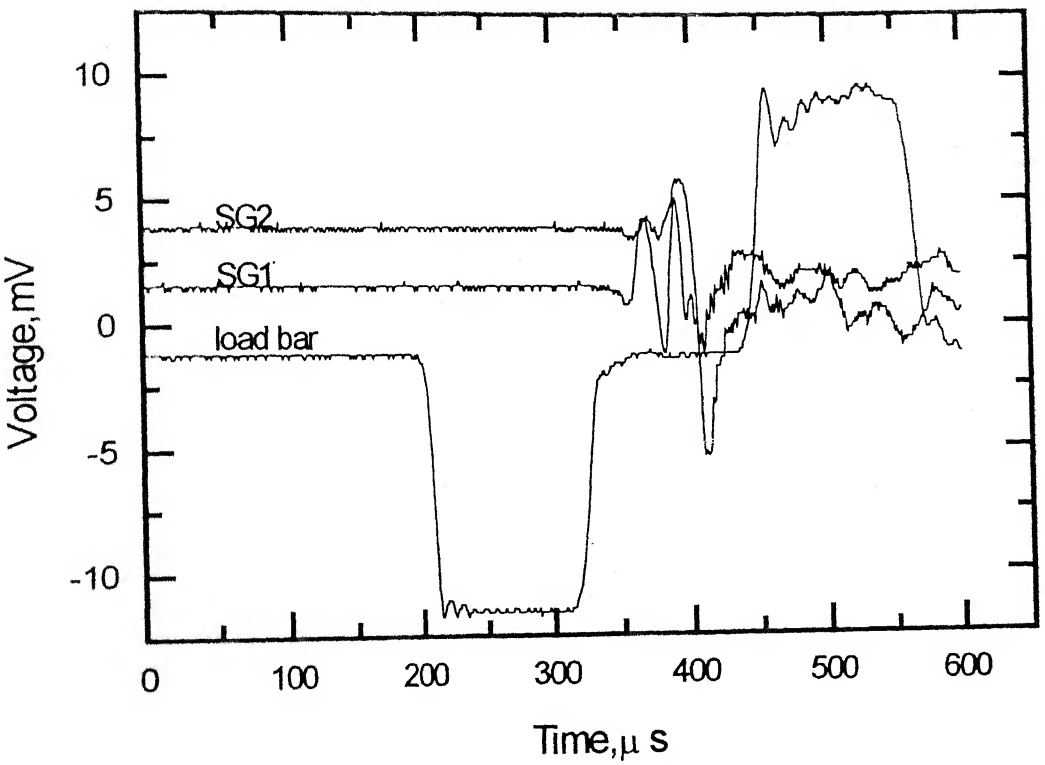

Fig. A.2.8(a) Oscilloscope Records Expt. S-9

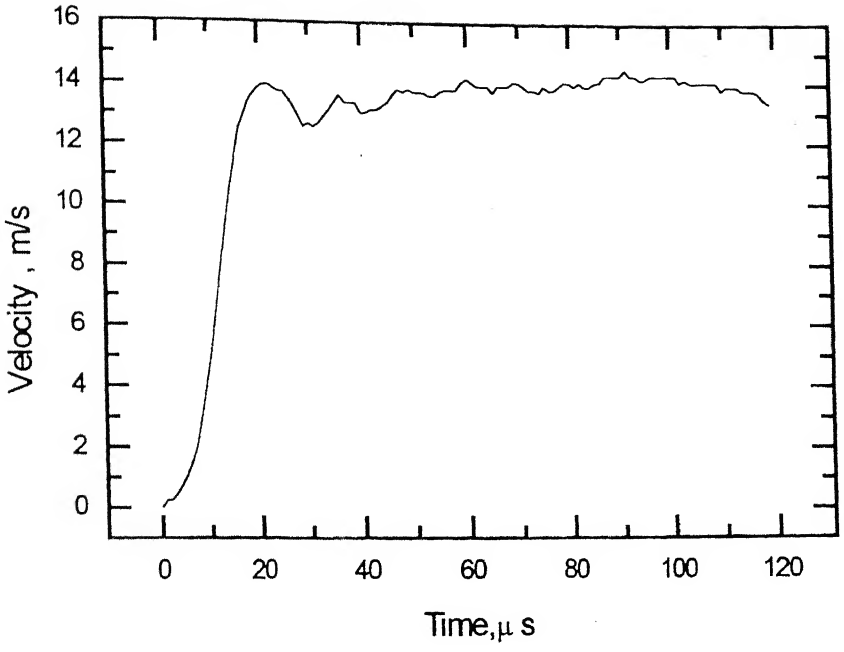

Fig. A.2.8(b) Velocity of load bar end Expt. S-9

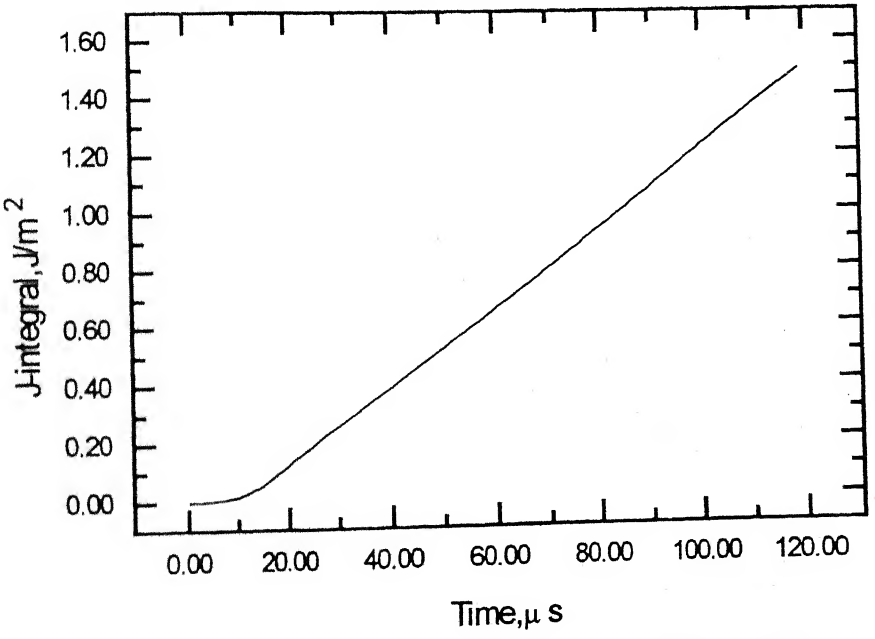

Fig. A.8(c) Displacement of cantilever end Expt. S-9

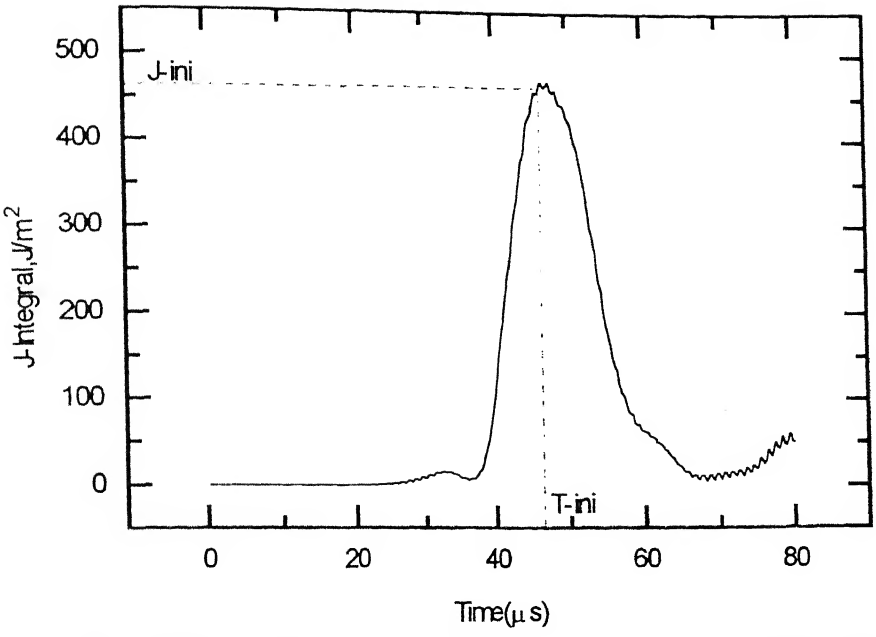

Fig. A.2.8(d) Variation of J-integral for stationary crack Expt. S-9

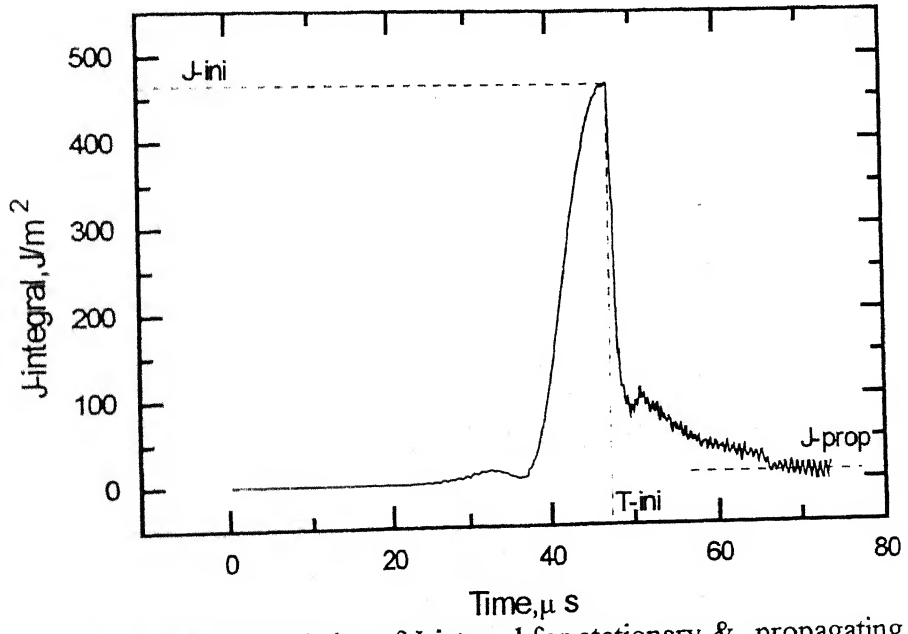

Fig. A.2.8(e) Variation of J-integral for stationary & propagating crack Expt. S-9

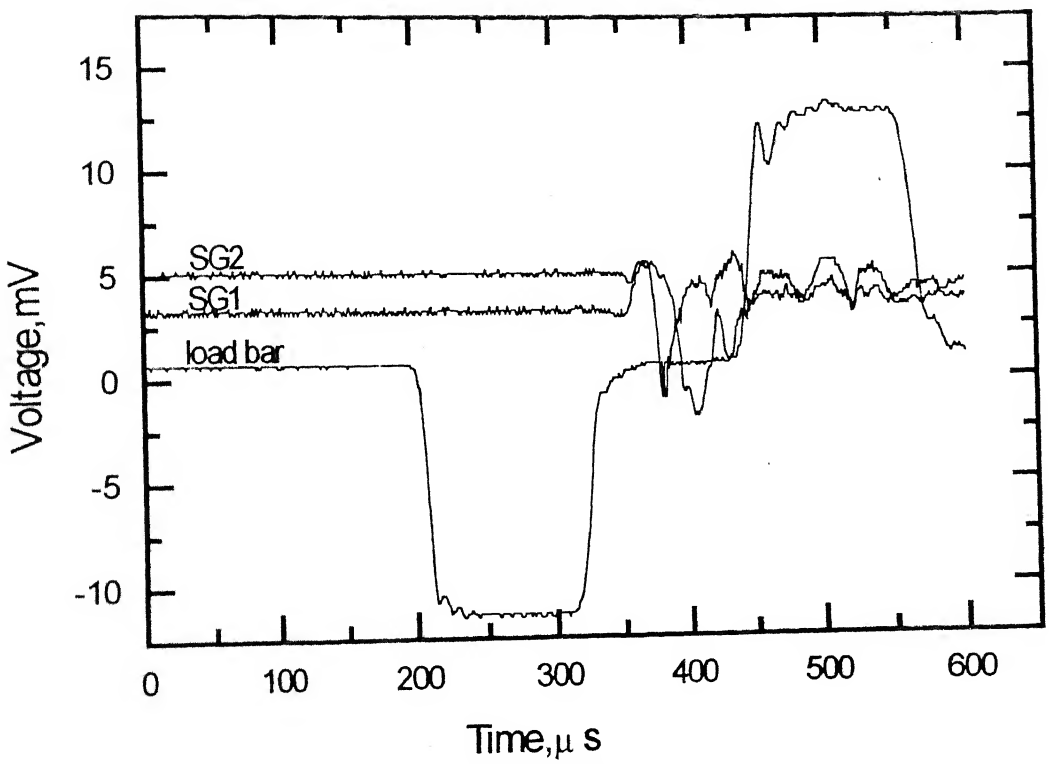

Fig. A.2.9(a) Oscilloscope Records Expt. S-10

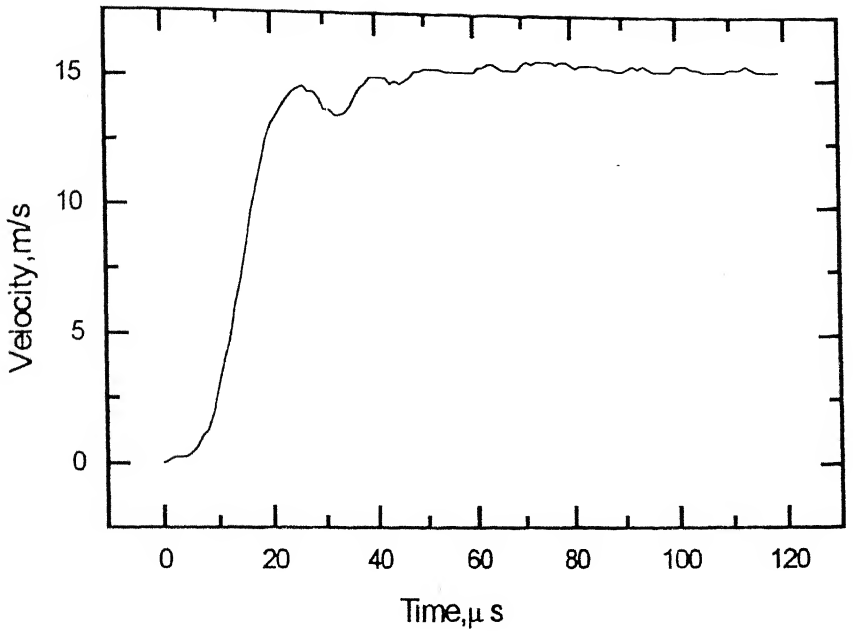

Fig. A.2.9(b) Velocity of load bar end Expt. S-10

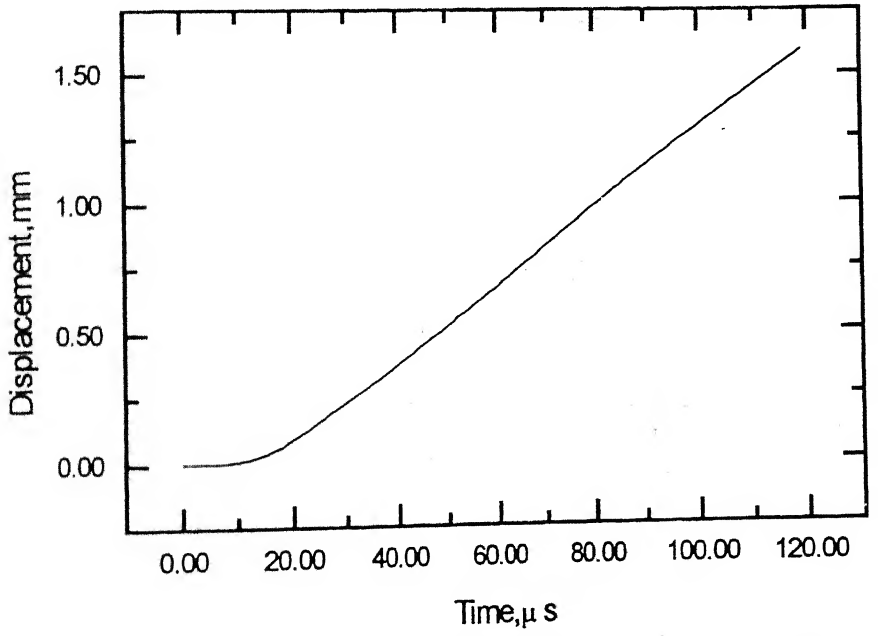

Fig. A.2.9(c) Displacement of cantilever end Expt. S-10

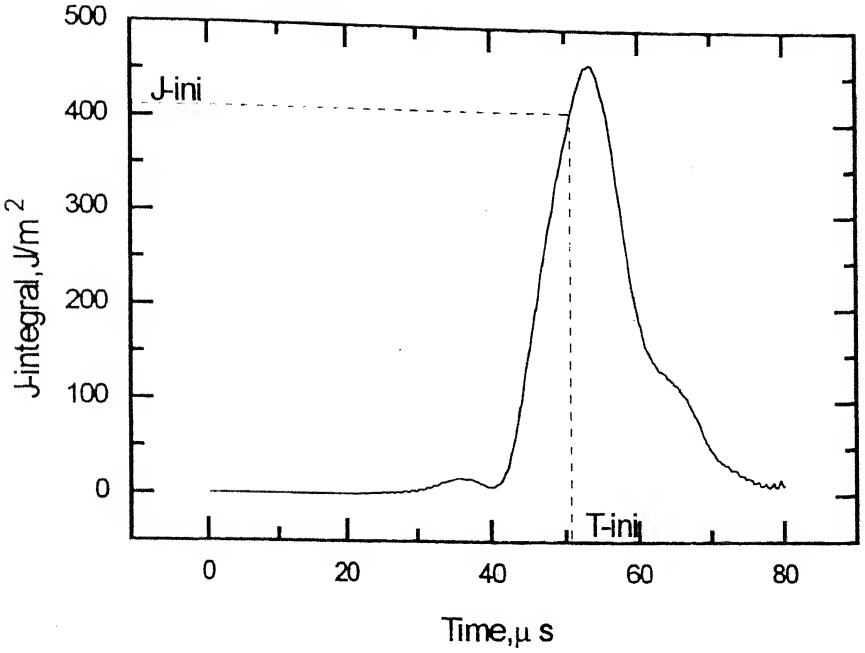

Fig. A.2.9(d) Variation of J-integral for stationary crack Expt.S-10

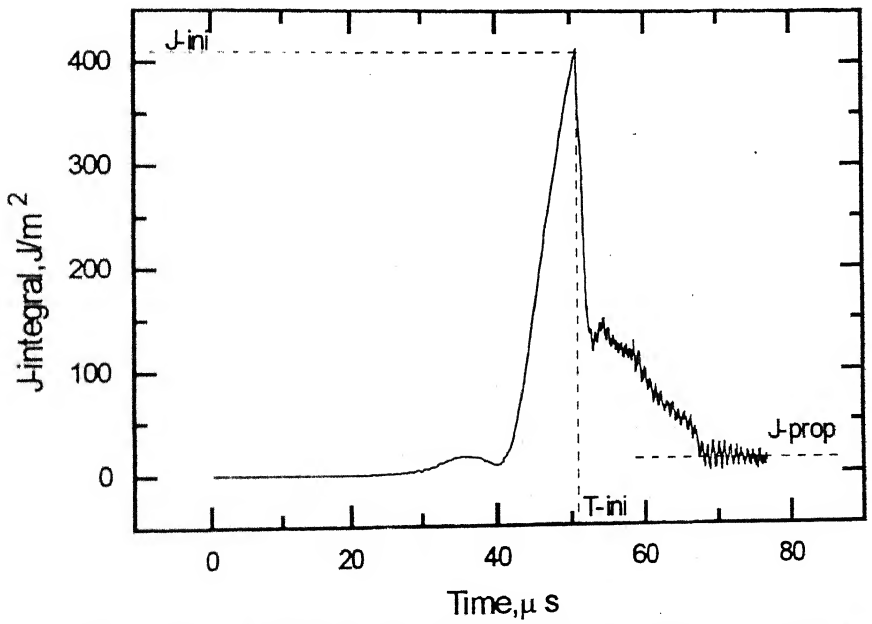

Fig. A.2.9(e) Variation of J-integral for stationary & propagating crack Expt. S-10

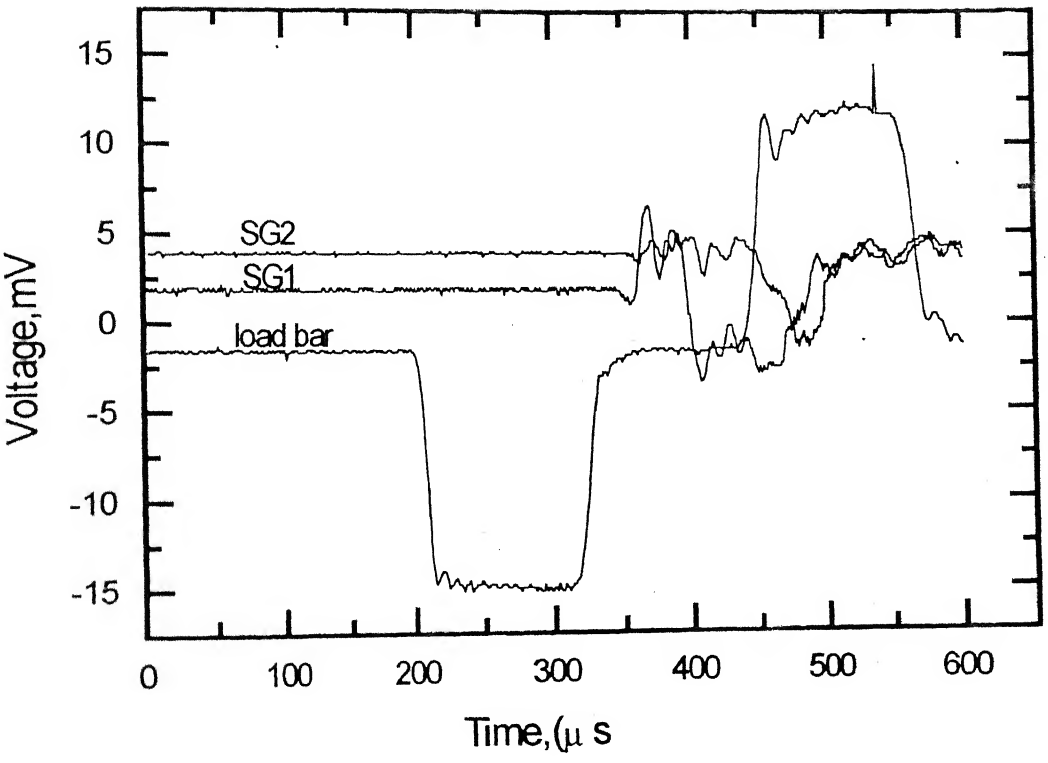

Fig.A.2.10(a) Oscilloscope Records Expt. S-11

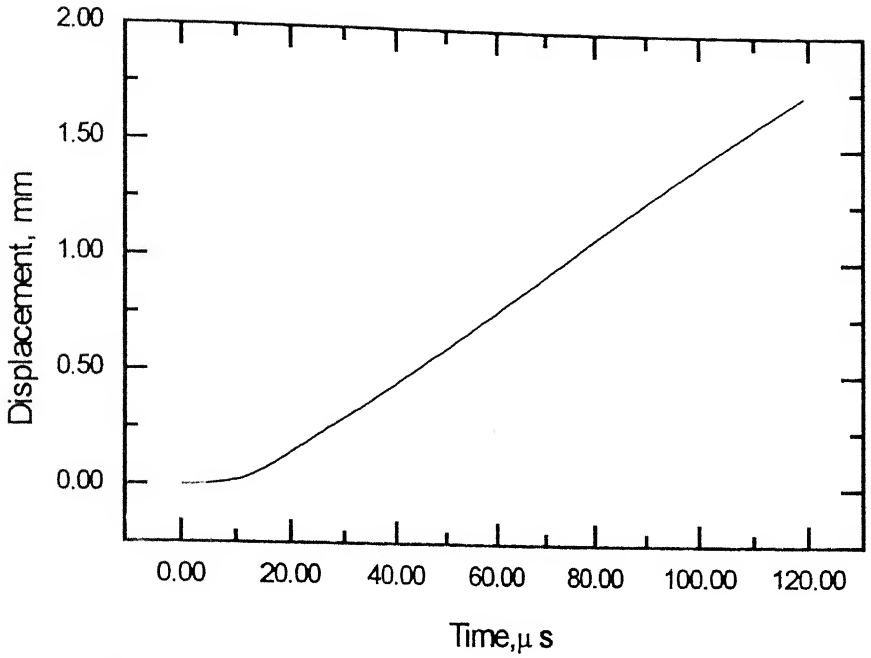

Fig. A.2.10(c) Displacement of cantilever end Expt. S-11

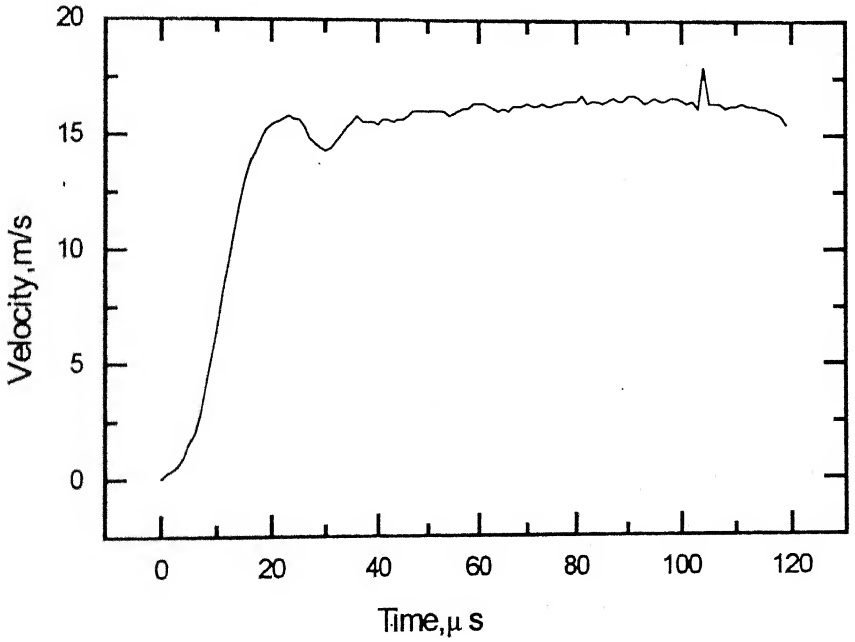

Fig. A.2.10(b) Velocity of load bar end Expt. S-11

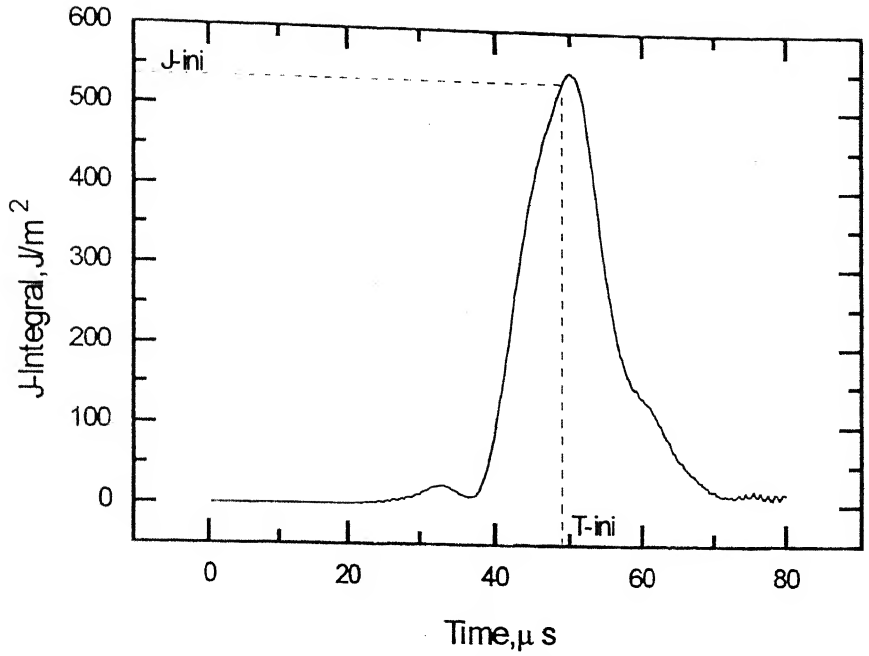

Fig. A.2.10(d) Variation of J-integral for stationary crack Expt. S-11

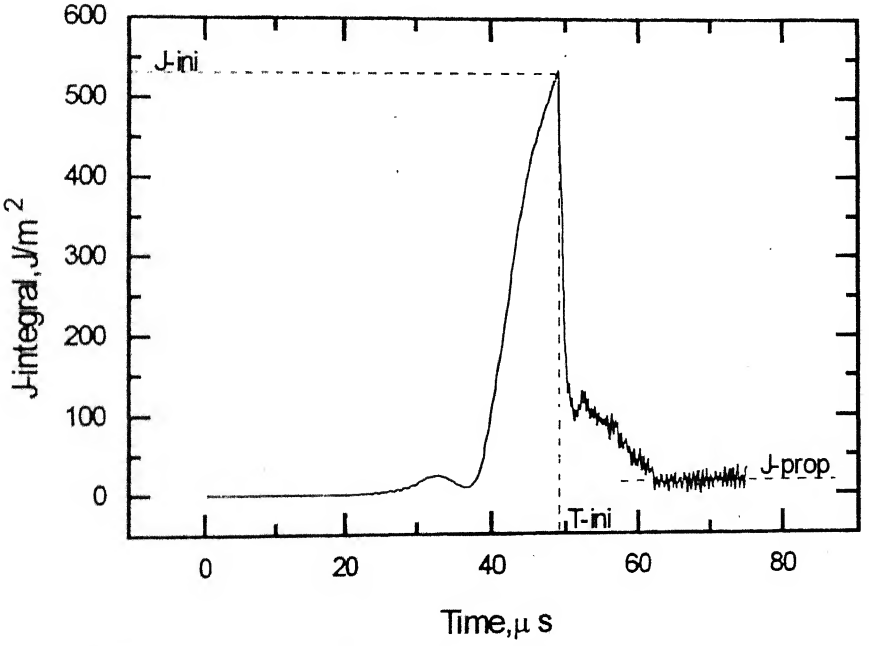

Fig. A.2.10(e) Variation of J-integral for stationary & propagating crack Expt. S-11

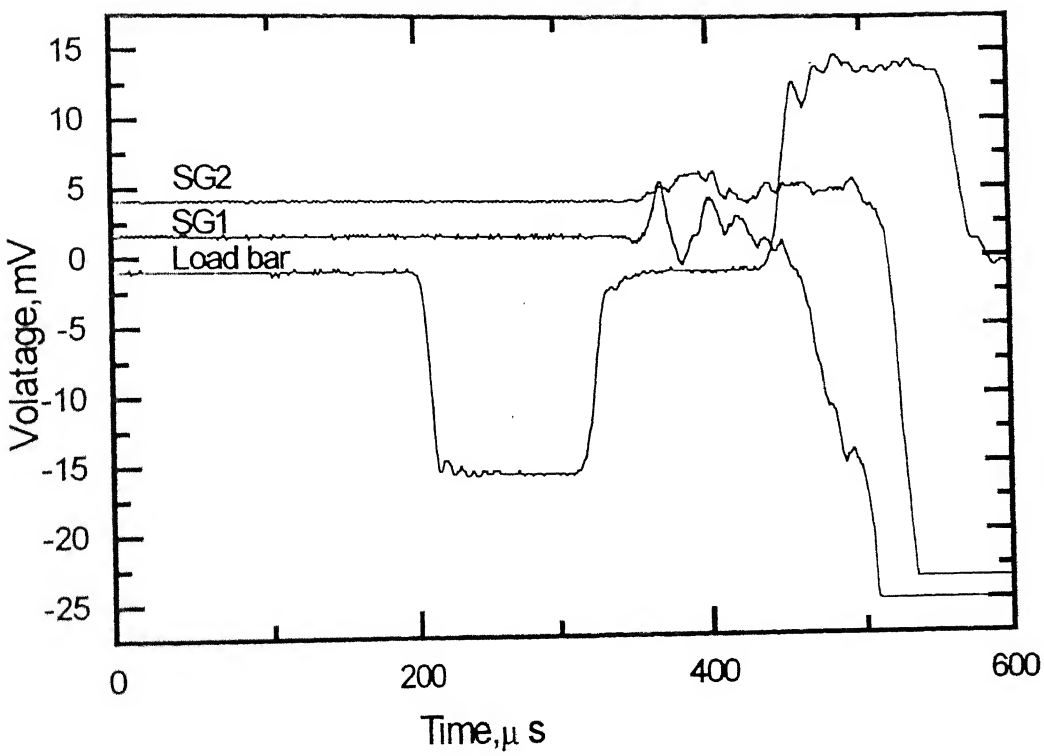

Fig. A.2.11(a) Oscilloscope Records Expt. S-12

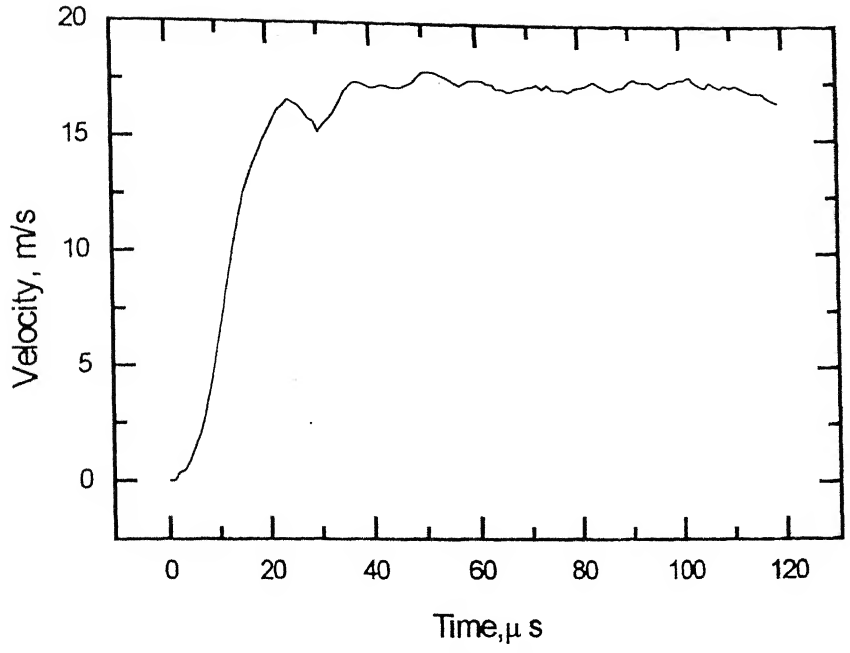

Fig. A.2.11(b) Velocity of load bar end Expt. S-12

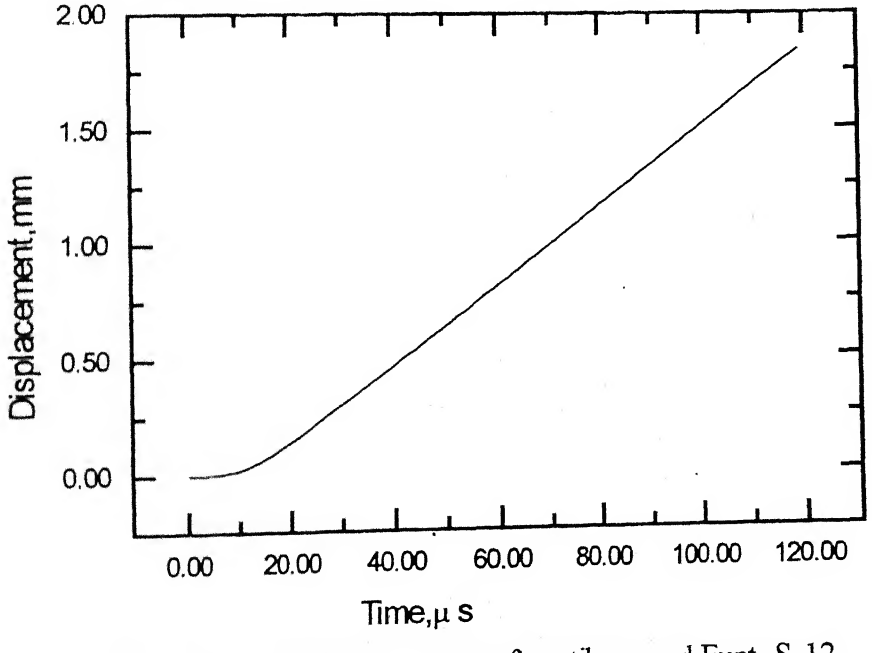

Fig. A.2.11(c) Displacement of cantilever end Expt. S-12

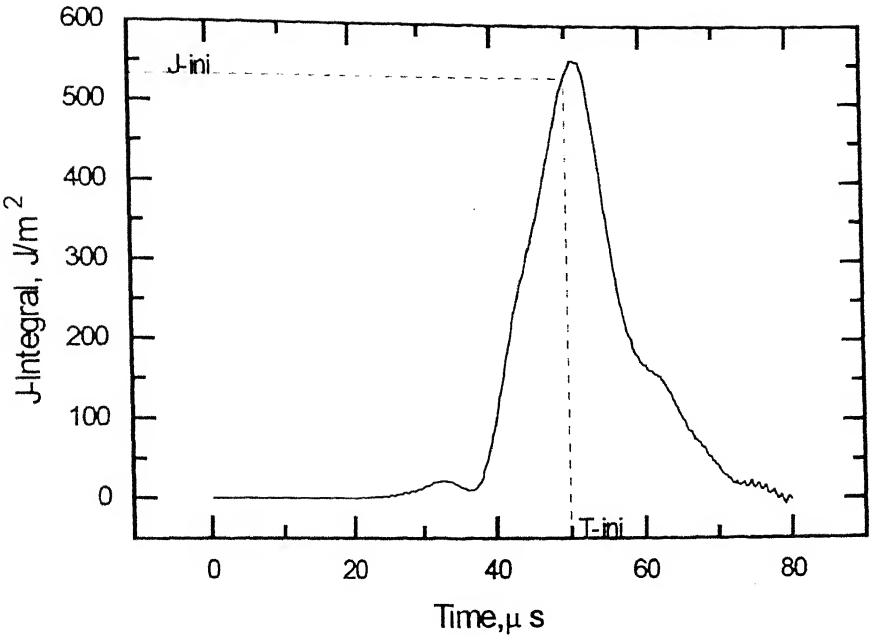

Fig. A.2.11(d) Variation of J-Integral for stationary crack Expt. S-12

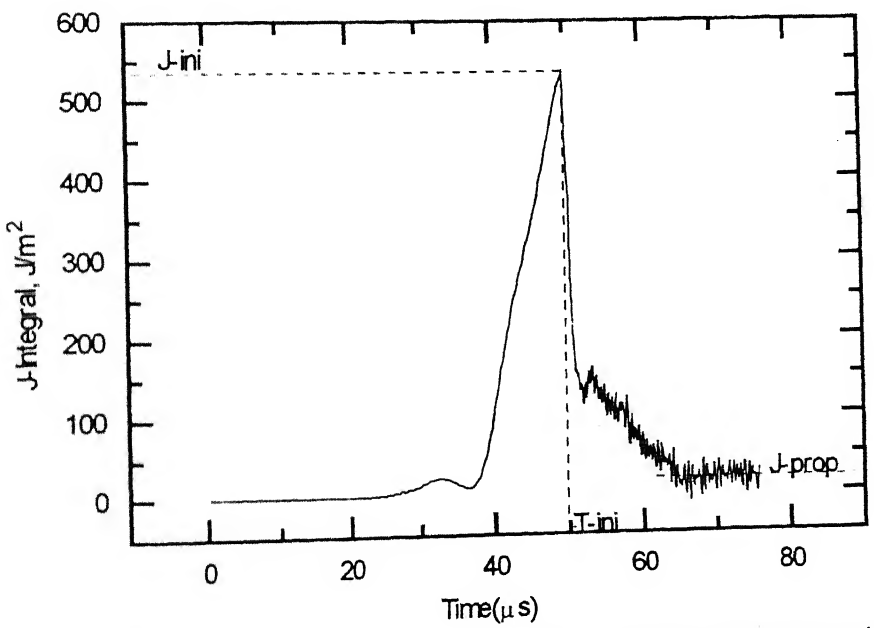

Fig. A.11(e) Variation of J-Integral for stationary & propagating crack Expt. S-12

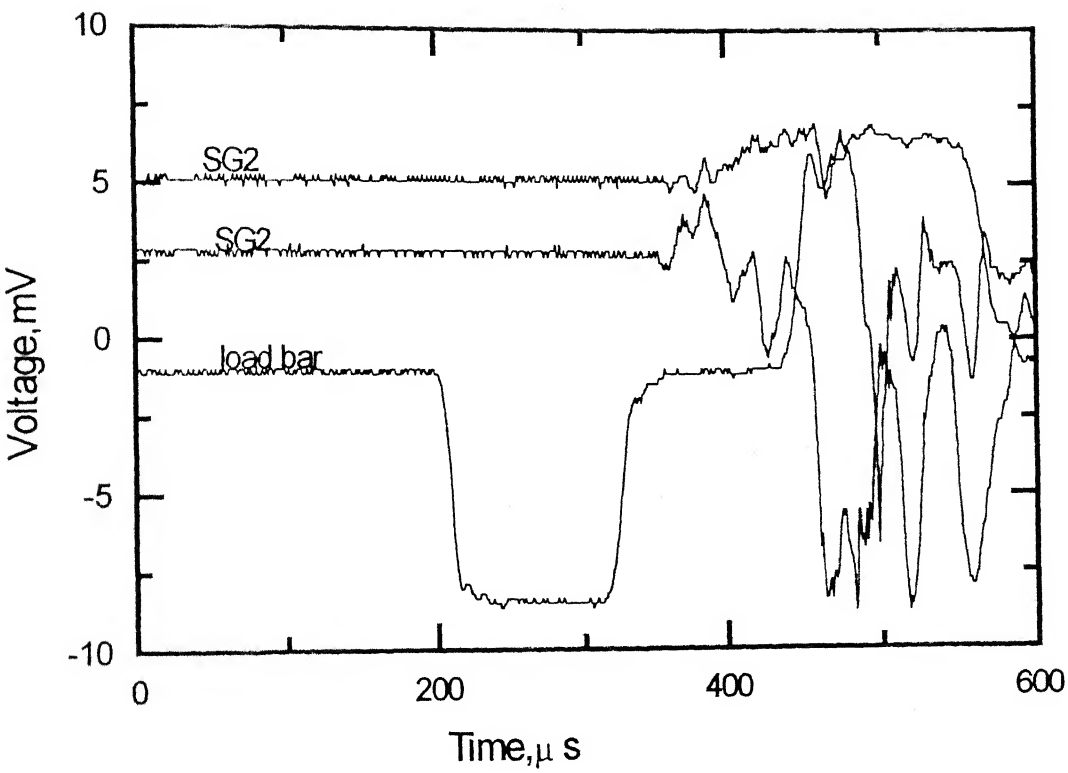

Fig. A.2.12(a) Oscilloscope Records Expt. S-13

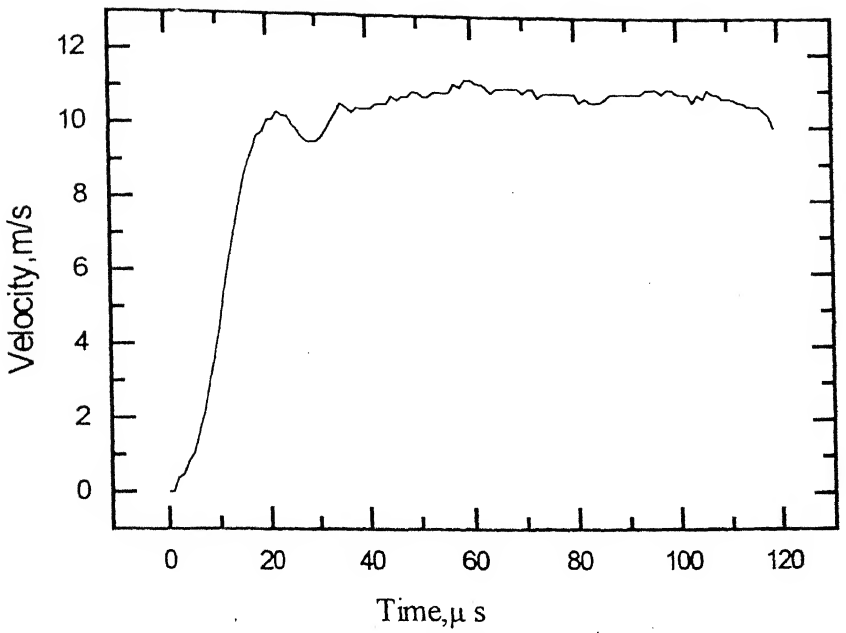

Fig. A.2.12(b) Velocity of load bar end Expt. S-13

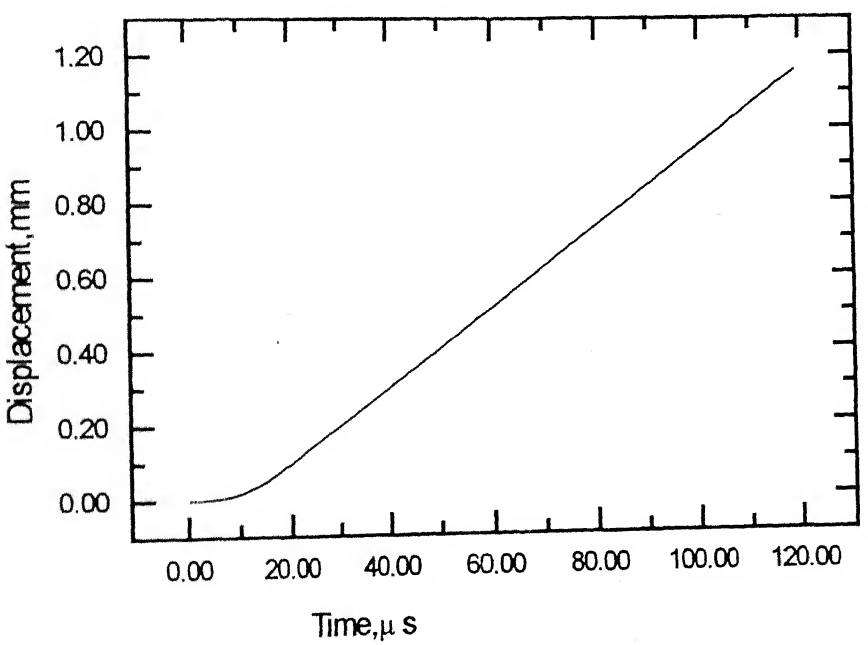

Fig. A.2.12(c) Displacement of cantilever end Expt. S-13

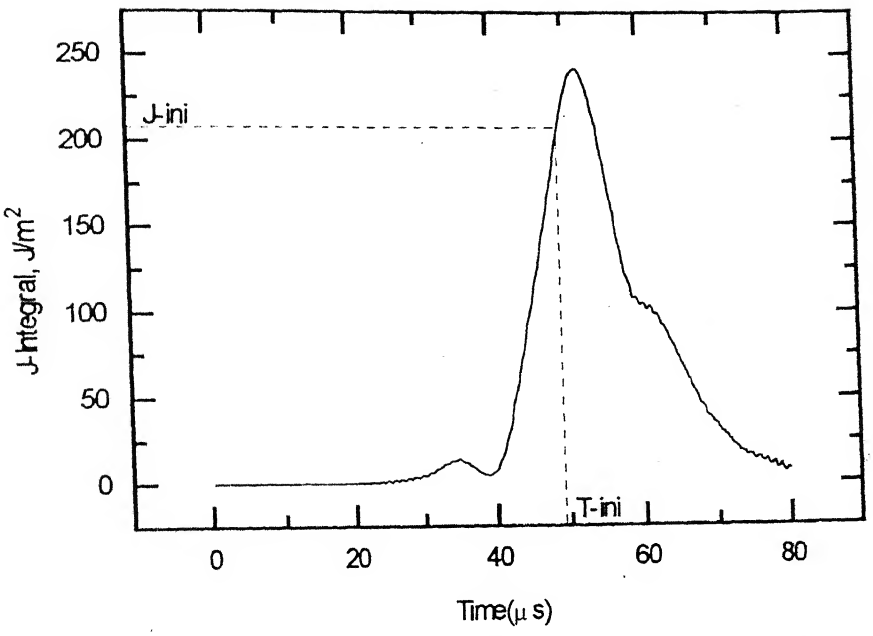

Fig. A.2.12(d) Variation of J-Integral for stationary crack Expt. S-13

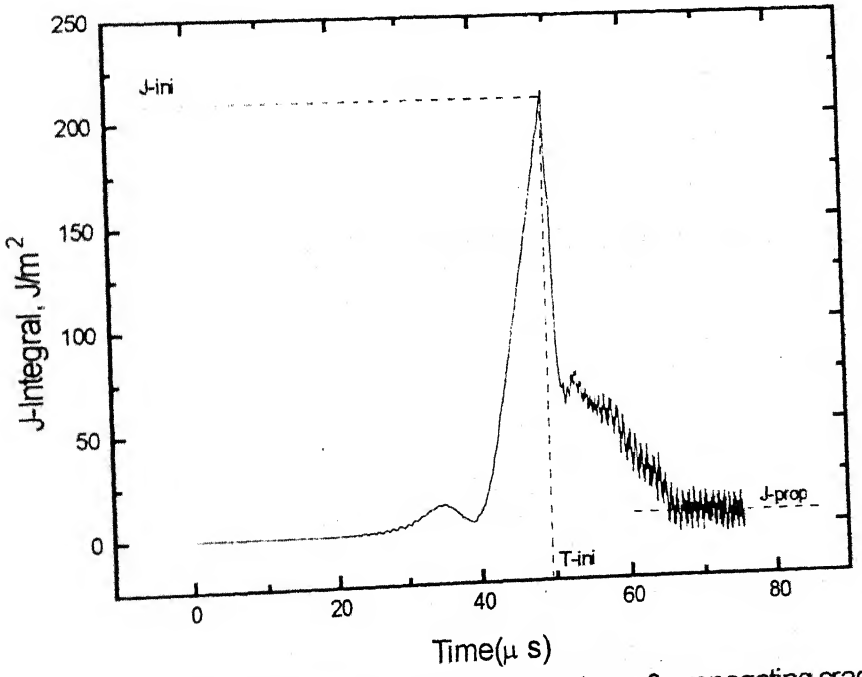

Fig:4.23(e) Variation of J-Integral for stationry & propagating crack

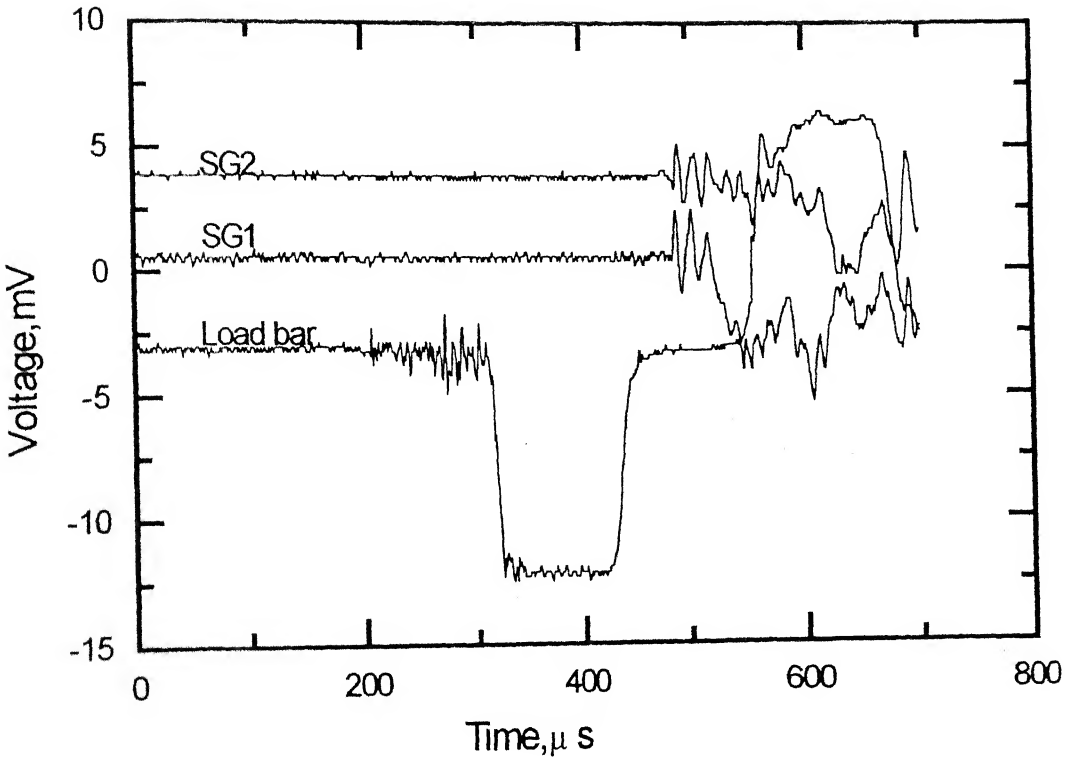

Fig. A.2.13(a) Oscilloscope Records Expt. L-1

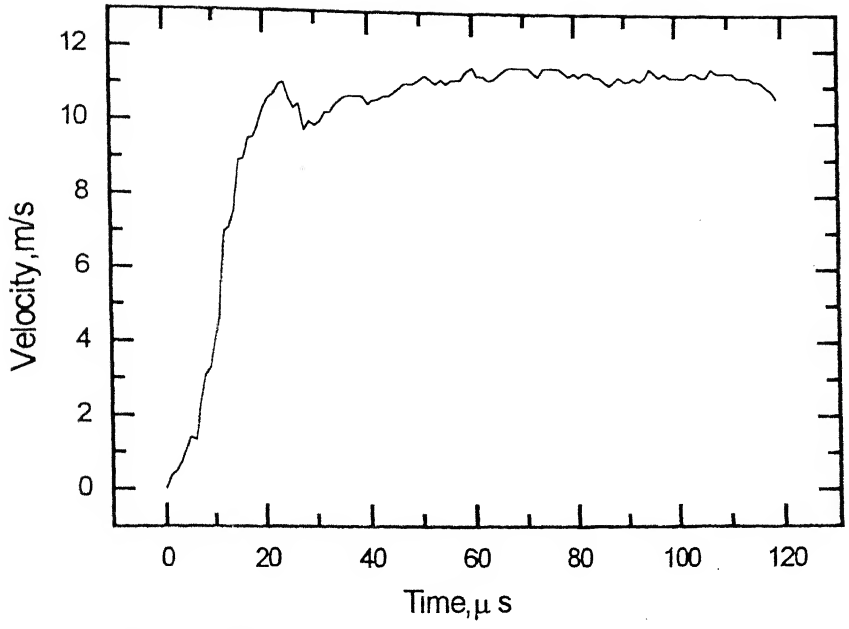

Fig.A.2.13(b) Variation of velocity of load bar end Expt. L-1

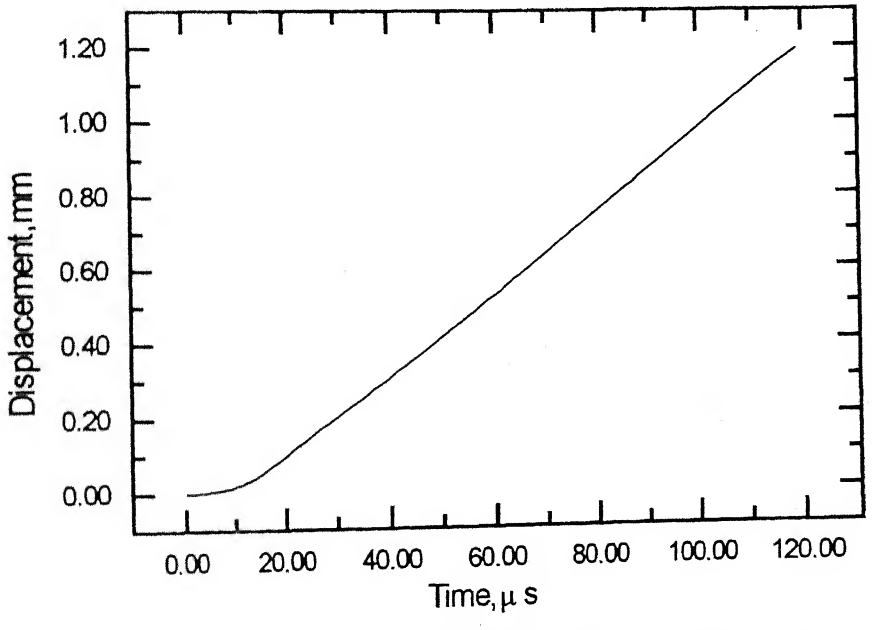

Fig.A.2.13(c) Displacement of cantilever end Expt. L-1

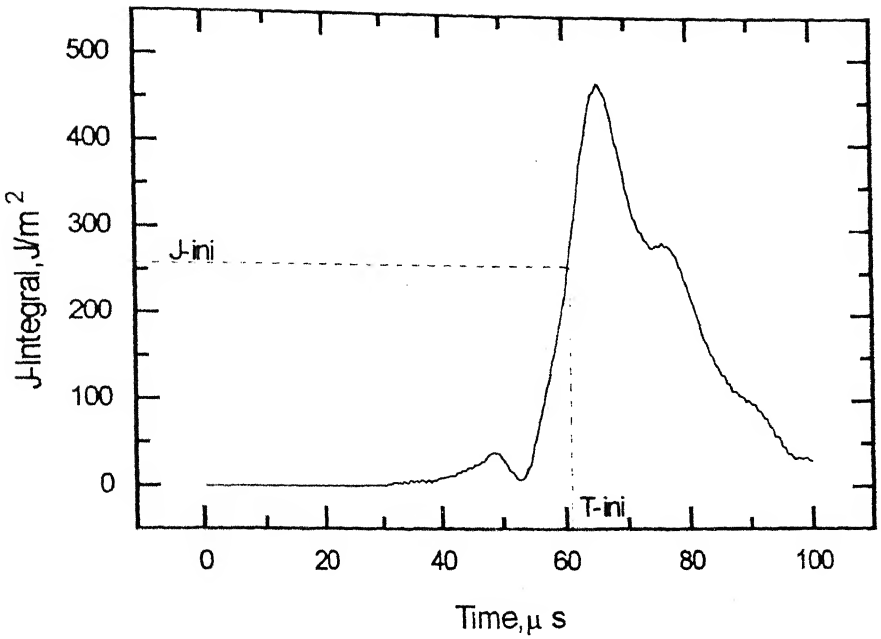

Fig. A.2.13(d) Variation of J-Integral for stationary crack Expt.L-1

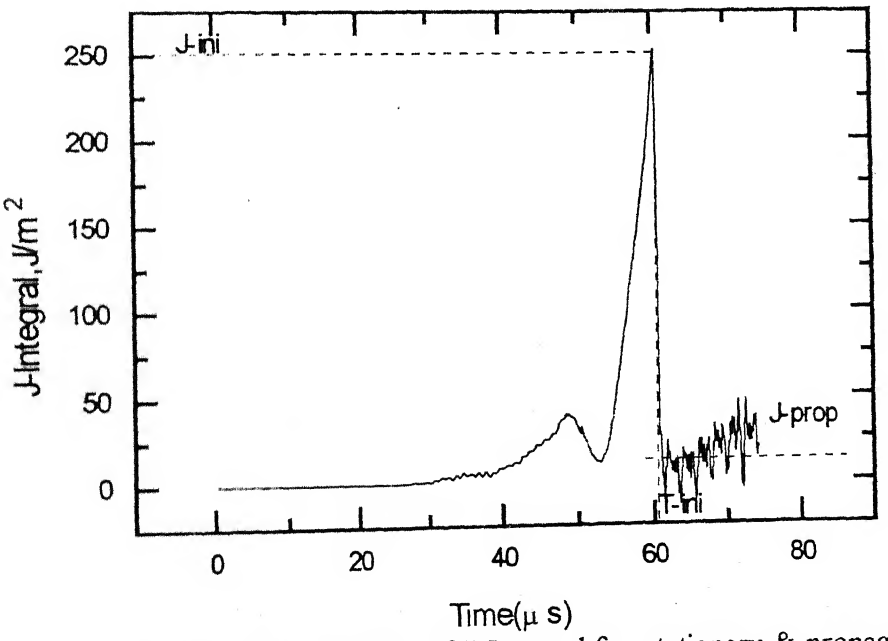

Fig. A.2.13(e) Variation of J-Integral for stationary & propagating crack Expt.L-1

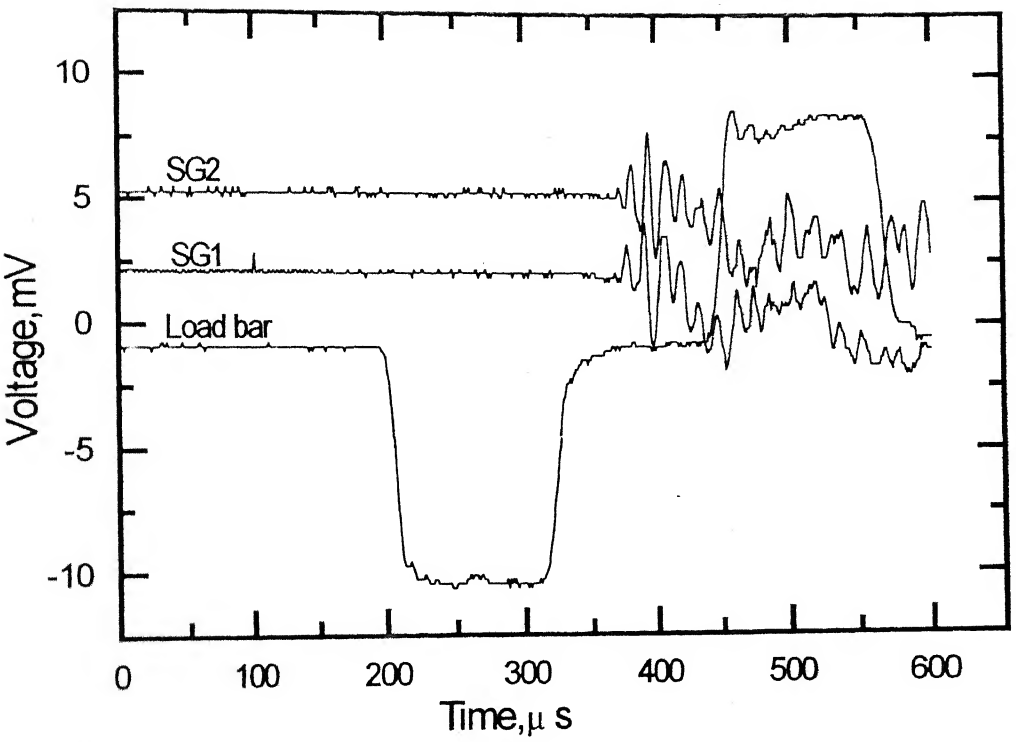

Fig. A.2.14(a) Oscilloscope Records Expt. L-2

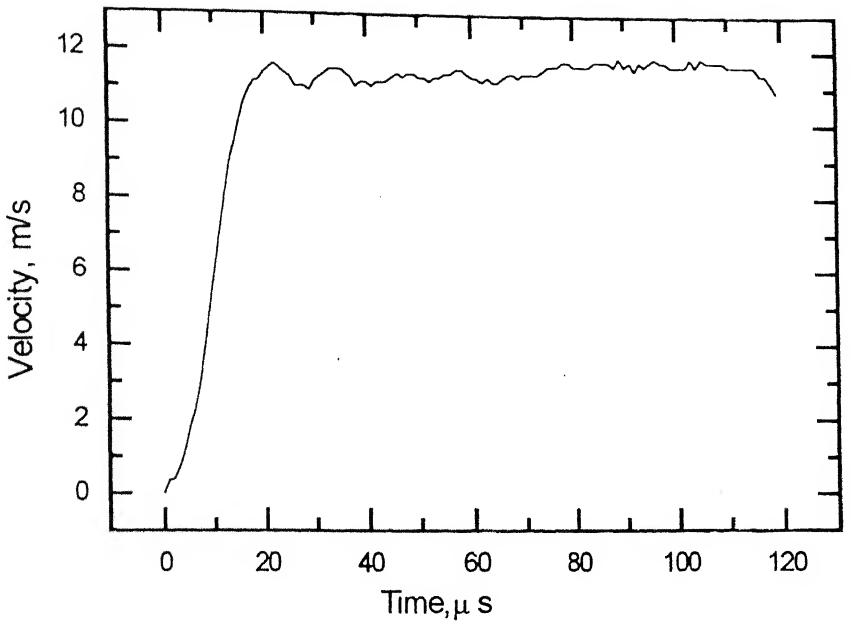

Fig. A.2.14(b) Velocity of cantilever end Expt. L-2

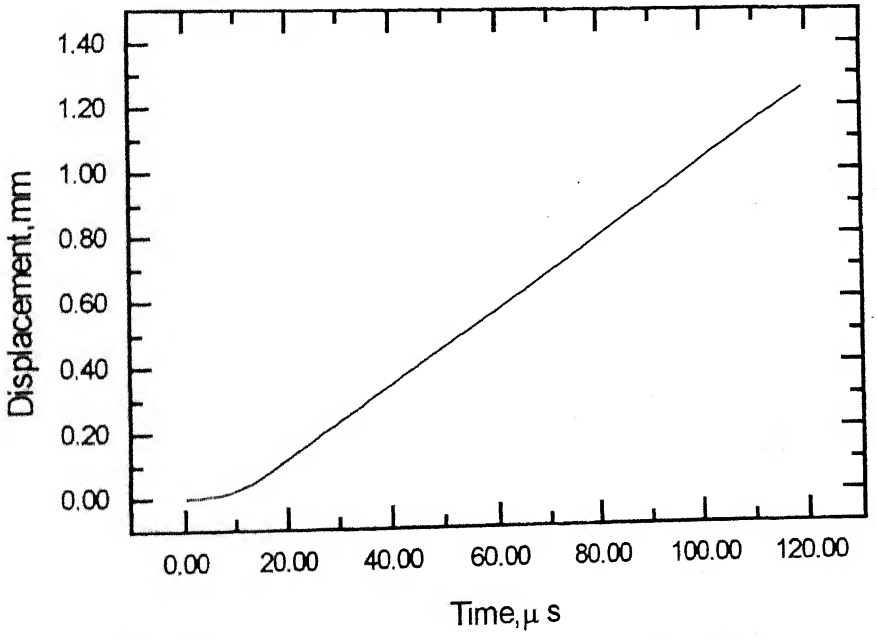

Fig. A.2.14(c) Displacement of cantilever end Expt. L-2

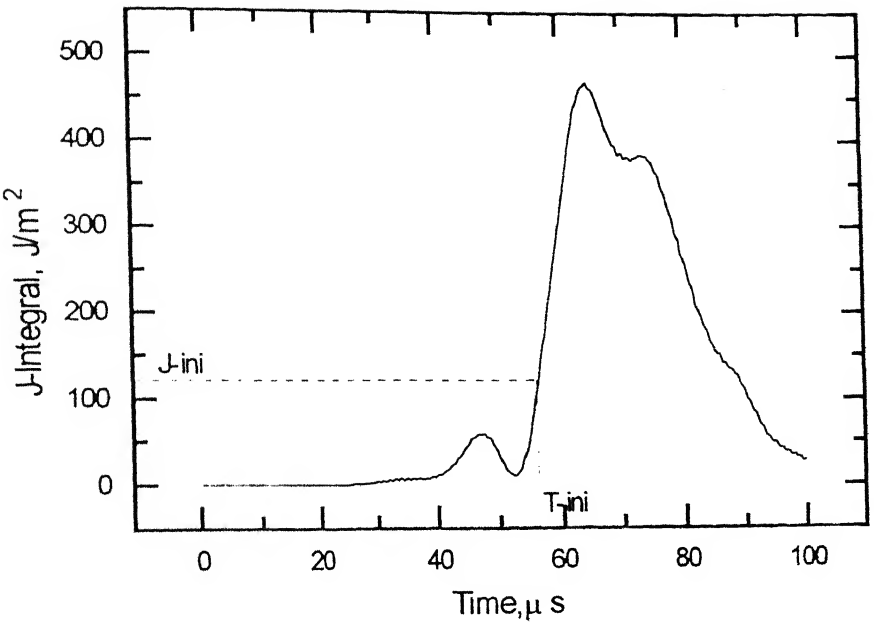

Fig. A.2.14(d) Variation of J-Integral for stationary crack Expt. L-2

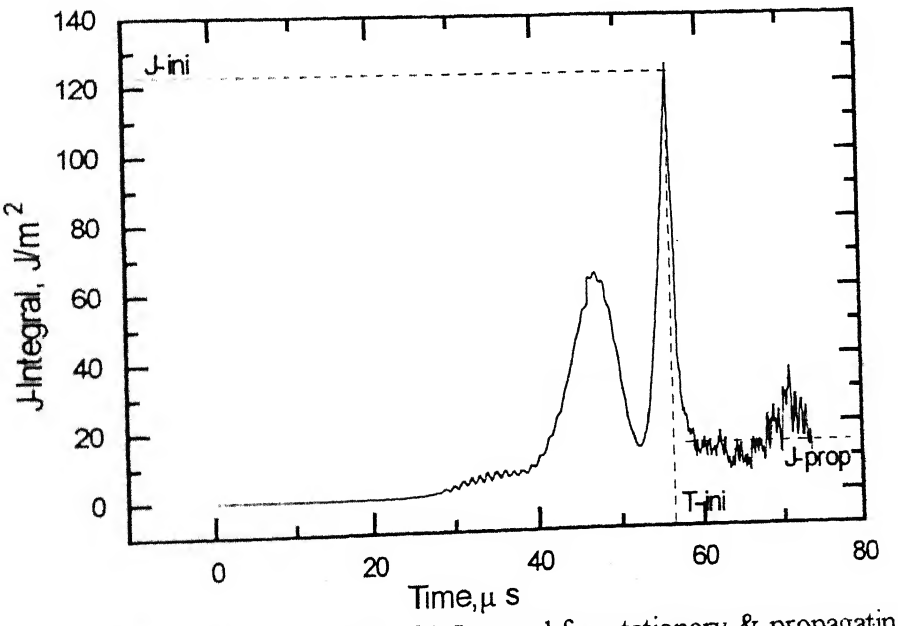

Fig. A.14(e) Variation of J-Integral for stationary & propagating crack Expt. L-2

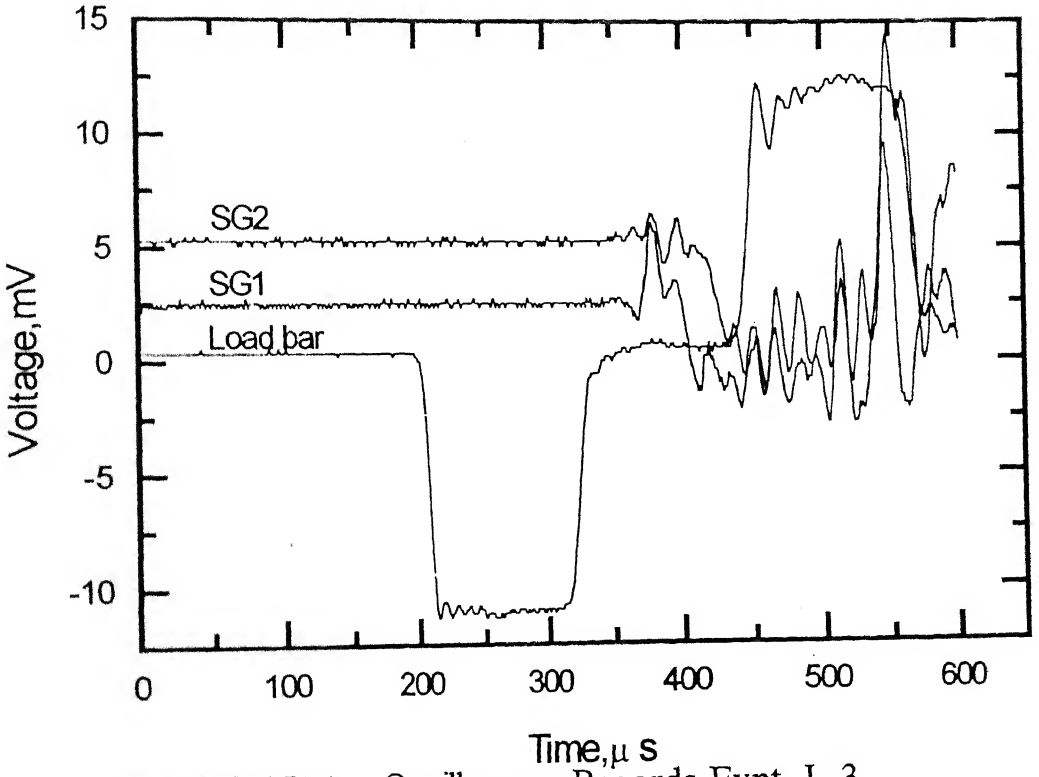

Fig. A.2.15(a) Oscilloscope Records Expt. L-3

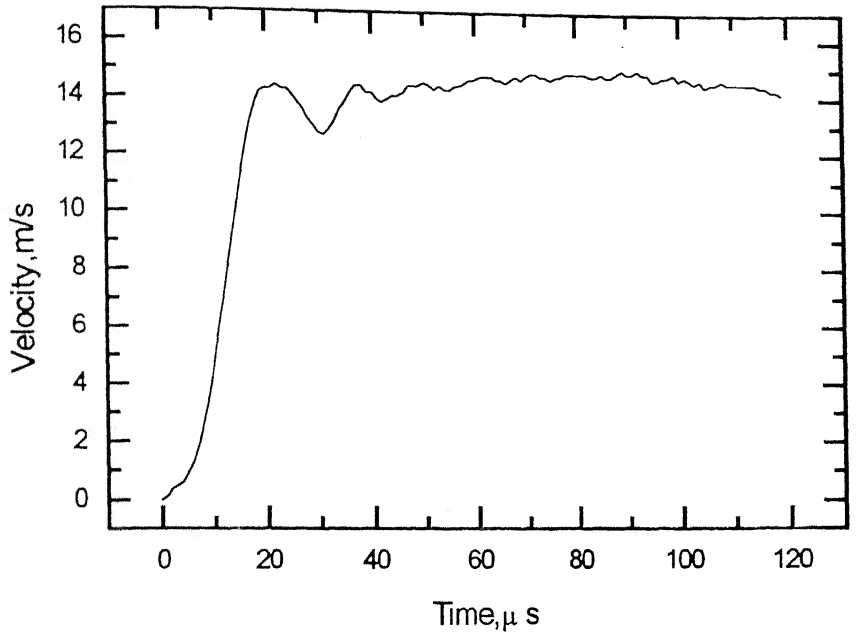

Fig. A.2.15(b) Velocity of load bar end Expt. L-3

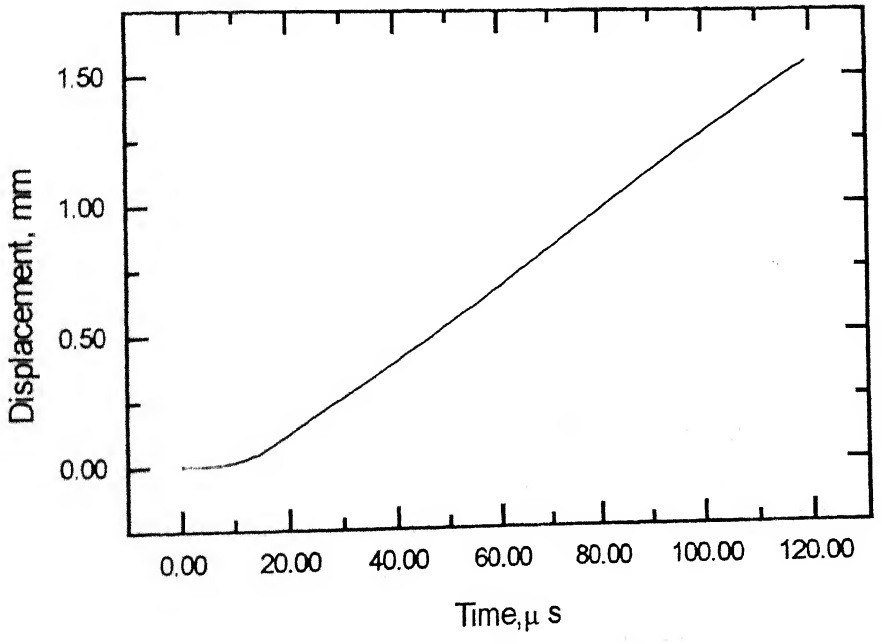

Fig. A.2.15(c) Displacement of cantilever end Expt. L-3

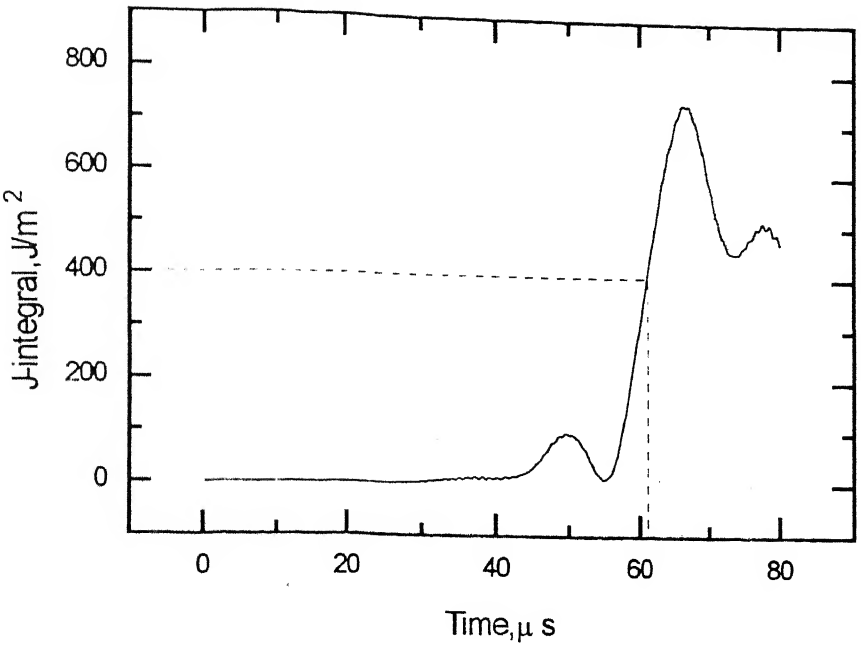

Fig. A.2.15(d) Variation of J-integral for stationary crack Expt. L-3

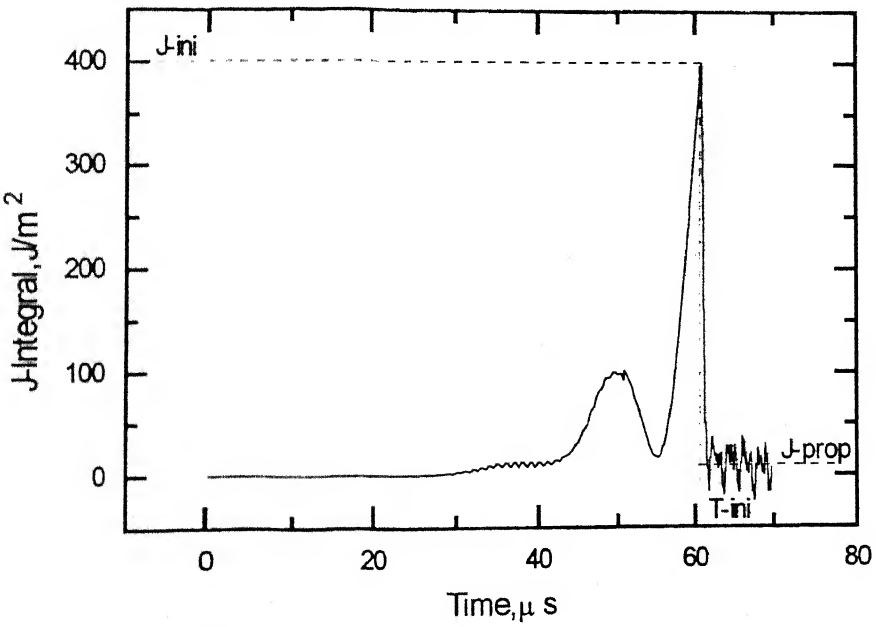

Fig. A.2.15(e) Variation of J-integral for stationary & Propagating crack Expt. L-3

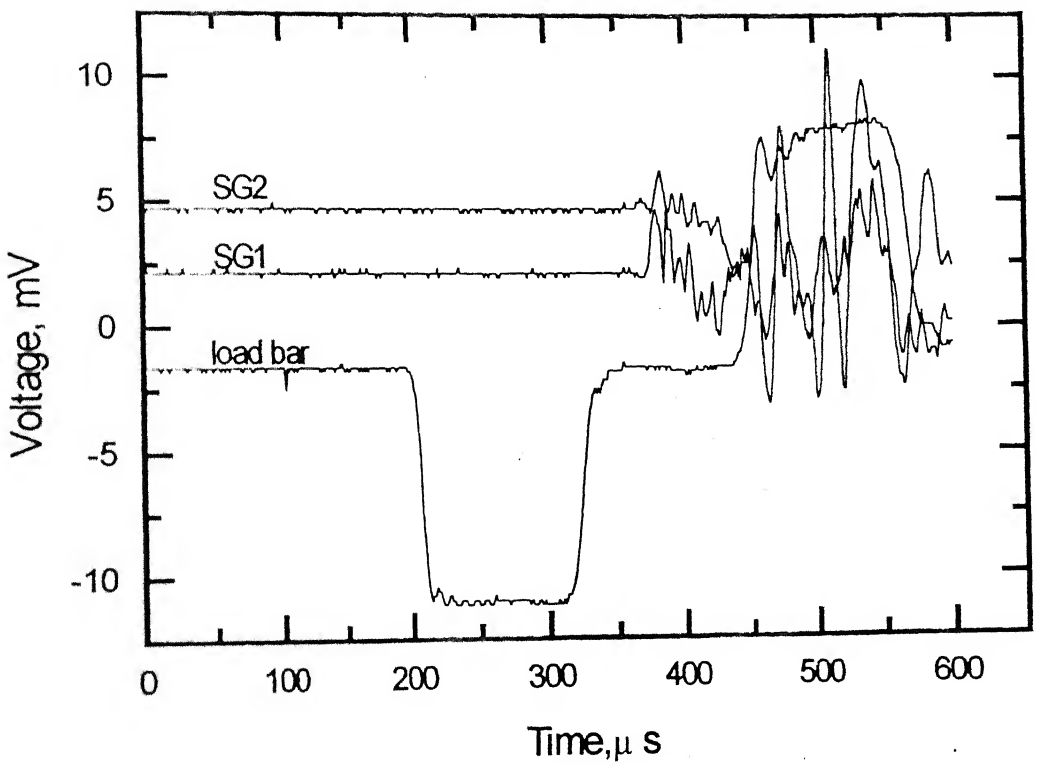

Fig. A.2.16(a) Oscilloscope Records Expt. L-4

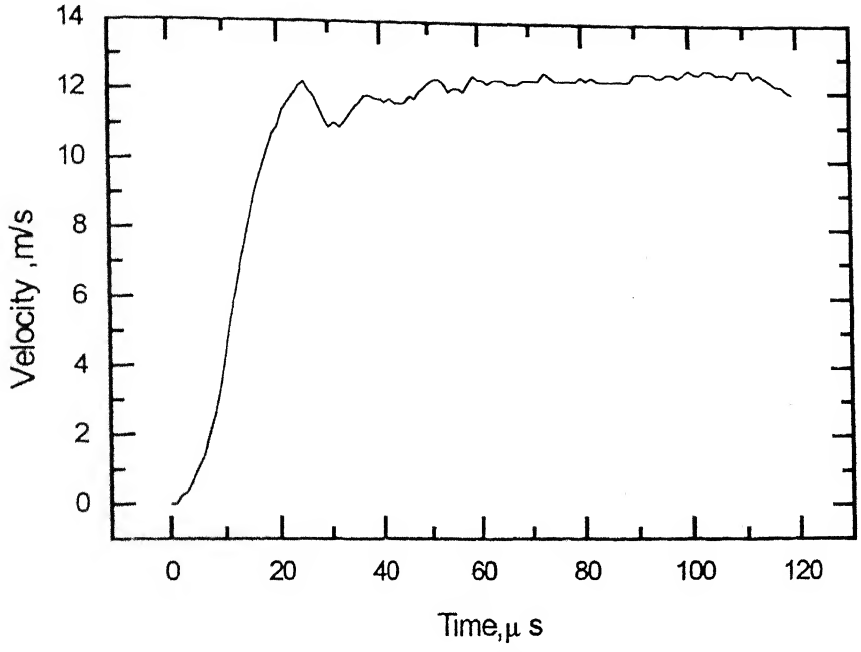

Fig. A.2.16(b) Velocity of load bar end Expt. L-4

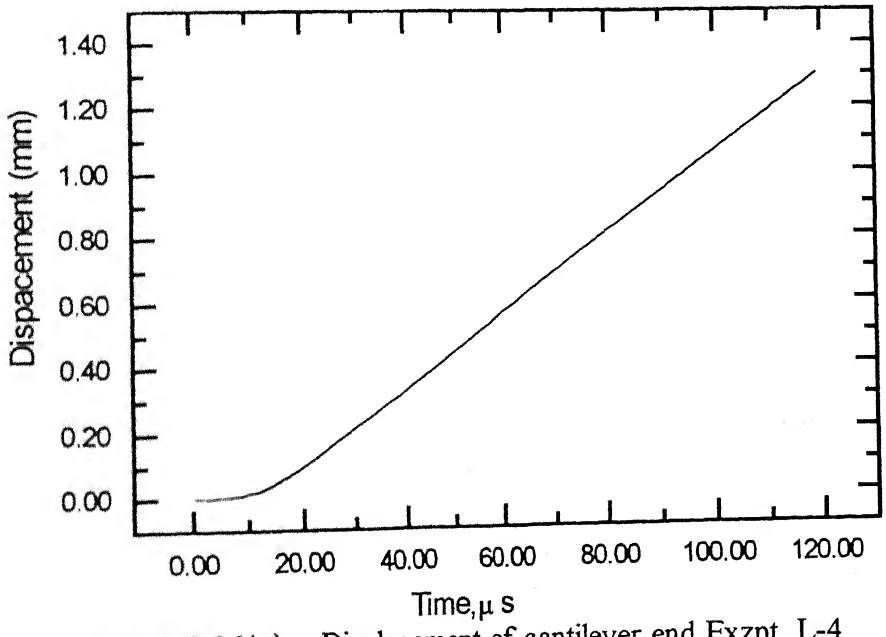

Fig. A.2.16(c) Displacement of cantilever end Exzpt. L-4

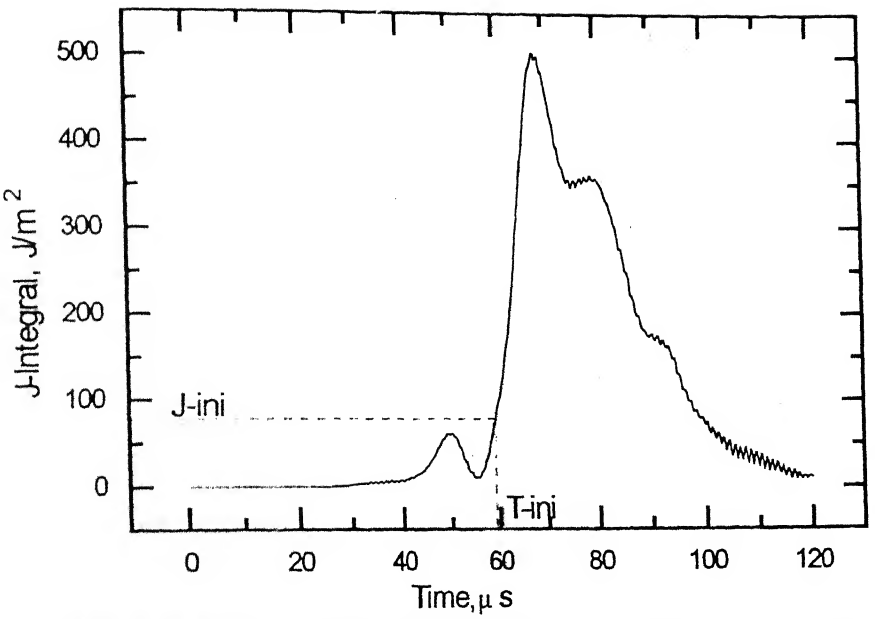

Fig. A 2.16(d) Variation of J-Integral for stationary crack Expt. L-4

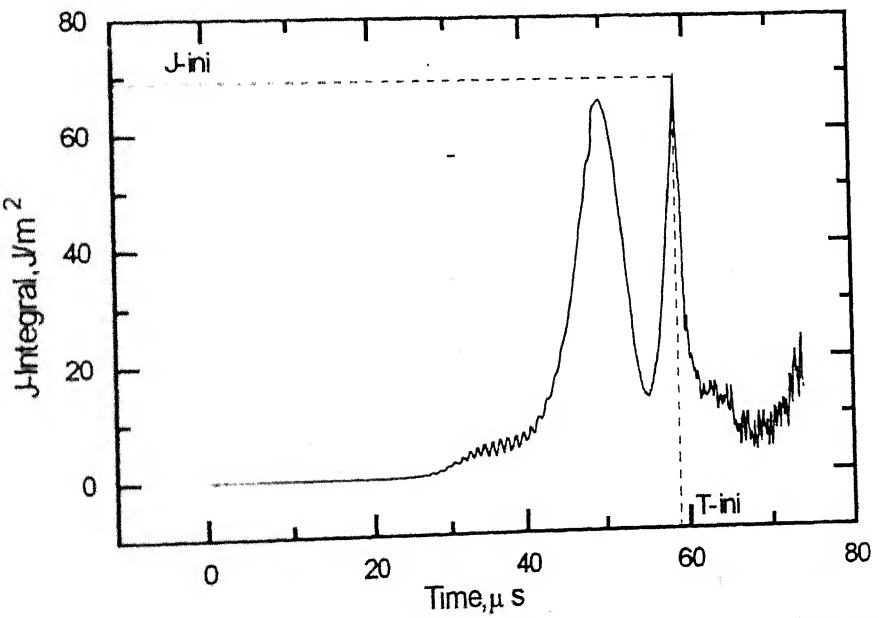

Fig. A 2.16(e) Variation of J-Integral for stationary &propagating crack Expt. L-4

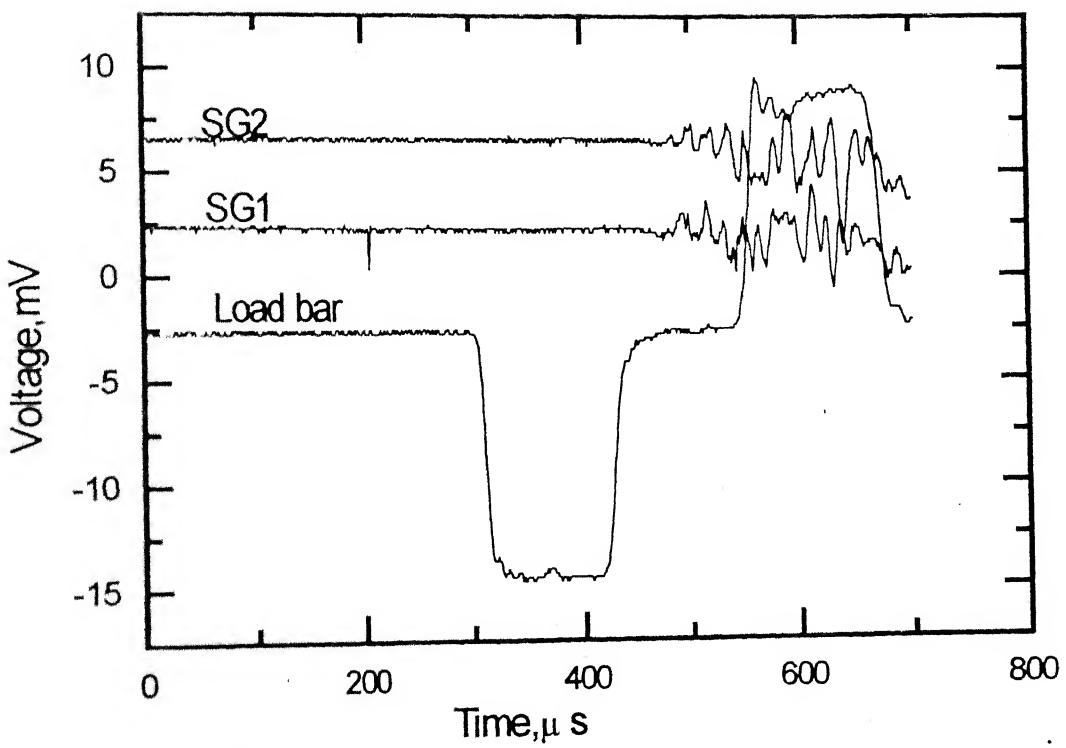

Fig. A.2.17(a) Oscilloscope Records Expt. L-5

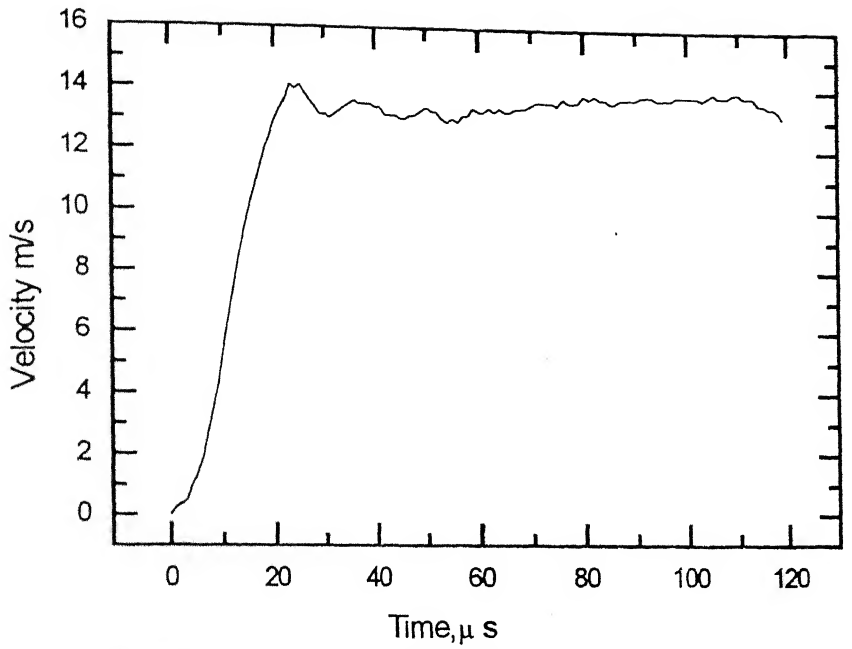

Fig. A.2.17(b) Velocity of load bar end Expt. L-5

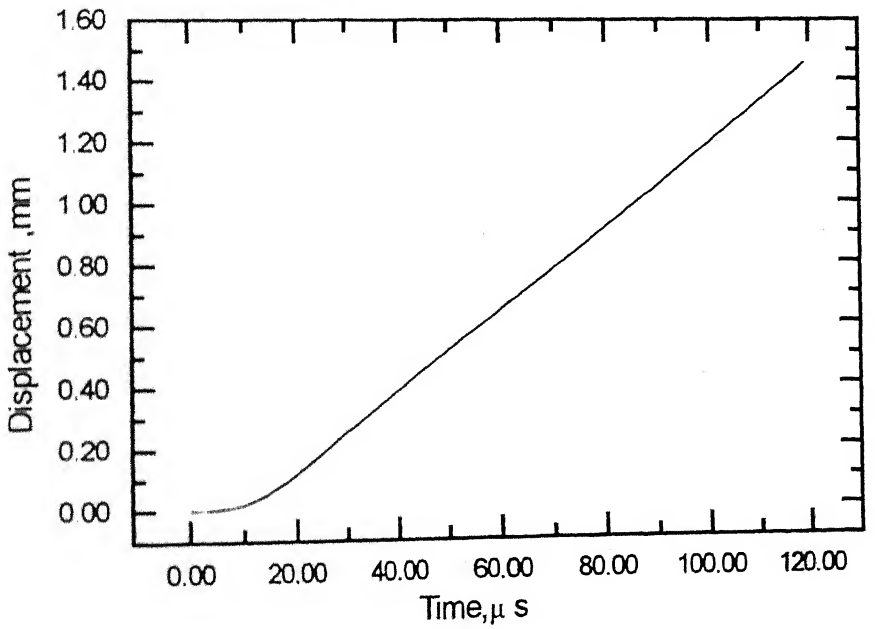

Fig. A.2.17(c) Displacement of cantilever end Expt. L-5

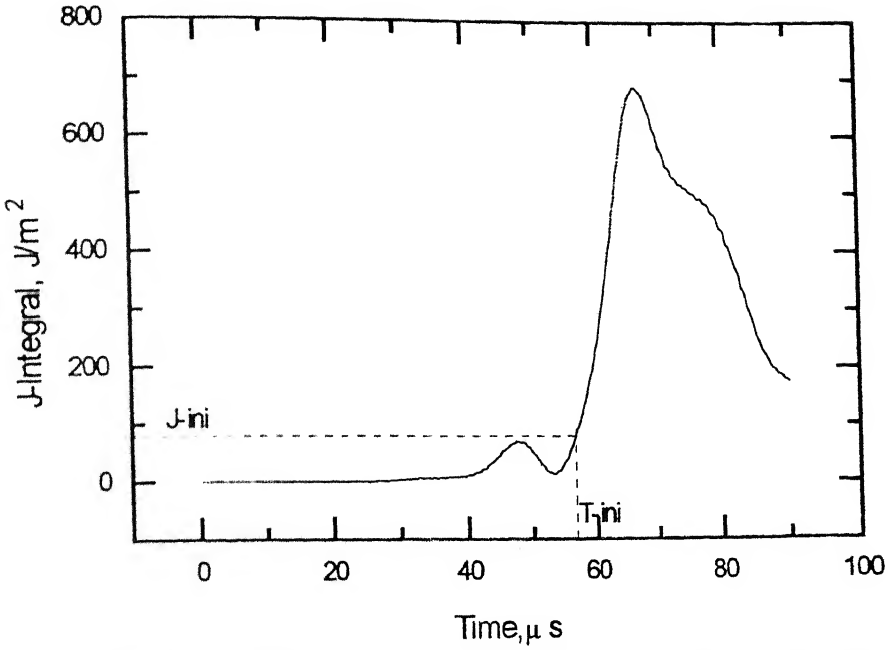

Fig. A.2.17(d) Variation of J-integral for staionary crack Expt. L-5

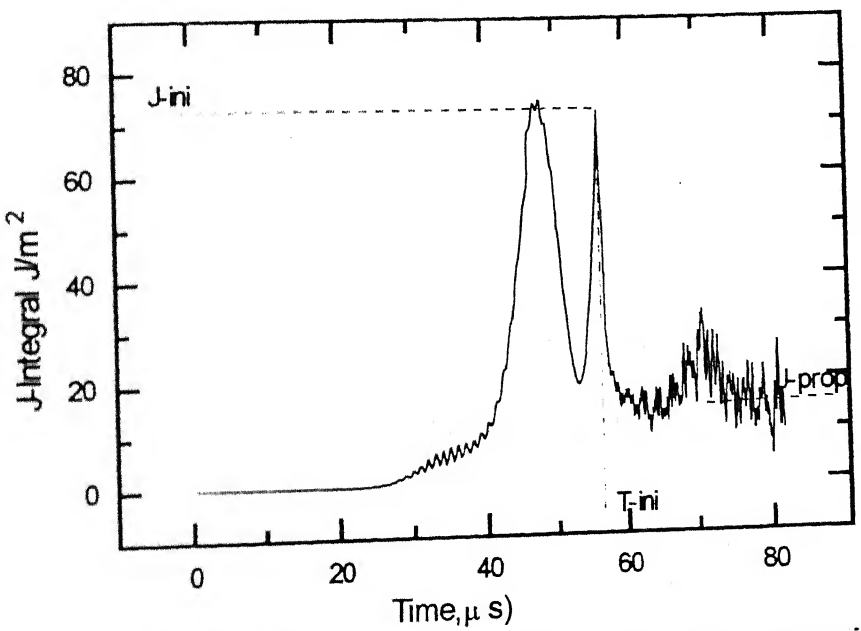

Fig. A.2.17(e) Variation of J-integral for stationary & propagating crack Expt. L-5

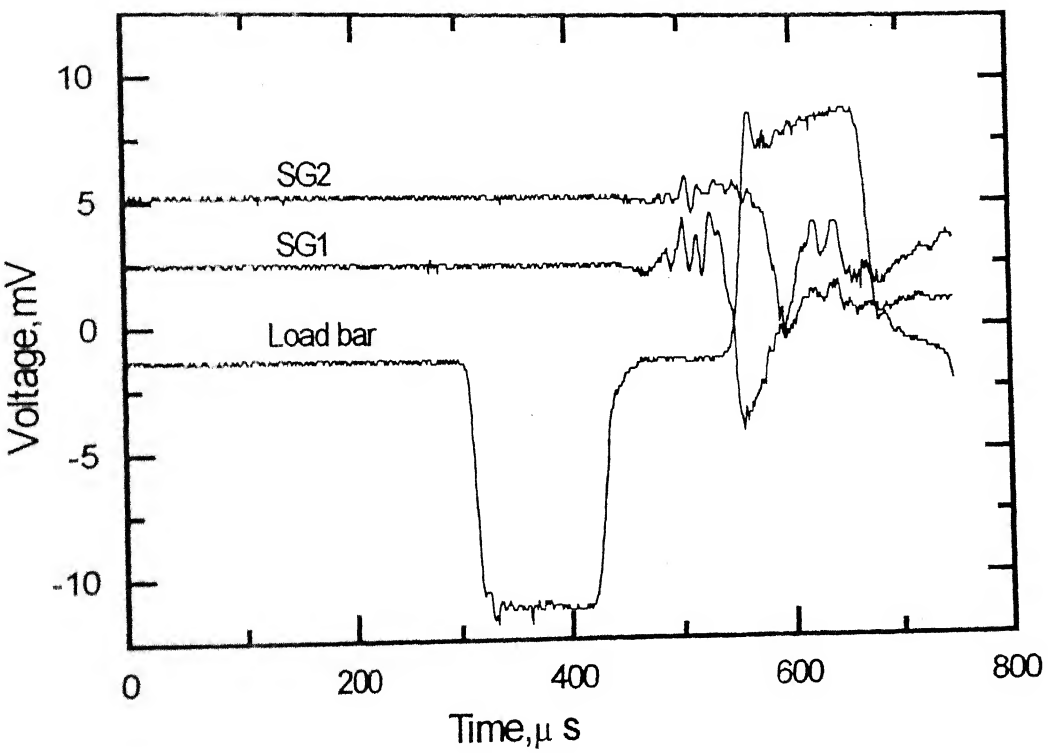

Fig. A.2.18(a) Oscilloscope Records Expt. L-6

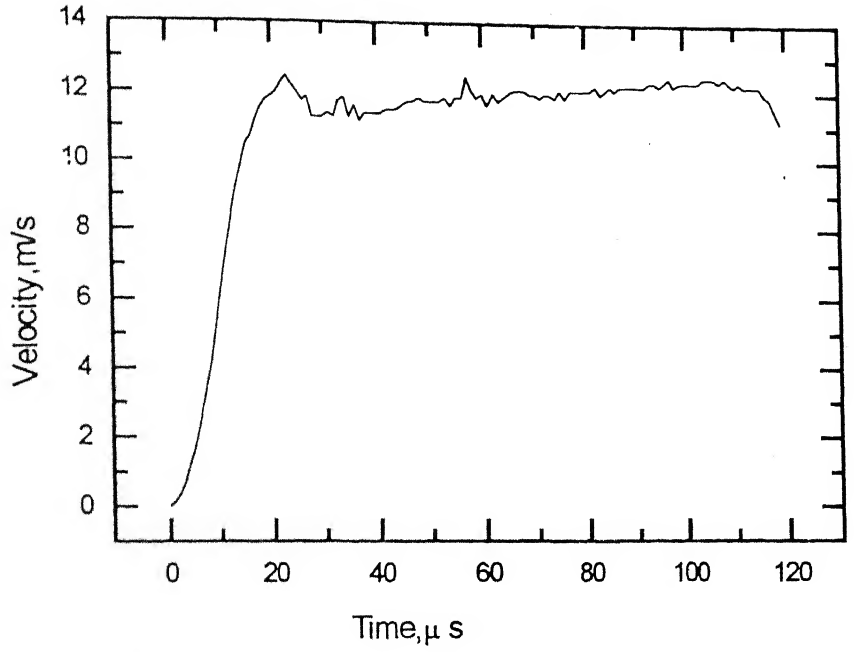

Fig. A.2.18(b) Velocity of load bar end Expt. L-6

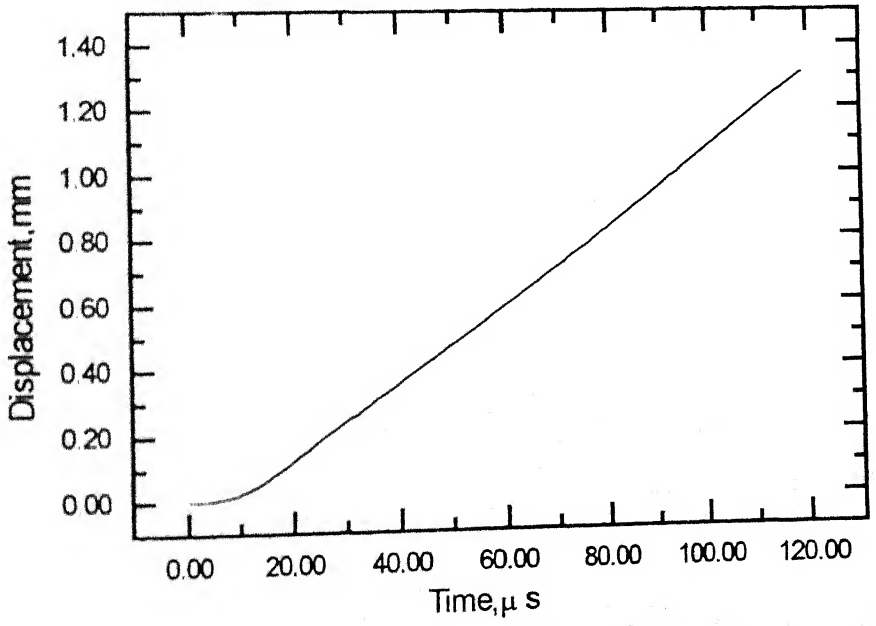

Fig. A.2.18(c) Displacement of cantilever end Expt. L-6

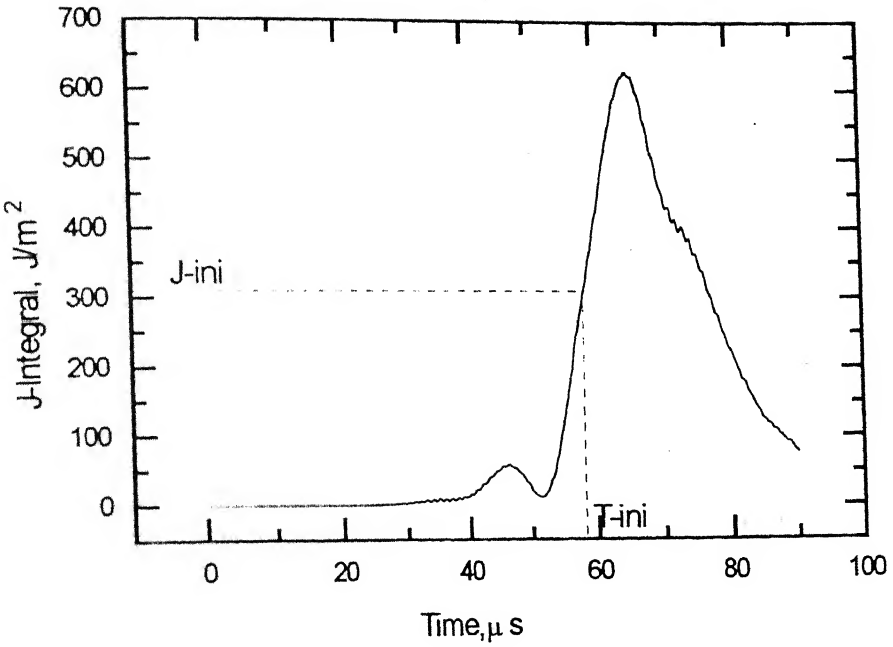

Fig. A. A. 18(d) Variation of J-integral for stationary crack Expt. L-6

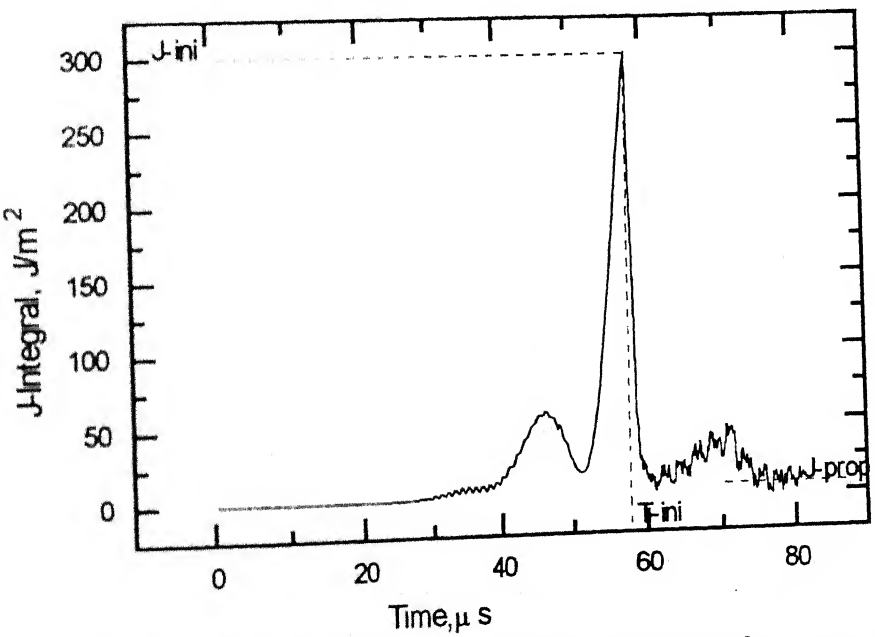

Fig. A 2. 18(e) Variation of J-integral for stationary & propagating crack Expt. L-6

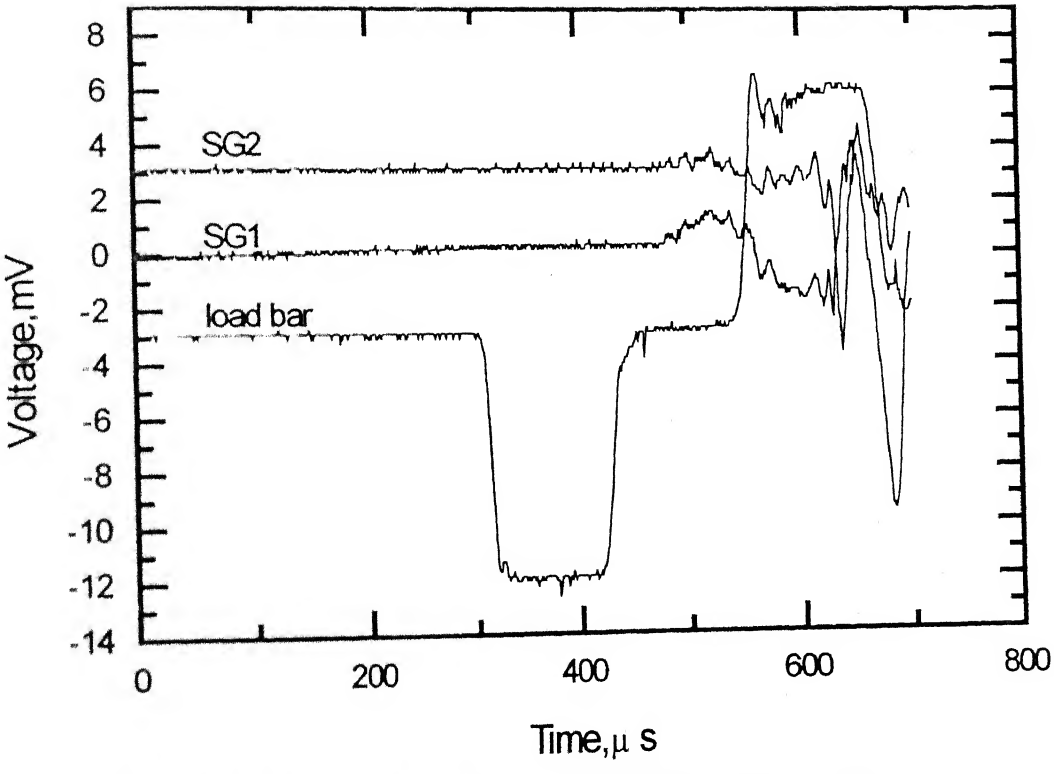

Fig. A.2.119(a) Oscilloscope Records Expt. L-7

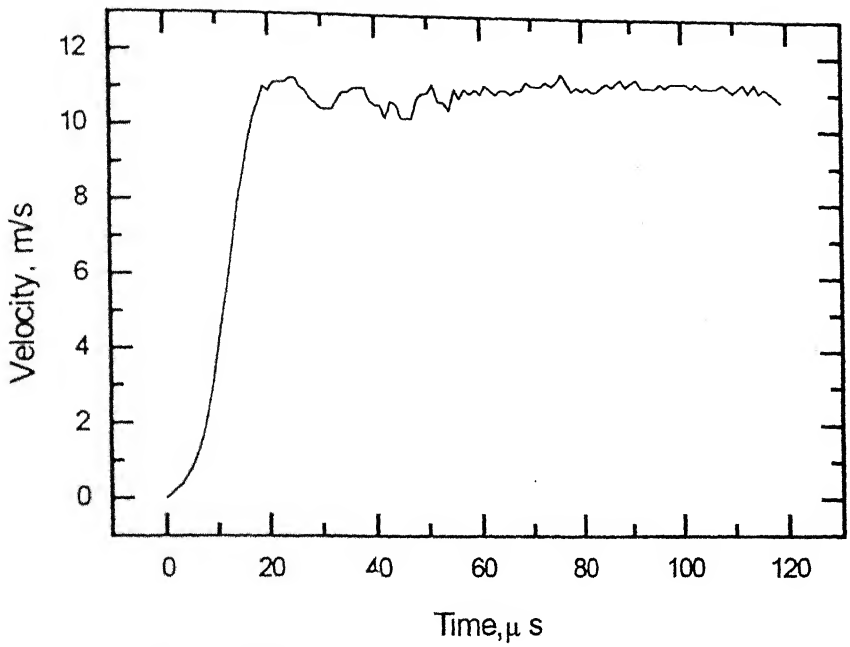

Fig A.2.19(b) Velocity of load bar end Expt. L-7

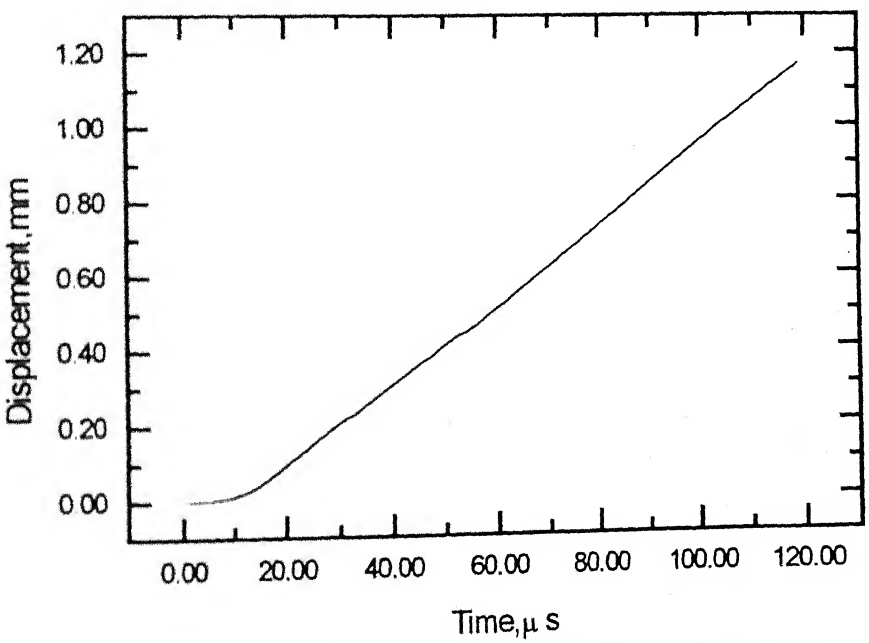

Fig.A.2.19(c) Displacement of cantilever end Expt. L-7

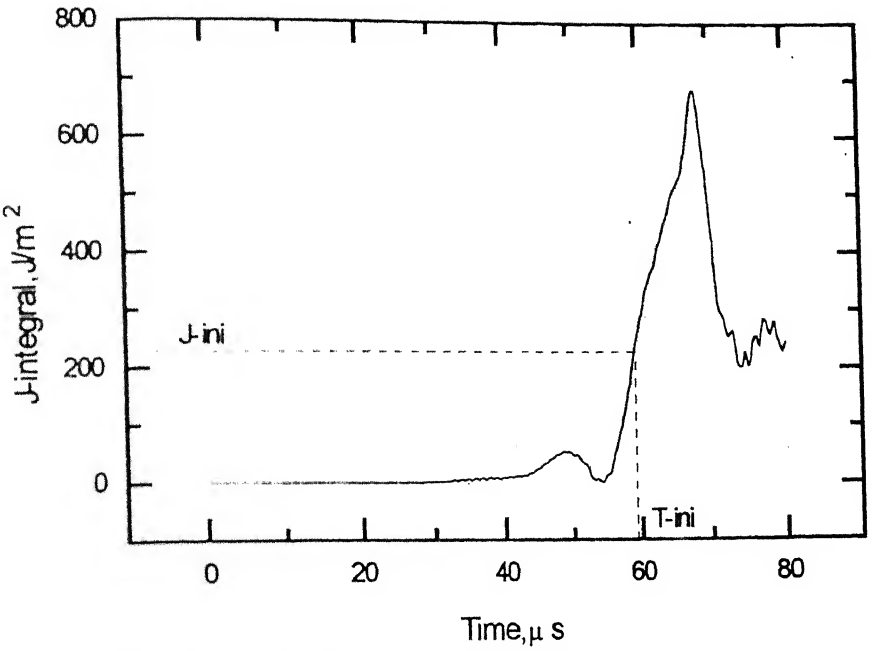

Fig A.2.19(d) Variation of J-integral for stationary crack Expt. L-7

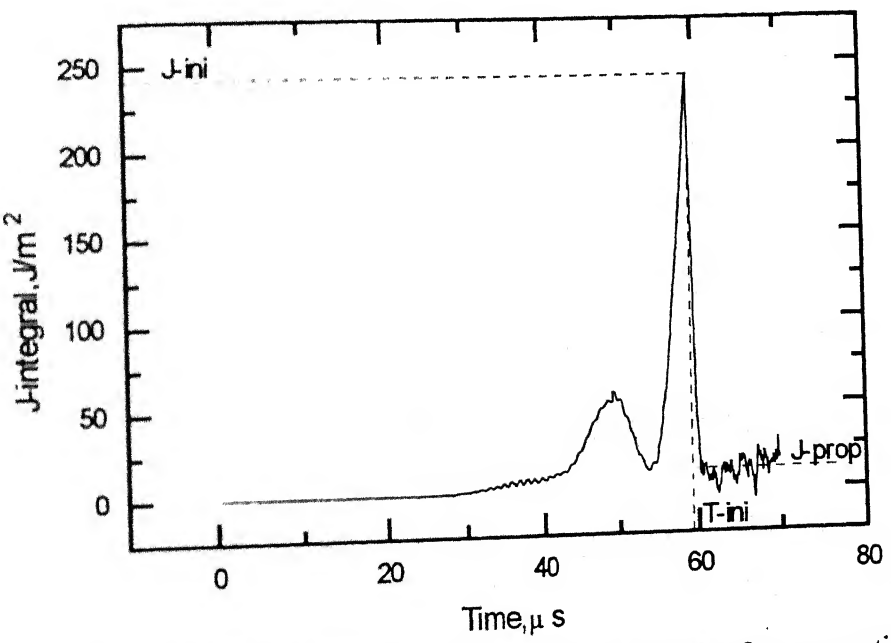

Fig A.2.19(e) Variation of J-integral for stationary & propagating crack Expt. L-7

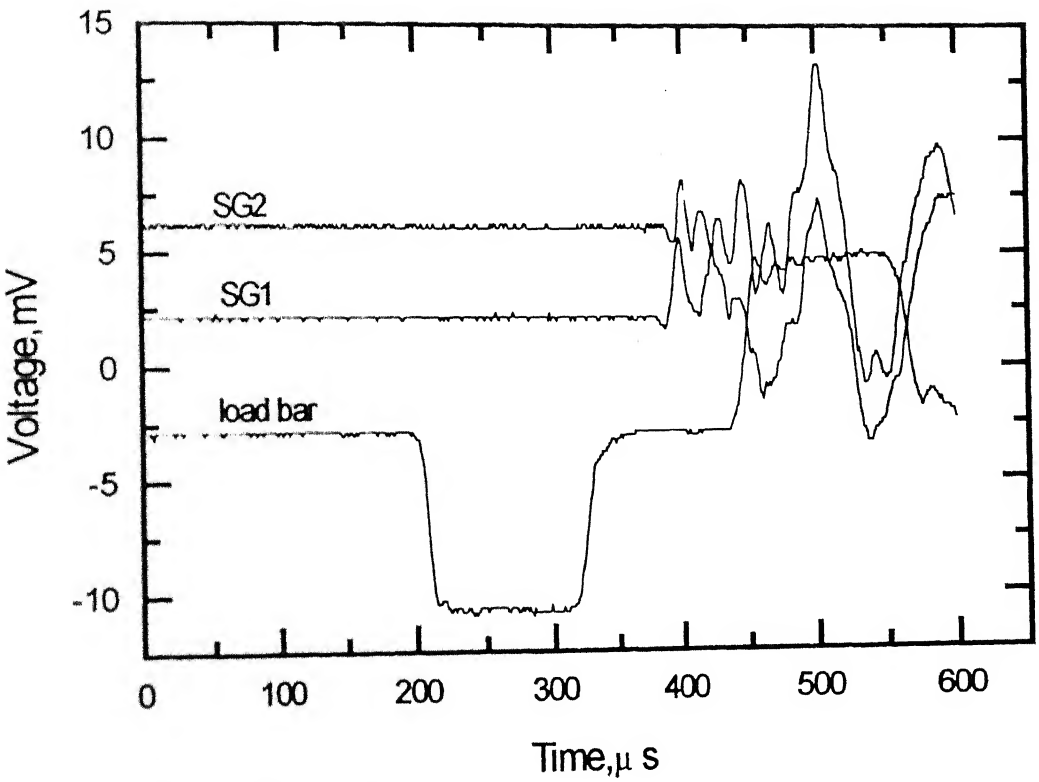

Fig. A.2.20(a) Oscilloscope Records Expt. L-8

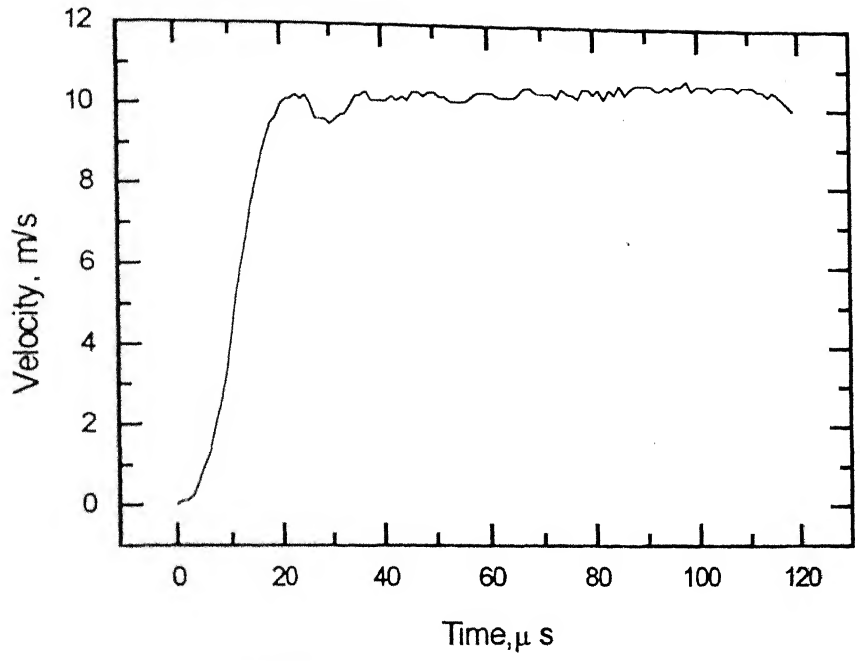

Fig. A 2.20(b) Velocity of load bar end Expt. L-8

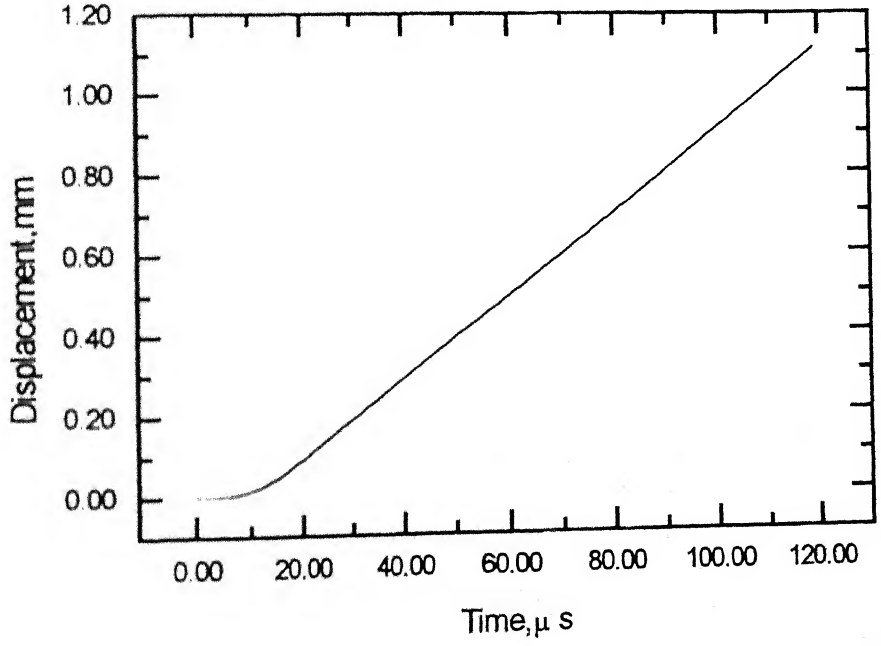

Fig. A 2.20(c) Displacement of cantilever end Expt. L-8

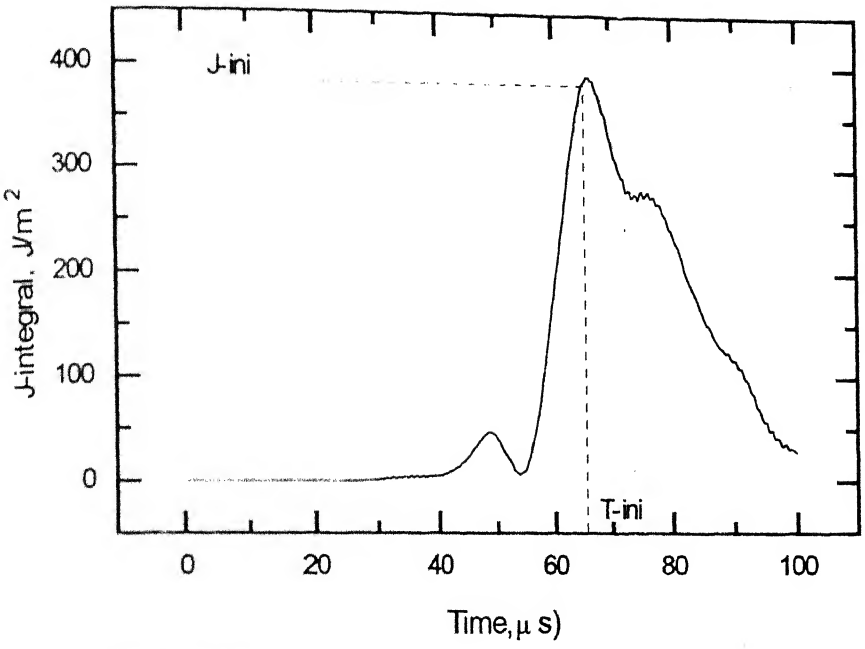

Fig A 2.20(d) Variation of J-integral for stationary crack Expt. L-8

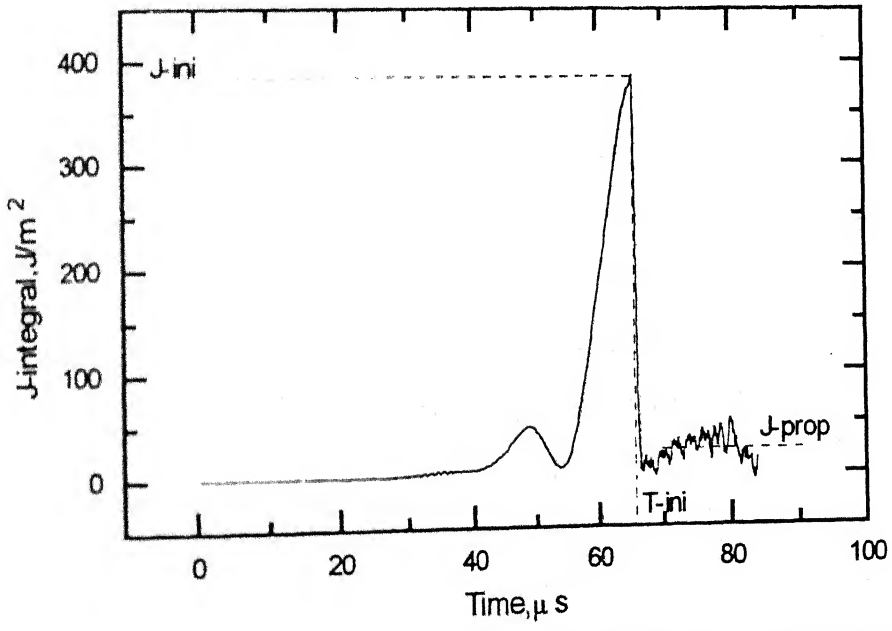

Fig. A 2.20(e) Variation of J-integral for stationary & propagating crack Expt. L-8

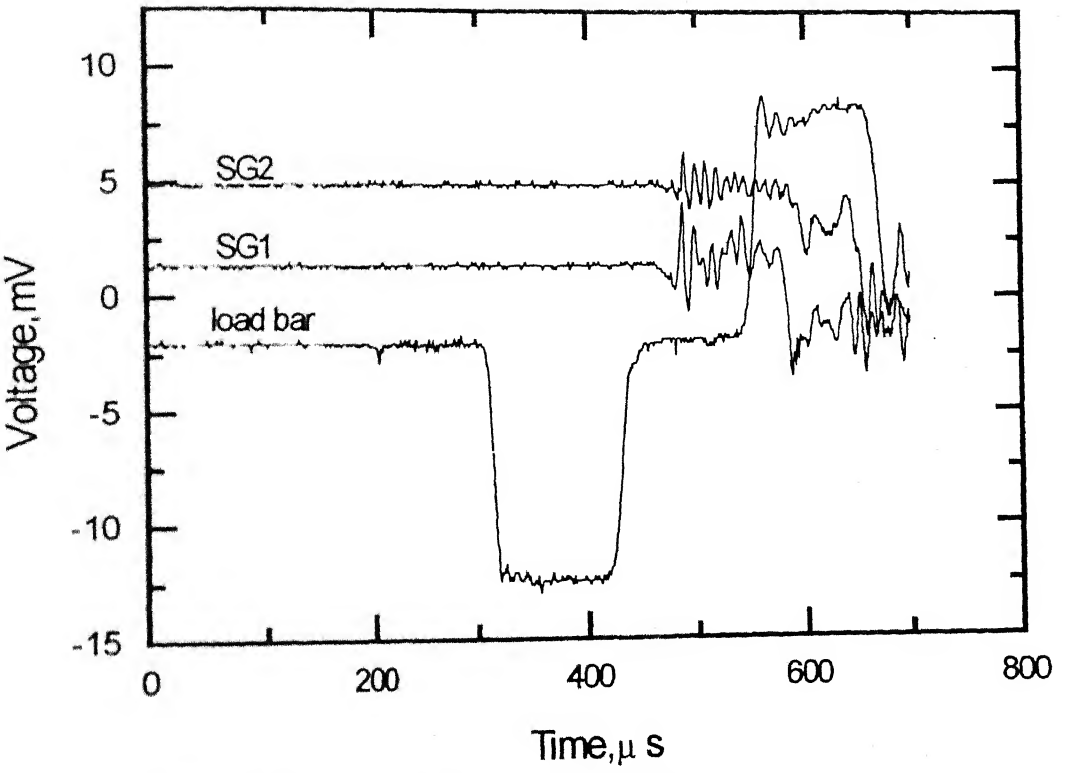

Fig. A.2.21(a) Oscilloscope Records Expt. L-9

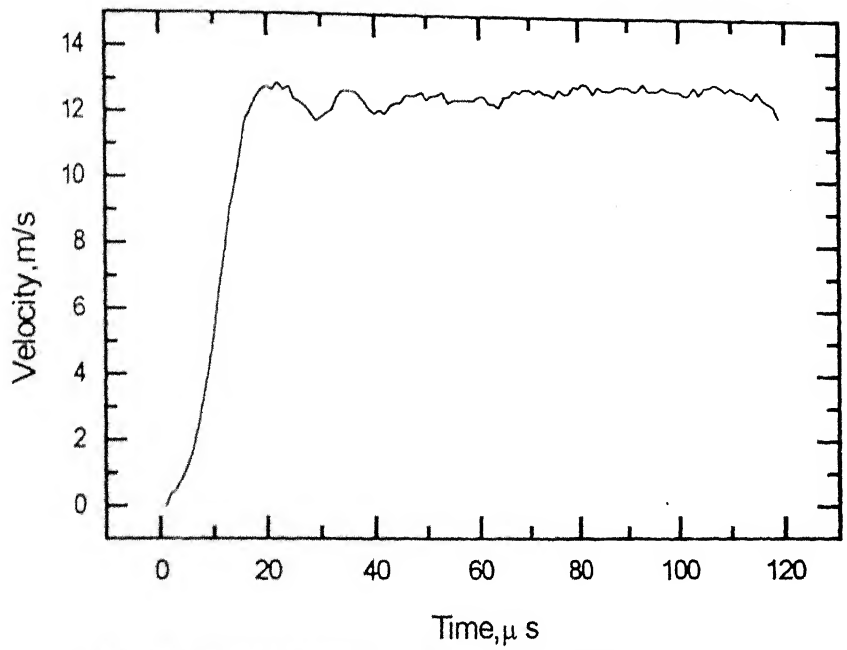

Fig A 2 21(b) Velocity of load bar end Expt.L-9

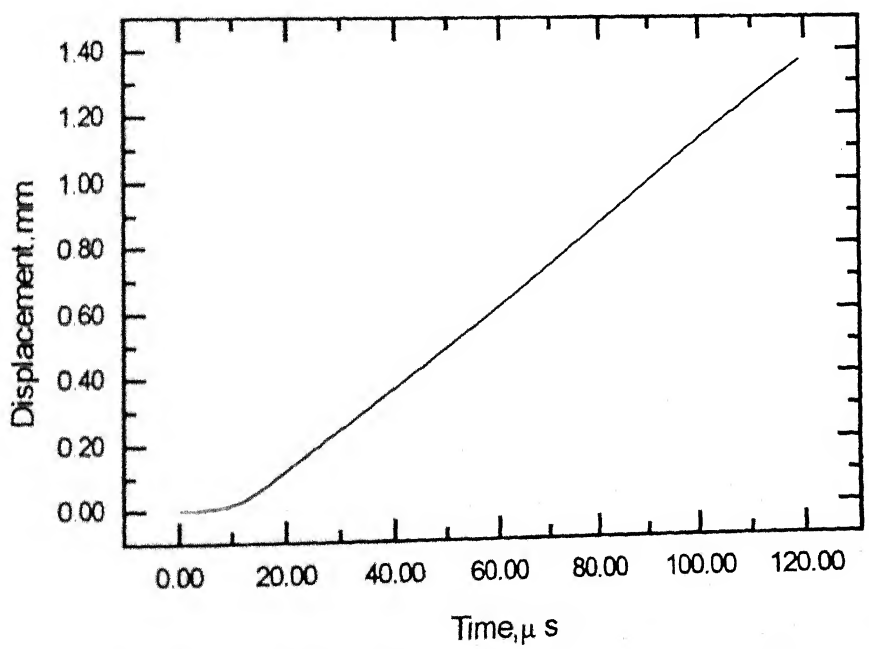

Fig A.2.21(c) Displacement of cantilever end Expt. L-9

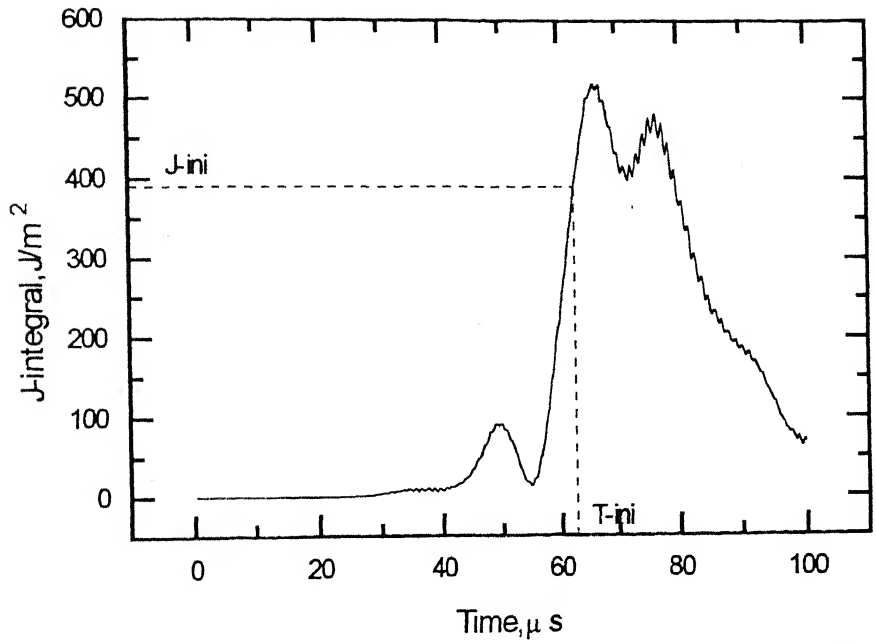

Fig. A.2.21(d) Variation of J-integral for stationary crack Expt. L-9

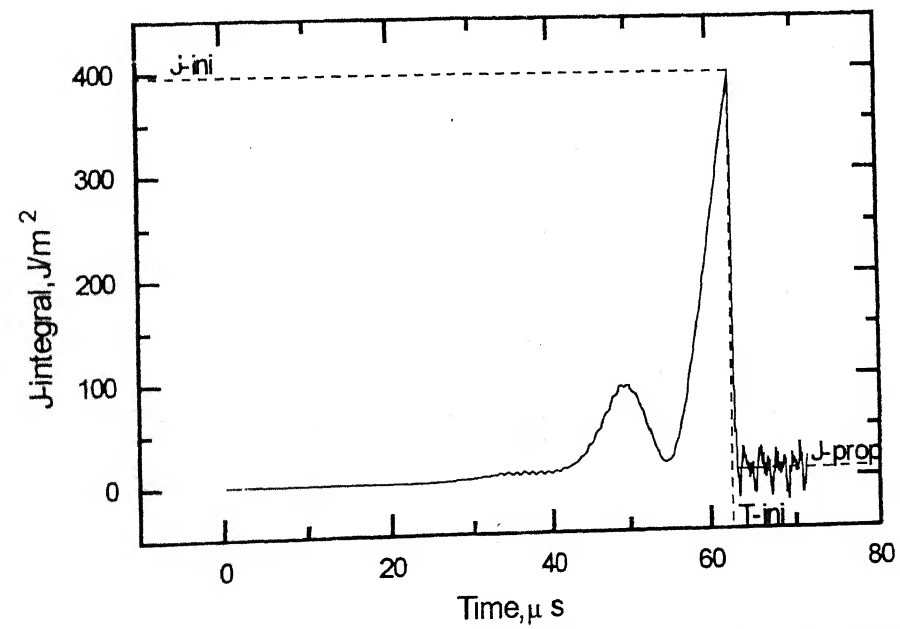

Fig. A.2.21(e) Variation of J-integral for stationary & propagating crack Expt. L-9

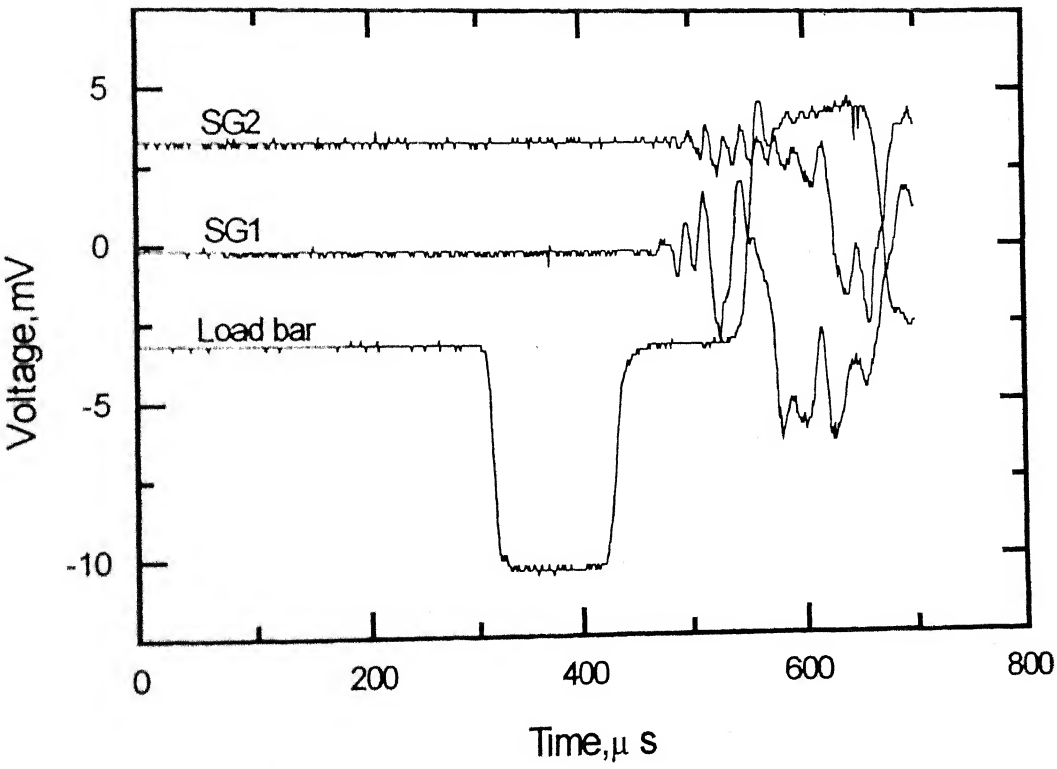

Fig. A.2.22(a) Oscilloscope Records Expt. L-10

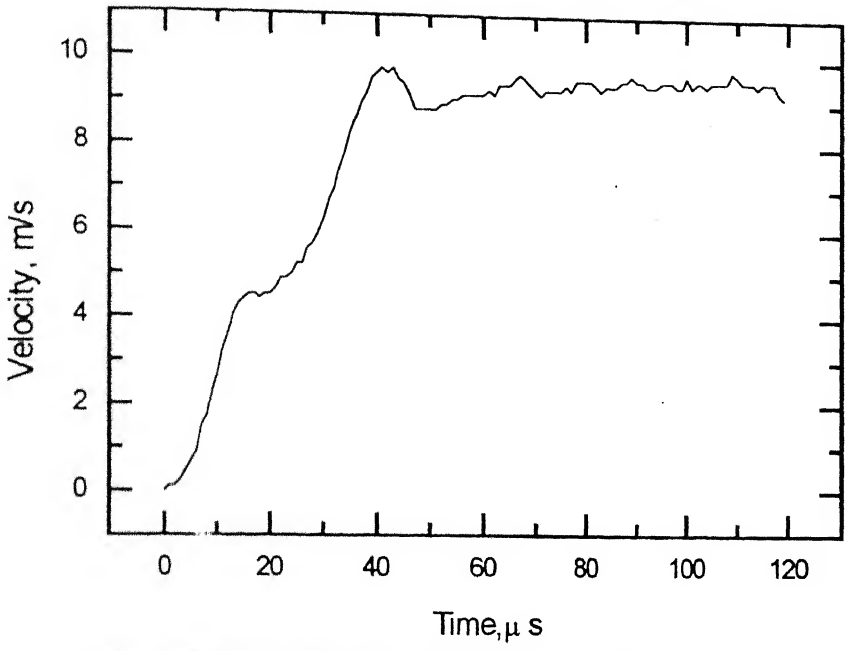

Fig. A.2.22(b) Velocity of load bar end Expt. L-10

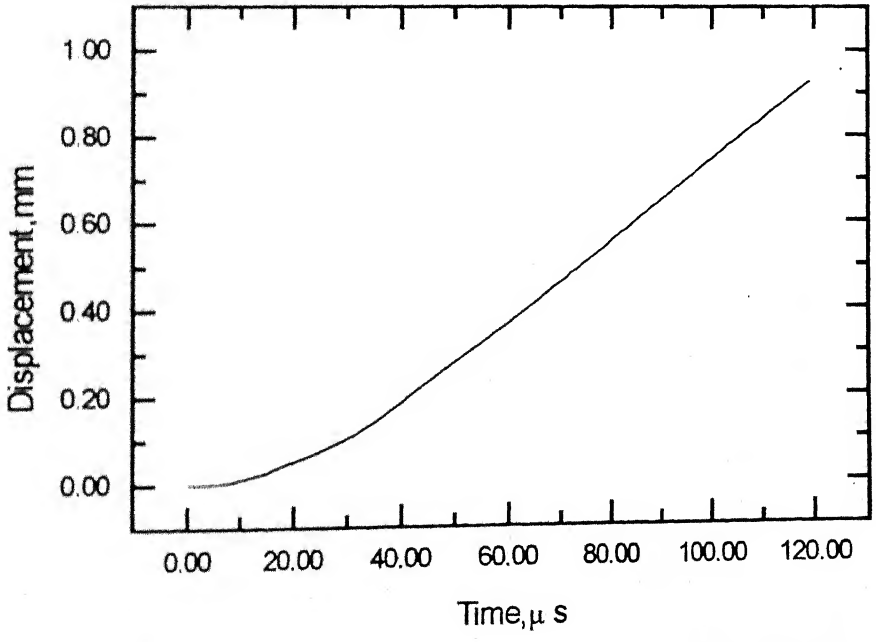

Fig. A.2.22(c) Displacement of cantilever end Expt. L-10

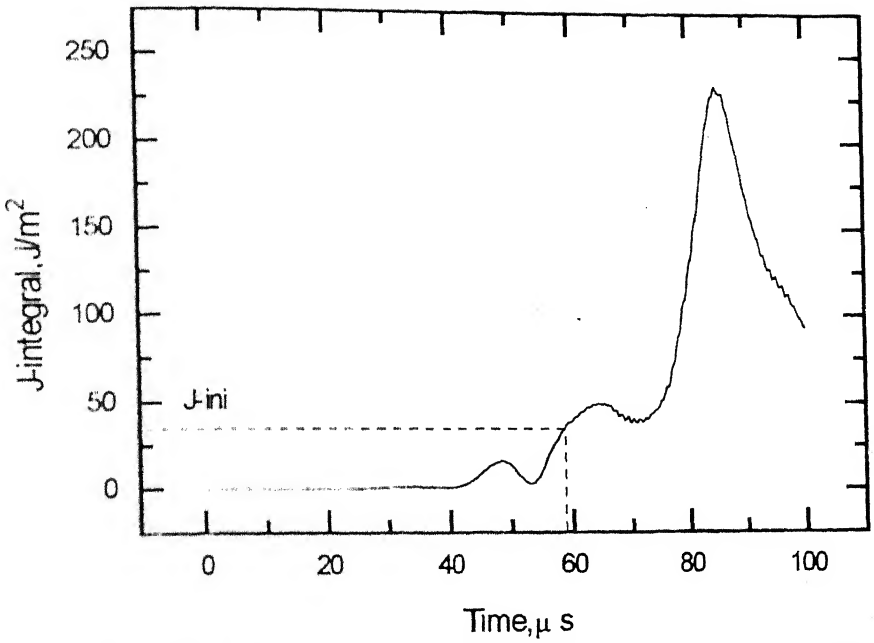

Fig A 2 22(d) Variation of J-integral for stationary crack Expt. L-10

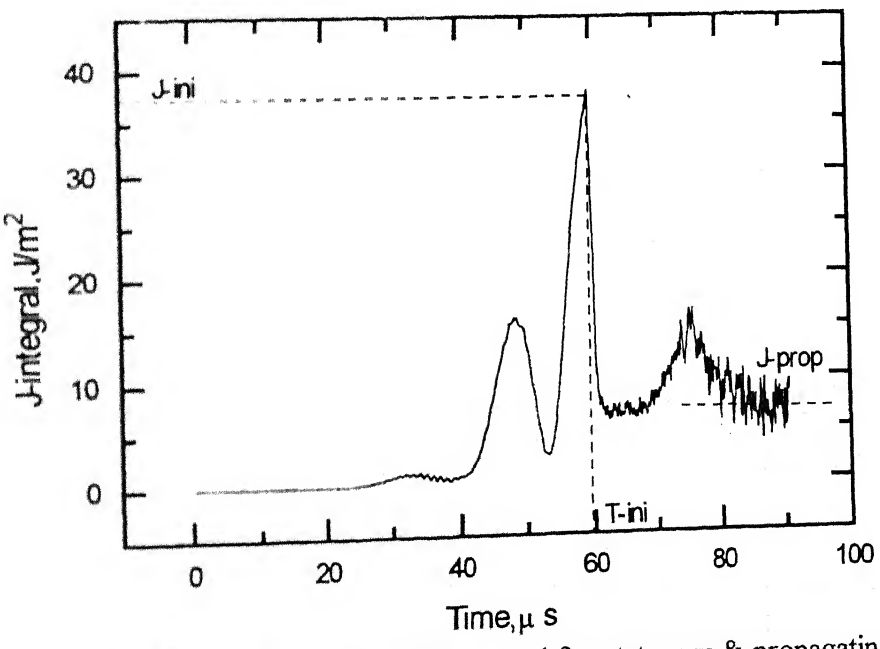

Fig A 2 22(e) Variation of J-integral for statonary & propagating crack Expt. L-10

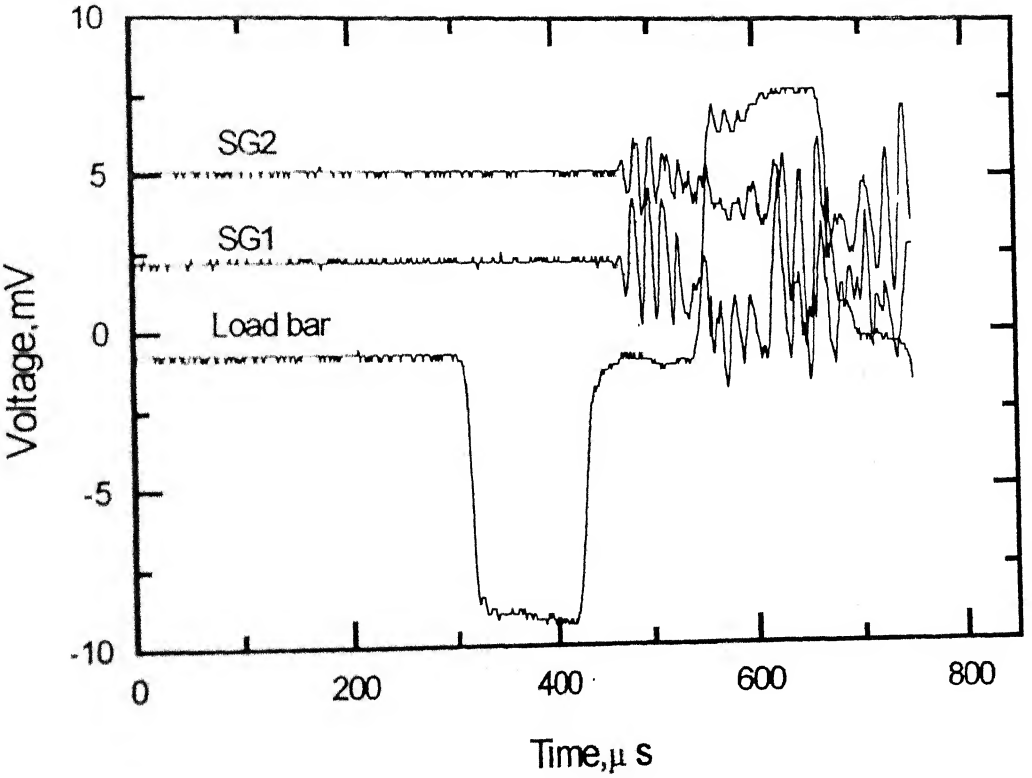

Fig.A.2.23(a) Oscilloscope Records Expt. L-11

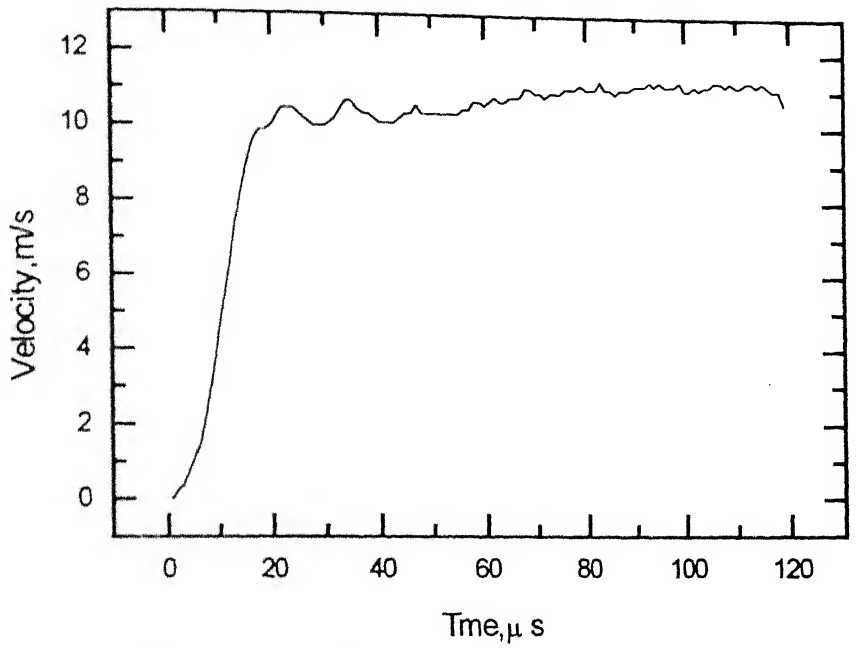

Fig A.2 23(b) Velocity of load bar end Expt. L-11

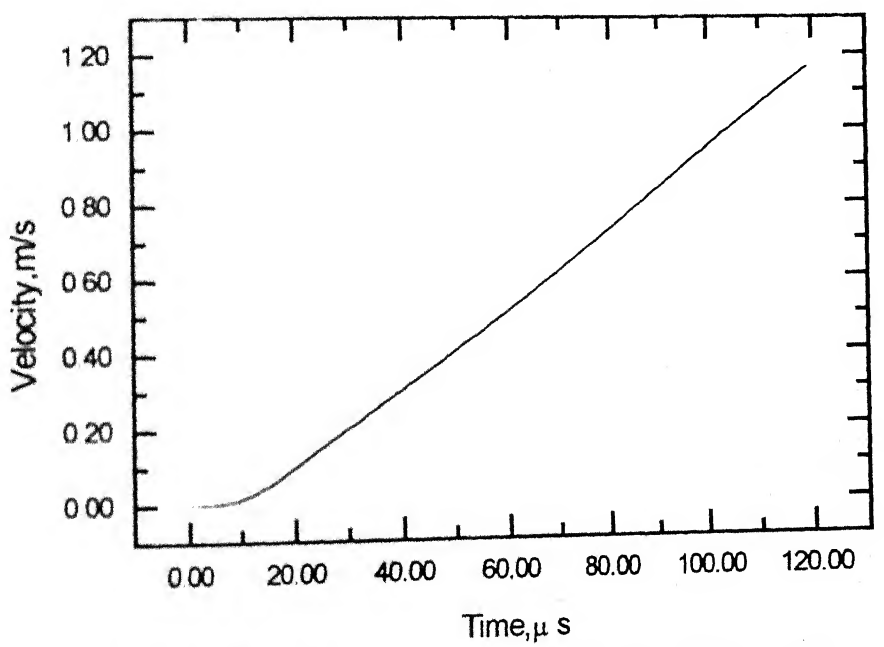

Fig A.2 23(c) Displacement of cantilever end Expt. L-11

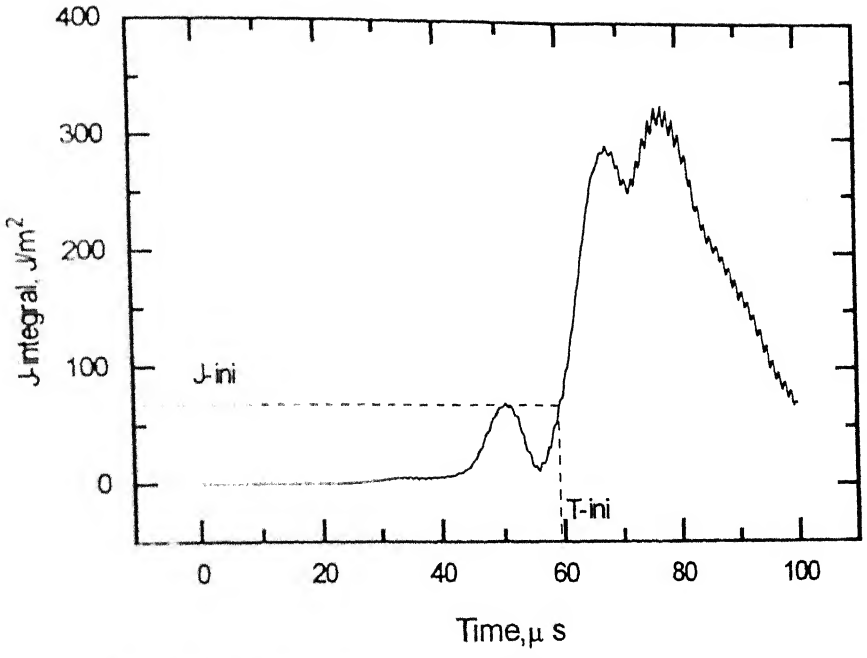

Fig A 2.23 Variation of J-integral for stationary crack Expt. L-11

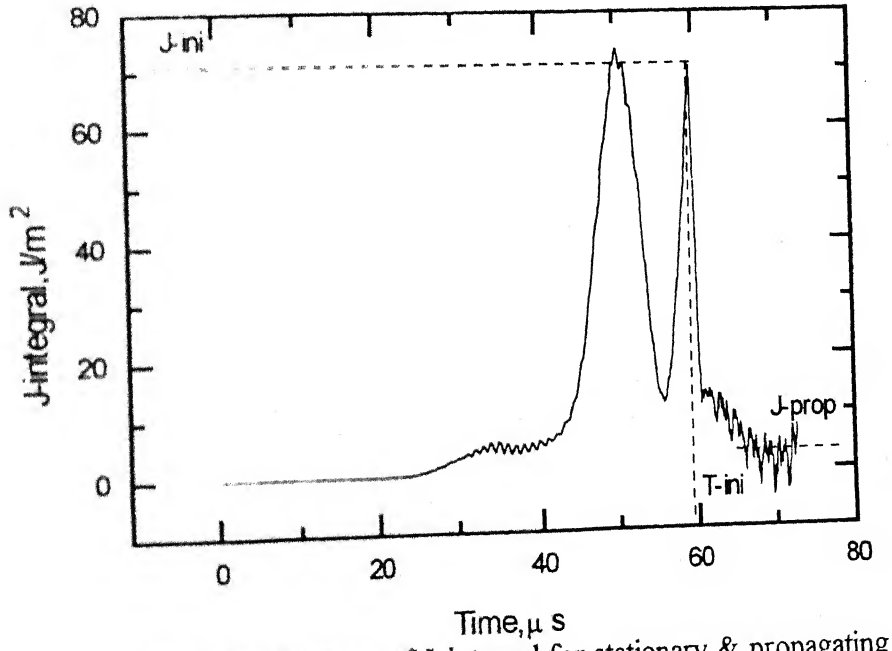

Fig A 2 23 Variation of J-integral for stationary & propagating crack Expt. L-11

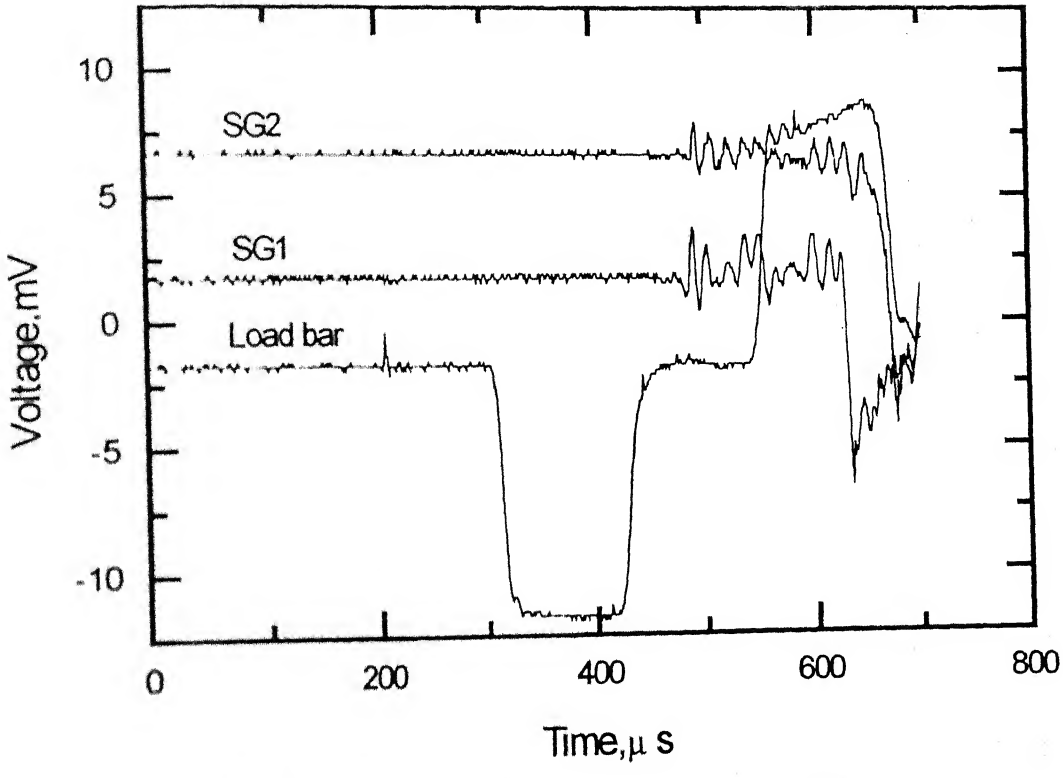

Fig. A.2.24 Oscilloscope Records Expt. L-12

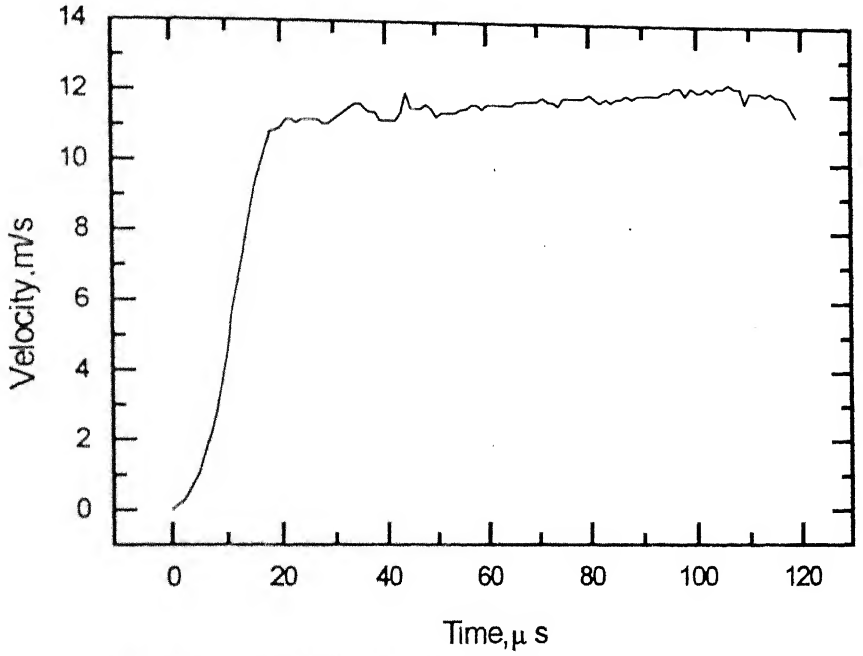

Fig A 2.24(b) Velocity of load bar end Expt. L-12

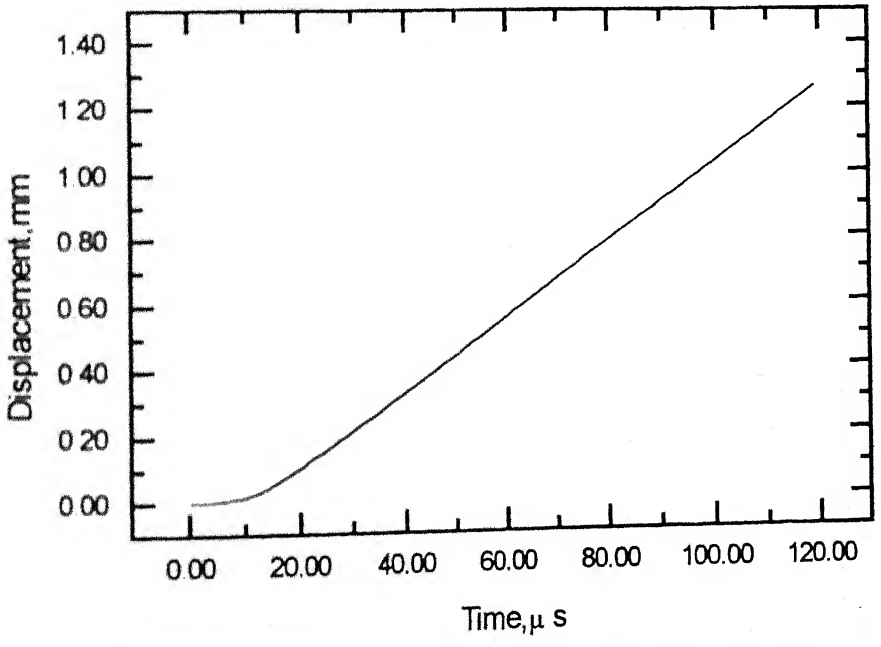

Fig. A 2.24 Displacement of cantilever end Expt. L-12

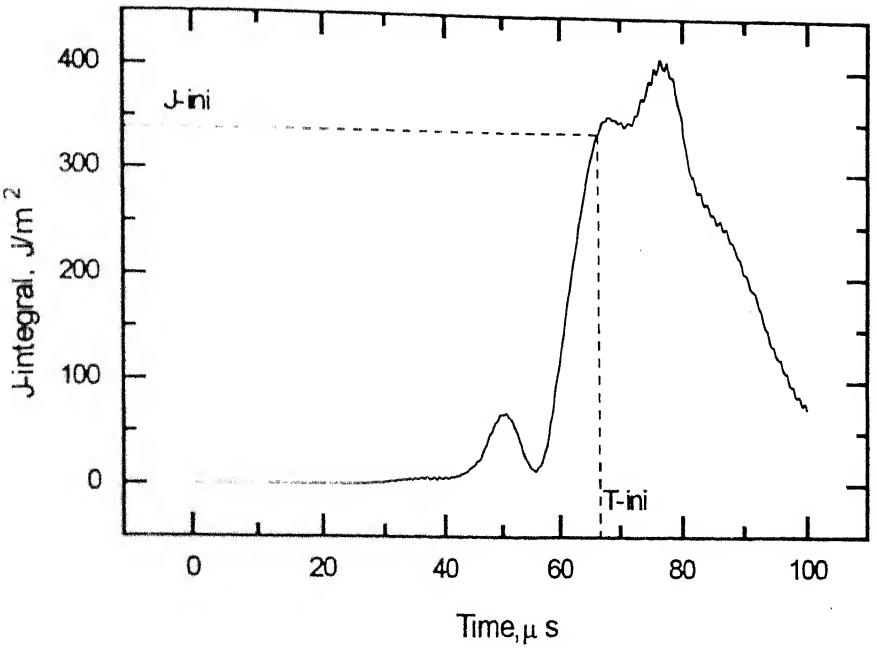

Fig A 2.24 Variation of J-integral for stationary crack Expt. L-12

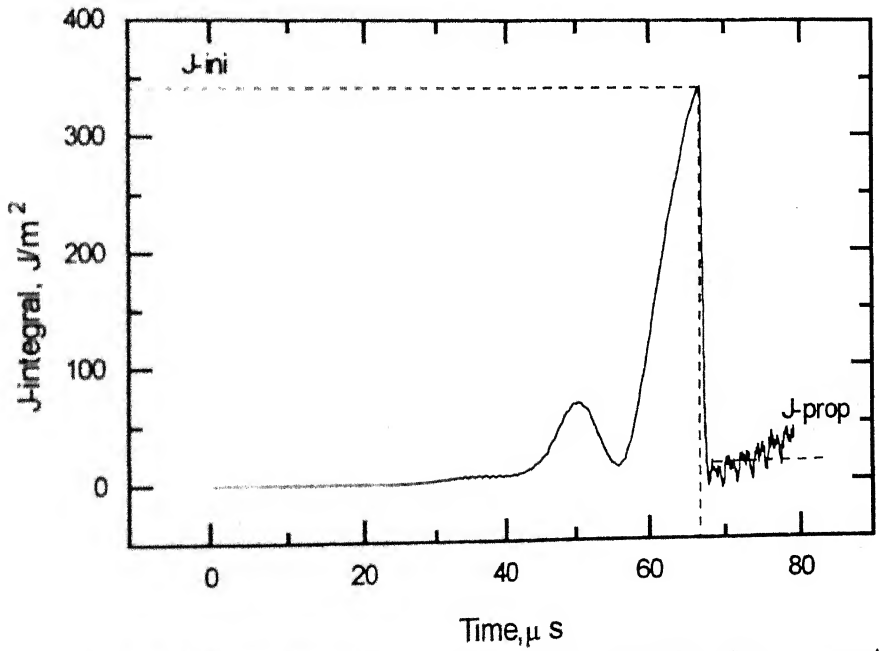

Fig A 2 24(e) Variation of J-integral for stationary & propagating crack Expt. L-12

Appendix 3

Quasistatic Interlaminar Toughness

To compare the dynamic interlaminar toughness with quasistatic interlaminar toughness experiments are conducted to determine the quasistatic interlaminar toughness (G_{Ic}) through a standard test (P. Kumar (1999)). The test involves pulling a DCB specimen in displacement control mode. Specimen used to determine quasistatic interlaminar toughness is identical to that of a impact testing specimen. It is made of 64 laminae. The load is applied until the crack extends by a small distance (5 - 10 mm) The machine is stopped until the crack becomes stationary and then the specimen is unloaded The specimen, now with a longer crack length, is loaded again. The compliance of the specimen is determined through the loading curve (Fig.A.3.1). The specimen is subjected to several loading – unloading compliance and critical load for several crack lengths. With proper data reduction scheme (P. Kumar (1999)), the critical energy release rate is evaluated. Value of G_{Ic} is determined from equation

$$G_{Ic} = \frac{3}{2}\frac{A_1 A_2^2}{B} \tag{1}$$

where A_1 and A_2 are given by

$$\ln(A_1) = \frac{1}{n}\left[-3\Sigma\ln(a) + \Sigma\ln(C)\right] \tag{2}$$

$$\ln(A_2) = \frac{1}{n}\left[\ln(a) + \Sigma\ln(P_c)\right] \tag{3}$$

and P_c and a are critical load and crack length respectively. Crack length, a, compliance, C and critical load P_c are tabulated in Table A.3.1 for Expt. 1.

Table A.3.1 Logarithmic value of a, c and P_c

S.No.	Crack length A (mm)	Displacement at P_c u (mm)	Critical load P_c (N)	Compliance $C = u/P_c$ (mm/N)	In (C)	In (a)	In (P_c)
1	31.0	2.1	270.0	0.00778	-4.856	3.433	5.598
2	40.5	3.1	227.0	0.0136	-4.297	3.701	5.425
3	50.5	5.0	212.5	0.0235	-3.750	3.922	5.358
4	60.0	6.5	175.0	0.0375	-3.283	4.094	5.165
				Sum of column (Σ)	-16.186	15.15	21.546

By suing Eqs. (1), (2) and (3)

$A_1 = 2.032 \times 10^{-7}$ and

$A_2 = 964.31$

$G_{Ic} = 944.7\ J/m^2$

Similarly, one more experiment is conducted that gives

$G_{Ic} = 904.1\ J/m^2$

Table A.3.2 shows the average value of G_{Ic} of the two experiments.

Expt No	Specimen	Quasistatic Interlaminar Toughness (J/m^2)	Average Value (J/m^2)
1	$[0^o]_{64}$	904.1	924.4
2	$[0^o]_{64}$	944.7	

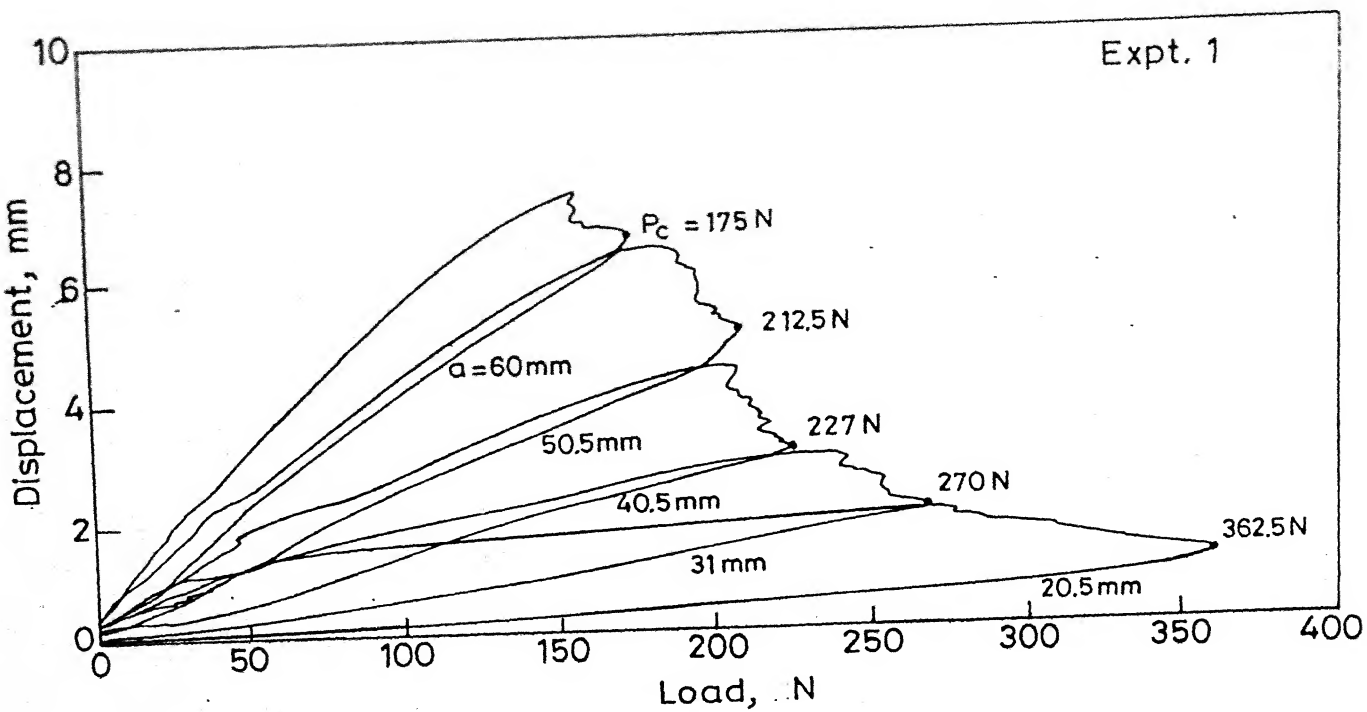

Fig. A.3.1 Load displacement curves.